Vol. 294, No. 2, August 19, 1994 ISSN 0003-2670

ANALYTICA CHIMICA ACTA

An international journal devoted to all branches of analytical chemistry

ELSEVIER

ANALYTICA CHIMICA ACTA

Scope. *Analytica Chimica Acta* publishes original papers, rapid publication letters and reviews dealing with every aspect of modern analytical chemistry. Reviews are normally written by invitation of the editors, who welcome suggestions for subjects. Letters can be published within **four months** of submission. For information on the Letters section, see inside back cover.

Submission of Papers

Americas

Prof. Harry L. Pardue
Department of Chemistry
1393 BRWN Bldg, Purdue University
West Lafayette, IN 47907-1393
USA

Tel:(+1-317) 494 5320
Fax:(+1-317) 496 1200

Computer Techniques

Prof. J.T. Clerc
Universität Bern
Pharmazeutisches Institut
Baltzerstrasse 5, CH-3012 Bern
Switzerland

Tel:(+41-31) 6314191
Fax:(+41-31) 6314198

Prof. Sarah C. Rutan
Department of Chemistry
Virginia Commonwealth University
P.O. Box 2006
Richmond, VA 23284-2006
USA
Tel:(+1-804) 367 7517
Fax:(+1-804) 367 8599

Other Papers

Prof. Alan Townshend
Department of Chemistry
The University
Hull HU6 7RX
Great Britain

Tel:(+44-482) 465027
Fax:(+44-482) 466410

Prof. Willem E. van der Linden
Laboratory for Chemical Analysis
Department of Chemical Technology
Twente University of Technology
P.O. Box 217, 7500 AE Enschede
The Netherlands
Tel:(+31-53) 892629
Fax:(+31-53) 356024

Prof. Paul Worsfold
Dept. of Environmental Sciences
University of Plymouth
Plymouth PL4 8AA
Great Britain

Tel:(+44-752) 233006
Fax:(+44-752) 233009

Submission of an article is understood to imply that the article is original and unpublished and is not being considered for publication elsewhere. *Anal. Chim. Acta* accepts papers in English only. There are no page charges. Manuscripts should conform in layout and style to the papers published in this issue. See inside back cover for "Information for Authors".

Publication. *Analytica Chimica Acta* appears in 16 volumes in 1994 (Vols. 281-296). *Vibrational Spectroscopy* appears in 2 volumes in 1994 (Vols. 6 and 7). Subscriptions are accepted on a prepaid basis only, unless different terms have been previously agreed upon. It is possible to order a combined subscription (*Anal. Chim. Acta* **and** *Vib. Spectrosc.*).
Our p.p.h. (postage, packing and handling) charge includes surface delivery of all issues, except to subscribers in the U.S.A., Canada, Australia, New Zealand, China, India, Israel, South Africa, Malaysia, Thailand, Singapore, South Korea, Taiwan, Pakistan, Hong Kong, Brazil, Argentina and Mexico, who receive all issues by air delivery (S.A.L.-Surface Air Lifted) at no extra cost. For Japan, air delivery requires 25% additional charge of the normal postage and handling charge; for all other countries airmail and S.A.L. charges are available upon request.

Subscription orders. Subscription prices are available upon request from the publisher. Subscription orders can be entered only by calendar year and should be sent to: Elsevier Science B.V., Journals Department, P.O. Box 211, 1000 AE Amsterdam, The Netherlands. Tel: (+31-20) 5803 642, Telex: 18582, Telefax: (+31-20) 5803598, to which requests for sample copies can also be sent. Claims for issues not received should be made within six months of publication of the issues. If not they cannot be honoured free of charge. Readers in the U.S.A. and Canada can contact the following address: Elsevier Science Inc., Journal Information Center, 655 Avenue of the Americas, New York, NY 10010, U.S.A. Tel: (+1-212) 6333750, Telefax: (+1-212) 6333990, for further information, or a free sample copy of this or any other Elsevier Science journal.
Advertisements. Advertisement rates are available from the publisher on request.

US mailing notice - Analytica Chimica Acta (ISSN 0003-2670) is published 3 times a month (total 48 issues) by Elsevier Science B.V. (Molenwerf 1, Postbus 211, 1000 AE Amsterdam). Annual subscription price in the USA US$ 3035.75 (valid in North, Central and South America), including air speed delivery. Second class postage paid at Jamaica, NY 11431. *USA Postmasters*: Send address changes to Anal. Chim. Acta, Publications Expediting, Inc., 200 Meacham Av., Elmont, NY 11003. Airfreight and mailing in the USA by Publication Expediting.

ANALYTICA CHIMICA ACTA

An international journal devoted to all branches of analytical chemistry

(Full texts are incorporated in CJELSEVIER, a file in the Chemical Journals Online database available on STN International; Abstracted, indexed in: Aluminum Abstracts; Anal. Abstr.; Biol. Abstr.; BIOSIS; Chem. Abstr.; Curr. Contents Phys. Chem. Earth Sci.; Engineered Materials Abstracts; Excerpta Medica; Index Med.; Life Sci.; Mass Spectrom. Bull.; Material Business Alerts; Metals Abstracts; Sci. Citation Index)

VOL. 294 NO. 2 CONTENTS AUGUST 19, 1994

ELSEVIER

Analytica Chimica Acta 294 (1994) 113–126

ANALYTICA CHIMICA ACTA

Identification of the procedural steps that affect recovery of semi-volatile compounds by solid-phase extraction using cartridge and particle-loaded membrane (disk) devices

Mary L. Mayer, Colin F. Poole *

Department of Chemistry, Wayne State University, Detroit, MI 48202, USA

Received 28th December 1993; Revised manuscript received 7th March 1994

Abstract

The experimental conditions are optimized for the recovery of a test mixture of neutral semi-volatile analytes on a cartridge and particle-loaded membrane (disk) device used for solid-phase extraction. The experimental variables investigated include: (1) selection of the type and volume of eluting solvent; (2) drying time between sample processing and elution of analytes; (3) the need for a preconditioning step prior to sample processing; (4) the need for an eluent permeation period prior to elution; (5) the use of organic solvents, surfactants and neutral inorganic salts as sample processing aids to enhance sample flow rates and recovery; (6) sample flow rate. The disk device is easier to work with, allows faster sample processing, requires a smaller eluent volume for analyte recovery, and provides recoveries virtually independent of the sample and eluent flow rates. On the other hand, preconditioning of the disk with an organic solvent prior to sample application is absolutely essential for normal operation, but is not essential when the cartridge device is used. There is greater variability in results obtained on different cartridge devices because of differences in their packing density and heterogeneous flow characteristics. The recovery of analytes from the cartridge device shows significant flow rate dependence when the sample volume exceeds the breakthrough volume of the analyte. When used under optimized conditions both devices show excellent recovery of the analytes (> 90%, except for dodecane on the cartridge device) and similar method precision.

Key words: Chromatography; Solid-phase extraction; Particle-loaded membrane (disk) devices; Semi-volatile compounds

1. Introduction

Solid-phase extraction cartridges were introduced in the late 1970s and rapidly gained acceptance as a replacement for liquid–liquid extraction techniques for the isolation of organic analytes in a form suitable for chromatographic analysis [1–6]. Liquid–liquid extraction procedures were viewed as being too labor intensive, difficult to automate, and required the use of relatively large volumes of high purity solvents that were

* Corresponding author.

SSDI 0003-2670(94)00131-5

expensive to purchase and, in some cases, equally as expensive to dispose of in an environmentally acceptable manner. The selectivity of the extraction process was limited by the narrow range of immiscible solvents available and emulsion formation could add to the difficulty of obtaining two distinct phases. Solid-phase extraction cannot be viewed as a panacea for all of these problems but its wide acceptance as an extraction technique attests to the fact that it has been successful in addressing some of these issues in individual cases.

The basic design of solid-phase extraction devices has changed little since their inception. A typical solid-phase extraction cartridge consists of a small column (generally an open syringe barrel) containing a sorbent with an average nominal particle size of about 40 μm packed between porous metal or plastic frits. The dimensions of the sorbent bed are deliberately miniaturized to minimize the difficulty in sample processing using gravity or suction-aided sample flow and to reduce the amount of solvents consumed in conditioning the sorbent. This design has certain attendant disadvantages which can be summarized as follows: (1) the small cross-sectional area of the extraction cartridges results in slow sample processing rates and a low tolerance to blockage by particles and adsorbed matrix components; (2) channeling reduces the capacity of the cartridge bed to retain analytes (causes premature breakthrough of the analyte); (3) sorbent properties are inconsistent from lot-to-lot and between manufacturers; (4) incomplete reversibility of the sorption of some analytes from active sorbent sites lowers their expected recovery; and (5) contamination of the isolated analytes by impurities originating from the manufacturing and packaging process. It is possible that some of these problems could be remedied by redesign of the solid-phase extraction cartridge in the form of a low profile disk.

Commercial products for solid-phase extraction in disk form have appeared in the last few years [7–9]. Particle-loaded membranes in the form of flexible disks of various diameters and 0.5 mm thickness consist of sorbent particles of about 8 μm diameter (90% w/w) immobilized in a web of poly(tetrafluoroethylene) microfibrils. For general use the membranes are supported on a fritted glass disk in a standard filtration apparatus, using suction to generate the desired flow of sample through the membrane. Glass microfiber disks impregnated with chemically bonded sorbent are the most recent addition to the marketplace. The microfiber disks are rigid eliminating the necessity for an external support. The specific advantages claimed for the disk format over the cartridge format can be summarized as follows: (1) shorter sample processing times due to the larger cross-sectional area and decreased pressure drop enabling higher sample flow rates to be used; (2) decreased plugging by particles due to reduced channeling and improved kinetic performance resulting from the use of smaller sorbent particles and the greater mechanical stability of the sorbent bed; and (4) cleaner background and lower interferences by optimization of the bed mass to reduce non-specific matrix adsorption. From this perspective the disk technology can be considered a further evolution in the solid-phase extraction concept attempting to address some of the deficiencies in cartridge devices identified above.

While a great deal of information is available concerning the use and applications of solid-phase extraction cartridges (reviewed in [1–7]) the pedigree of solid-phase extraction devices using disk technology is short, since these products have been available for a relatively short period of time. A few applications using particle-loaded membranes for the recovery of industrial chemicals, pesticides and herbicides from water [7,10–20] and drugs from serum [21] have appeared. Recent papers on the mechanism of solid-phase extraction using particle-loaded membranes have characterized the kinetic properties of these membranes [22] and suggested a method for the prediction of breakthrough volumes based on a solvation parameter model [23]. The glass microfiber disks have been validated for the isolation of drugs of abuse from biological fluids including the use of on disk derivatization reactions to enhance the separation and detection charac-

teristics of the isolated analytes without the need for a separate analyte elution step [9,24].

This study is part of a larger effort to define a theoretical model that allows the optimized sampling conditions in solid-phase extraction to be predicted for any desired analyte entirely from rapid experiments performed by liquid chromatography. To this end we have previously developed a model that successfully predicts the breakthrough volume of a substance of known structure or chromatographic retention and extended this approach to the selection of sampling conditions and optimized solvents for matrix simplification and analyte recovery [22,23,25]. As part of these studies it was necessary to develop a standard protocol for sample processing conditions using disks and cartridges to validate the results predicted by liquid chromatography.

2. Experimental

2.1. Materials

All organic solvents and water were Omnisolv grade from EM Science (Gibbstown, NJ). Dodecane, *n*-propylbenzene, 1,2,4-trichlorobenzene, acetophenone, 1-bromoheptane, and heptanal were general laboratory grade chemicals in the highest purity available from Aldrich (Milwaukee, WI). The Empore™ particle-loaded membranes in the form of 47-mm disks were obtained from Varian Sample Preparation Products (Harbor City, CA) and the 6-ml solid-phase extraction cartridges from J.T. Baker (Phillipsburg, NJ). Both cartridges and disks contained nominally 500 mg of octadecylsilanized silica packing material.

Preparation of standard solutions

Standard solutions containing approximately 1000 ppm of analytes were prepared in methanol. Unless stated otherwise, 0.5 ml of the primary standard was added to 50 to 1000 ml of water adjusted to give a final aqueous solution containing from 0.5–1.0% (v/v) methanol.

To correct for injection volume differences and instability in the split injection conditions in gas chromatography acenaphthene or 2-nonanone were added to standard solutions and the eluents from the extraction experiments at a concentration of 25–30 ppm to calculate recoveries.

2.2. Optimized extraction conditions for standard substances

Numerous conditions were used to study the influence of experimental parameters on the recovery of the standard compounds from water. Reported below are the optimized experimental procedures for the recovery of the standard compounds from water using particle-loaded membranes (disks) and cartridges.

The particle-loaded membranes were mounted in the usual way on the fritted glass support disk of a standard vacuum filtration apparatus (Millipore, Bedford, MA) connected to a water aspirator via a flow metering valve, as described by Hagen et al. [7]. Prior to use, the membranes were washed by sucking 10 ml of acetonitrile through them to remove any contaminants. The wash solvent was allowed to permeate the disk for a few minutes, before pulling it through the membrane, which was then dried by pulling air through it for about 10 min. The disk was then conditioned with methanol, 10 ml, by allowing it to permeate the disk for a few minutes, followed by sucking the solvent through the membrane and releasing the vacuum before the last drop of methanol had passed through the membrane. The disk was then washed with water, 10 ml, followed by application of the sample without allowing the disk to become dry. The samples were sucked through the membrane at a flow rate of 40 ± 3 ml/min. After the sample had been processed, the receiver was changed for elution of the standards. The disk was allowed to dry for about 30 s under suction and the standards were then eluted with two 5 ml aliquots of acetonitrile. The first aliquot was allowed to permeate the disk for a few seconds before sucking through the membrane followed by the second aliquot of acetonitrile without allowing the disk to become dry. The suction was continued until no more acetonitrile was recovered from the disk and its support. The combined aliquots of acetonitrile were then

transferred to a 10 ml volumetric flask, a suitable internal standard added, and the solution adjusted to the mark.

For the cartridge studies a standard filtration flask, 500 ml, connected to a water aspirator via a flow metering valve (similar arrangement to the disk study) was used. Cartridges were evaluated individually by mounting on a rubber stopper with a hole bored through it, which was inserted into the open mouth of the filtration flask. The cartridges were conditioned by slowly sucking 10 ml of methanol through them without a permeation step. Without letting the cartridge become dry this was followed by 10 ml of water. The sample was then applied to the cartridge just as the last drop of the previous solvent had reached the surface of the top frit in the cartridge. The pressure was adjusted to maintain a flow rate of 5 ± 1 ml/min throughout the sample application process. When all the sample had been processed, the cartridge was dried for about 3 min under suction, the vacuum broken, and the cartridge transferred to a second filtration apparatus containing a test tube to collect the eluent. The analytes were eluted from the cartridge using two 10 ml and one 5 ml volumes of acetonitrile at a flow rate of about 2 ml/min.

2.3. Instrumentation

The recovery of standards was determined by gas chromatography using a Varian 3700 gas chromatograph (Walnut Creek, CA), split injector, and flame ionization detector. The separations were performed on a 60 m × 0.32 mm i.d. fused silica capillary column (J&W Scientific, Folsom, CA) coated with DB-1, film thickness 0.25 μm. The column was temperature programmed from 50°C with a 5 min hold to 120°C at 7°C/min with hydrogen as the carrier gas at a flow rate of 1.1 ml/min. The injector and detector temperatures were 240°C and 300°C, respectively. Quantitation was based on peak areas recorded with a Hewlett-Packard 3396A (Avondale, PA) computing integrator.

3. Results and discussion

A typical procedure employing solid-phase extraction consists of four distinct steps. Initially, the sorbent bed is conditioned with solvent to improve the reproducibility of analyte retention and to reduce the carry through of sorbent impurities at the recovery stage. Subsequently the

Table 1
Repeatability of the observed recovery of standards for disks and cartridges

Compound	3 new devices		1 device reused 4 times	
	Average recovery (%)	Standard deviation ($n = 3$)	Average recovery (%)	Standard deviation ($n = 4$)
(i) Disk (sample volume 500 ml)				
Heptanal	85.0	3.0	89.5	5.9
n-Propylbenzene	85.6	2.6	87.2	3.0
1-Bromoheptane	82.8	3.1	84.7	3.7
Acetophenone	29.8	28	29.2	9.0
1,2,4-Trichlorobenzene	95.3	2.7	97.3	0.9
Dodecane	96.6	4.5	86.0	4.1
(ii) Cartridge (sample volume 50 ml)				
Heptanal	68.8	3.9	68.0	0.2
n-Propylbenzene	84.4	1.1	90.3	2.0
1-Bromoheptane	79.8	1.6	90.2	2.0
Acetophenone	97.2	1.7	100	0.0
1,2,4-Trichlorobenzene	83.6	2.5	86.5	2.3
Dodecane	20.2	10.7	35.9	8.2

sample is processed through the sampling device at a controlled flow rate. Optionally, after the sample has been processed, the sampling device may be rinsed with a weak solvent to displace undesired matrix components from the sampling device without displacing the analytes of interest. Finally the analytes of interest are eluted from the sorbent in a small volume of a strong solvent for subsequent chromatographic determination. Hidden in the above description of events are a number of sub-steps which can dramatically influence analyte recovery if not adequately optimized. Also, it may not be adequate to replace a disk for a cartridge in an established cartridge method without a significant change in the experimental protocol. A group of neutral, polar analytes were selected as model compounds to identify the critical steps in the above sampling procedure without interference from sorbent specific interactions which relate to the chemistry of the sorbent surface and not to the general processing conditions. For example, it is well established that the conditions required for the recovery of weak acids and bases from chemically bonded sorbents are often different from those of neutral compounds due to ion-exchange interactions with ionizable groups on the sorbent surface.

3.1. Reusability of disks and cartridges

Recovery data for the test compounds were recorded with the manufactures recommended conditions for three disks or cartridges from the same lot and for a single disk or cartridge reused sequentially for four samples with an intermediate wash step followed by reconditioning of the device for the next sample. These tests were performed to evaluate the range of recovery data that might be expected from device to device and to establish whether a single disk or cartridge could be reused several times without impairing the reliability of the results obtained. The results of these experiments are summarized in Table 1. At the 95% confidence level their is no difference in the mean recovery of the analytes except for dodecane on both disks and cartridges. In large

Table 2
Influence of eluting solvent on analyte recovery

Solvent	Compound [a]					
	Heptanal	Propyl-benzene	1-Bromo-heptane	Aceto-phenone	Trichloro-benzene	Dodecane
(i) Disks						
Acetonitrile	85(3.0)	86(2.6)	83(3.1)	29(4.3)	95(2.7)	97(4.5)
Methanol	90(5.8)	84(4.9)	80(5.2)	32(5.2)	95(2.8)	80(2.9)
Dichloromethane	65(4.3)	59(6.3)	50(3.3)	13(4.1)	71(2.2)	53(8.1)
Acetone	88(4.7)	80(3.8)	75(2.7)	24(6.6)	90(2.6)	86(8.1)
Chloroform	67(4.7)	84(1.8)	83(1.8)	15(5)	90(0.8)	68(6.5)
Ethyl acetate	64(4.5)	80(5.9)	79(5.8)	13(4.2)	86(4.6)	76(1.0)
Tetrahydrofuran	62(2.3)	71(2.1)	72(2.9)	15(2.5)	80(1.7)	79(6.6)
Dioxane	86(2.8)	81(0.8)	82(4.9)	22(0)	89(1.3)	86(3.8)
Methyl ethyl ketone	82(1.8)	82(2.8)	83(4.7)		88(3.5)	88(1.9)
(ii) Cartridges						
Acetonitrile	79(2.2)	76(1.1)	64(6.8)	38(3.7)	79(2.8)	46(1.3)
Methanol	77(1.6)	73(3.7)	56(5.0)	44(0.3)	73(3.7)	31(14)
Dichloromethane	83(3.4)	69(7.7)	56(8.2)	26(2.7)	78(5.3)	48(3.7)
Chloroform	67(10)	69(4.6)	55(4.5)	17(10)	81(2.2)	41(5.7)
Acetone	82(5.2)	76(3.9)	65(5)	33(0)	81(4.4)	40(6.6)
Ethyl acetate	71(1.7)	84(2.8)	78(4.2)	16(6.8)	89(1.9)	67(1.2)
Dioxane	80(8)	80(5.9)	74(2.3)	35(6.6)	86(2.1)	56(7)
Methyl ethyl ketone	69(7)	73(4.3)	55(3.9)	17(4.6)	76(4)	26.8(20)

[a] The term in parentheses is the R.S.D. (%).

measure this is due to incomplete elution of the sorbed sample as well as some non-specific losses during sample processing. The choice of solvent (solvent strength) and volume used for elution are the main factors requiring further optimization in this case. The standard deviations indicate that the precision of the measurements is acceptable except for acetophenone on the disks and dodecane on the cartridges. It will be shown later that the acetophenone data is less rugged because of breakthrough on the disks where a 500 ml sample volume was used.

In the practical sense, the only real concern encountered in reusing solid-phase extraction devices is whether residual analyte or matrix components are left on the device from the previous extraction which interfere in the sorption of the sample or contribute to enhanced recovery due to carry-over from one sample to the next. For the test mixtures used in our experiments matrix contamination of the solid-phase extraction device should not be a problem and, therefore, reusing the sampling devices is an attractive way of minimizing the variability between individual experiments. An efficient washing step and reconditioning step was used to ensure that carry-over was not a general problem, although, some of the variability in the data for dodecane on the cartridge devices could arise from this source.

Although not relevant to the data given in Table 1, we have noticed that when a disk has been used or reused to extract in excess of 6 l of water it fails to function adequately. The appearance of the disk changes, taking on a permanent wet look with perhaps a swollen center portion. There is no simple means to restore the sorption properties of the disk to normal after this point is reached, and the disk will no longer function adequately and must be discarded.

3.2. Selection of the eluting solvent

The selection of the eluting solvent is critical to all subsequent optimization steps. The eluting solvent must be able to displace all the analyte from the sampling device with the minimum volume. Solvents ranging widely in solvent strength and water miscibility were evaluated for this purpose (Table 2). In general, the lowest recoveries were obtained for solvents with low water solubility. Although not shown in the table, experiments using mixed solvents (specifically methanol–dichloromethane, acetonitrile–dichloromethane, methanol–tetrahydrofuran, and tetrahydrofuran–acetonitrile as 1:1 mixtures) showed no advantages over using a single solvent.

The volume of solvent required for complete elution of the analytes from the particle-loaded membranes was determined by collecting 5 ml aliquots of solvent and analyzing them independently to determine the recovery. Recovery was complete with a 10 ml volume of solvent for dichloromethane, chloroform, acetone and ethyl acetate. For acetonitrile and dioxane 15 ml was required and 20 ml for methanol to include just detectable amounts in the last fraction analyzed. Based on the recovery data (Table 2) and the volume required for complete elution 15 ml of acetonitrile was selected as the eluting solvent in further optimization steps.

For the cartridges the choice of eluting solvent had little influence on the observed recovery but significantly larger volumes of solvent were required for complete recovery of the analytes compared to the disks. The observed recoveries were

Table 3
Influence of drying time on analyte recovery

Compound	Time (min)					
	0	1	5	12	25	50
(i) Disks						
Heptanal	88	79	79	79	74	76
n-Propylbenzene	85	86	82	78	24	6
1-Bromoheptane	86	87	85	91	68	16
Acetophenone	94	96	95	95	90	89
1,2,4-Trichlorobenzene	93	88	86	91	85	47
Dodecane	83	85	90	87	87	87
(ii) Cartridges						
Heptanal	70	74	80	81	77	65
n-Propylbenzene	83	88	92	92	92	10
1-Bromoheptane	84	78	88	89	90	16
Acetophenone	71	67	70	74	72	64
1,2,4-Trichlorobenzene	90	90	93	100	89	42
Dodecane	30	31	34	29	33	37

also flow rate dependent, as discussed subsequently. In general, for eluting solvent flow rates of 2 ml/min, two 25 ml aliquots were collected with the majority of the analytes being in the first aliquot. However, at faster eluting flow rates three 25-ml aliquots were required to completely elute the analytes.

One of the more obvious problems in the above protocol is that the elution step was performed without first removing entrapped water from the sampling device. For water immiscible solvents this resulted in the separation of the recovered eluent into two layers. The holdup volume for the membrane is 0.25 ml [22]. However, the holdup volume for the sampling device is 3.33 ml, with the largest contribution coming from the fritted glass disk used to support the membrane (assuming a thickness of 4 mm for the fritted disk and a total permeability of 0.8). At 10 ml, for example, the number of bed volumes required to elute all of analytes is about 40. The holdup volume of the sorbent bed of the cartridge device is about 0.42 ml [25] and that of the frits at the top and bottom of the bed a further 0.40 ml, for a total of 0.82 ml. At 50 ml of eluting solvent about 120 bed volumes of solvent were required to elute all of the analytes. Clearly, these high values do not represent an efficient eluting system, while at the same time the design of the devices is far from optimum in terms of their system holdup volume. In the case of the particle-loaded membranes the problem resides in the membrane support which could conceivably be easily reduced by using screens in place of the glass frits currently used.

3.3. Drying the sampling device before the elution step

The presence of water in the sampling device can influence the capacity of the eluting solvent to extract the analyte from the stationary phase in two ways. Since the pores are filled with water, water immiscible solvents will be impeded to some extent from entering the pores and gaining access to the analytes until the water has been mechanically displaced from the pores. This is unlikely to be a rapid process. Water miscible solvents may penetrate the pore volume more effectively, but do so with concurrent mixing with water that reduces their elution strength [26]. Thus their effectiveness as eluting solvents is diminished until the concentration of water dissolved in the eluting solvent in immediate contact with the sorbent is reduced to a level that favors displacement of the analyte from the sorbent surface. This should be more efficient for the membrane device since the holdup volume for the membrane is substantially less than that of the cartridge unless precipitation of the analytes in the fritted glass disk support occurs as the eluent encounters a larger volume of water contained in the interstercities of the glass frit. Transport of the analyte through the frit will then depend on the volume of solvent required to wash out the water from the glass frit, redissolve the analyte, and mechanically carry it across the frit.

The simplest approach to reducing the volume of water retained in the sampling devices prior to elution would be to remove the bulk water and reduce the volume of film water by applying suction to the device for some specified time, or alternatively, to place the sampling device in a desiccator at atmospheric or reduced pressure. The latter approach was evaluated by McDonnell et al. [16] and was shown to be quite effective for the recovery of pesticides from particle-loaded membranes. For the compounds studied here it lead to low recoveries due to volatility losses so only drying by suction was investigated thoroughly.

Table 4
Influence on analyte recovery of allowing the eluting solvent to permeate the sampling device for three minutes prior to eluting the analytes

Compound	Permeation time (min)			
	Disk		Cartridge	
	0	3	0	3
Heptanal	85	86	60	58
n-Propylbenzene	85	84	71	76
1-Bromoheptane	83	86	72	77
Acetophenone	65	73	93	91
1,2,4-Trichlorobenzene	90	93	72	75
Dodecane	83	82	34	25

The influence of drying time on recovery for membranes using a water aspirator vacuum is summarized in Table 3. Two factors are obvious: drying the disk prior to eluting the sample does not increase the recovery of the analytes; and for long drying times there is a loss of the more volatile analytes. As well as volatility the loss of analytes is related to how tightly the analyte is bound to the stationary phase. Dodecane, acetophenone and heptanal are hardly influenced by the drying time (0 to 50 min in Table 3) while significant amounts of *n*-propylbenzene, 1-bromoheptane, and 1,2,4-trichlorobenzene are lost between 12–50 min. The results for the cartridge indicate that there is no significant change in the recovery of the test compounds for drying times of 0–25 min but longer drying times cause a significant loss of the more volatile analytes.

The benefit from employing a drying step is not that it leads to an increase in recovery but, rather, that it reduces the volume of water co-eluted from the sampling device permitting further concentration of the eluent by the gas-blow down method. The drying time will be important when the analytes are sufficiently volatile to be lost via evaporation and will have to be adjusted accordingly [10,20]. Since most of the bulk water is removed with a very short drying time most of the benefit is obtained in the first minute or so of the drying step. Thus for the present purposes a drying time of 1 min is a reasonable compromise.

Table 5
Influence of the eluent flow rate on the recovery of analytes from the disk with sufficient volume of eluent (15 ml) to ensure complete recovery

Compounds	Recovery (%)			
	Flow rate (ml/min)			
	108	60	13	9
	Velocity (mm/s)			
	1.88	1.05	0.23	0.16
Heptanal	90	94	97	94
n-Propylbenzene	84	86	89	89
1-Bromoheptane	86	88	90	88
Acetophenone	62	64	62	63
1,2,4-Trichlorobenzene	90	92	96	93
Dodecane	83	88	84	87

Table 6
Influence on analyte recovery of the eluent flow rate when a sufficient volume of eluent is available for quantitative recovery using the cartridge device

Compound	Recovery (%) volume = 75 ml			
	Flow rate (ml/min)			
	18.8	14.3	2.4	0.55
	Velocity (mm/s)			
	4.42	3.36	0.56	0.13
Heptanal	84	80	83	86
n-Propylbenzene	74	75	79	82
1-Bromoheptane	64	69	74	79
Acetophenone	91	84	86	86
1,2,4-Trichlorobenzene	69	69	80	88
Dodecane	13	56	18	49

3.4. Solvent permeation step and eluent flow rate

Having decided on a suitable drying time and a suitable eluting solvent the next steps were to see if a permeation step was required to improve the contact of the solvent with the sorbed analyte and whether there was a relationship between the volume of solvent used for elution and the flow rate of the eluting solvent on the observed recovery. The data in Table 4 confirm that provided the volume of eluting solvent is sufficient to recover all of the analyte from the sampling device allowing the solvent to permeate the disk or cartridge for 3 min prior to eluting the analytes does not improve the recovery. When the volume of eluting solvent exceeds the minimum volume required for complete elution of the analytes then the flow-rate used to elute the analytes is not a critical factor (Table 5) for the particle-loaded membranes.

The influence of eluent flow rate on the recovery of analytes from the cartridge is less clear cut (Table 6). The data for dodecane is erratic and the recovery of 1,2,4-trichlorobenzene is reduced at high flow rates compared to the results at lower flow rates. Some of this variability is probably accounted for by the variable packing density of the cartridges resulting in heterogeneous flow streams through the sorbent bed [25]. Flow rates around 2.0 ml/min are convenient for general use and result in reliable recovery data while

higher flow rates can result in lower recoveries for some compounds.

3.5. Conditioning step

An organic solvent such as methanol is used in the conditioning step to solvate the stationary phase and enhance interactions with the analytes in the sampling step, to remove accumulated contaminants from the unused disk, and to promote even and uniform flow through the membrane [7]. To gain a better understanding of the role played by the solvating or wetting agent, as it is sometimes called, the following set of experiments were performed. In method 1, the preconditioning step was omitted and no methanol was added to the sample; in method 2 the preconditioning step was omitted and 0.5% (v/v) methanol was added to the sample; in method 3 preconditioning of the membrane with 10 ml of methanol followed by 10 ml of water to rinse out excess methanol from the membrane was used combined with the addition of 0.5% (v/v) methanol to the sample; in method 4 preconditioning with 10 ml of methanol was employed together with the addition of 10% (v/v) methanol to the sample solution. The results of these experiments are summarized in Table 7. The observed analyte recovery for the disk device is universally low unless the disk is preconditioned prior to processing the sample. Adding methanol to the sample is not as effective as preconditioning the disk with methanol. The highest recoveries are observed when the disk is preconditioned with methanol and a small volume of methanol is added to the sample prior to processing. Increasing the amount of methanol added to the sample from 0.5 to 10% (v/v) does not significantly influence the recovery of the analytes except that it reduces the breakthrough volume so that in those cases were the breakthrough volume is less than the sample volume (acetophenone) the recovery is lower for the sample containing a larger amount of methanol.

An equally important aspect of the use of methanol as a conditioning agent is its affect on the sample processing time. In the absence of a

Table 7
The influence of methanol as a conditioning agent on the observed recovery and sample processing time

Compound	Method 1	Method 2	Method 3	Method 4
	Preconditioning step			
	No	No	Yes	Yes
	Volume of methanol added to sample (% v/v)			
	0	0.5	0.5	10
(i) Disk (sample volume 200 ml)				
Heptanal	62	73	85	84
n-Propylbenzene	53	66	90	90
1-Bromoheptane	70	82	89	90
Acetophenone	41	39	71	58
1,2,4-Trichlorobenzene	64	78	92	94
Dodecane	57	62	85	86
Sample processing time (min)	180	90	3	4.2
(ii) Cartridge (sample volume 200 ml)				
Heptanal	85	77	79	86
n-Propylbenzene	81	86	84	83
1-Bromoheptane	83	82	82	86
Acetophenone	75	84	79	45
1,2,4-Trichlorobenzene	100	99	100	100
Dodecane	57	55	57	58
Sample processing time (min)	4.5	4.5	7.5	7.5

preconditioning step with methanol and addition of methanol to the sample 3 h is required to process a 500 ml sample at a constant vacuum; adding 0.5% (v/v) methanol to the sample reduces the time to 1.5 h; while preconditioning the disk with methanol and adding methanol to the sample reduces this time to 3–4 min. The high surface tension of water combined with the microporosity of the disk results in slow and uneven flow of sample through the disk. The surface tension of water is reduced dramatically at low methanol concentrations with only a small increase in its viscosity [27]. For the disk the reduction in surface tension is more important than the increase in viscosity of the sample solution for increasing sample flow through the membrane. The improvement in sample recovery and reduction in sample processing time clearly demonstrate the importance of the conditioning step for effective use of the disks in solid-phase extraction.

For the cartridges, preconditioning the sorbent with methanol and/or adding methanol (0.5% v/v) to the sample had no obvious influence on recovery of the analytes (Table 8). Whether this reflects differences in the sorbent characteristics or is related to properties of the poly(tetrafluoroethylene) matrix support used in fabricating the disks is impossible to say. In terms of the procedural steps used in SPE this represents a significant difference in how the two devices should be used.

It is difficult to quantify changes in the sample processing time under different conditions for the cartridges because of substantial flow rate variations between individual cartridges. There is no evidence, however, that adding methanol to the sample as a processing aid is effective at reducing

Table 8
Influence of sample flow rate on analyte recovery

(i) Disks (sample volume 200 ml)						
Compound	Flow rate (ml/min)					Mean Recovery (%) [a]
	94.8	79	36.5	24.1	16.1	
	Velocity (mm/s)					
	1.64	1.37	0.63	0.42	0.28	
Heptanal	96	95	93	90	91	93 (2.5)
n-Propylbenzene	90	92	84	86	83	87 (3.9)
1-Bromoheptane	88	92	85	86	85	87 (2.9)
Acetophenone	64	64	59	65	64	63 (2.4)
1,2,4-Trichlorobenzene	93	96	90	93	89	92 (2.8)
Dodecane	81	88	88	77	86	84 (4.5)
(ii) cartridges (sample volume 200 ml)						
	Flow rate (ml/min)					
	44.4	31.6	22.8	12.9	8.7	
	Velocity (mm/s)					
	10.4	7.4	5.4	3.0	2.0	
Heptanal	76	80	84	76	75	78 (3.8)
n-Propylbenzene	95	89	87	92	86	90 (3.7)
1-Bromoheptane	85	81	79	81	80	81 (2.3)
Acetophenone	87	87	84	81	88	85 (2.9)
1,2,4-Trichlorobenzene	100	98	98	94	88	96 (4.8)
Dodecane	53	50	48	43	49	49 (3.6)

[a] Values in parenthesis are the standard deviations.

the sample processing time. It is possible that the increase in solution viscosity actually results in longer sample processing times for the cartridges.

3.6. Sample flow rate

The results obtained for the influence of the sample flow rate on analyte recovery are summarized in Table 8. The disks showed no dependence for the recovery of the analytes with sample flow rate over the range 0.28–1.64 mm/s (95–16 ml/min), indicating that this is not a critical parameter, even for acetophenone whose breakthrough volume is less than the sample volume processed. For the cartridges the observed recovery is independent of the sample flow rate over the range 0.28–1.64 mm/s (44–9 ml/min). In other studies with cartridges we have observed that the recovery may show a distinct flow rate dependence when the sample volume is greater than the breakthrough volume [25].

3.7. Surfactants and salt as sample processing aids

The possibility of adding a surfactant, Triton X-100, to the sample to improve analyte recovery for the disks was evaluated. The results are summarized in Table 9. A 1% (v/v) solution of Triton X-100 in water was less effective than methanol as a preconditioning agent and gave lower recoveries. On the other hand, adding 1% (v/v) Triton X-100 to the sample and preconditioning the disk with methanol had no significant influence on the observed recovery of the analytes. Adding Triton X-100 to the sample or using a solution of Triton X-100 as a preconditioning agent leads to a significant increase in the sample processing time. There seems to be no advantage to using a surfactant in place of methanol as a sample processing aid with the particle-loaded membranes.

Adding sodium chloride to the sample in amounts from 0 to 5% (w/v) had no significant influence on analyte recovery for the disks, except, perhaps for a small increase in the recovery of acetophenone, which was the only analyte with a breakthrough volume less than the sample volume processed. As a general procedure, it is unlikely that the recovery of neutral analytes can be significantly influenced by adding salt to samples prior to processing by SPE using the particle-loaded membranes.

Although the addition of surfactant and salt had little influence on the observed recovery of the analytes, variation of the ionic strength and contamination of natural waters with surfactants is quite common. The above observations suggest that these two factors need not be monitored too strictly and robust analytical methods can be designed for neutral compounds in which ionic strength and surfactant contamination vary between samples.

Table 9
Influence of surfactant (Triton X-100) on analyte recovery using disks (sample volume 200 ml)

Compound	Recovery		
	Preconditioning agent		
	Methanol	Methanol	Triton-X-100 (1%)
	Added to sample (v/v)		
	0.5% Methanol	1% TritonX-100	1% Triton X-100
Heptanal	86	82	34
n-Propylbenzene	89	87	82
1-Bromoheptane	89	85	82
Acetophenone	75	67	61
1,2,4-Trichlorobenzene	95	93	86
Dodecane	81	78	62
Sample processing time (min)	1.67	2.65	7.63

3.8. Optimized procedure

Finally, the breakthrough volumes and mean recoveries of the test compounds under optimized conditions were determined for the cartridge and disk devices (Table 10). The optimized experimental conditions are those described in the experimental section. The recovery for each compound was determined for a series of samples in which the sample volume was varied in the order 25, 50, 100, 200, 350, 500, 750, 1000, 1250, 1500, 1750, and 2000 ml. Thus, when breakthrough occurred between two measurements it is indicated as a range in Table 10 and the statistics quoted for the mean recovery refer to this data and not a constant sample volume (the mean recovery is independent of the sample volume provided that the breakthrough volume is not exceeded). The breakthrough volumes for all compounds except for acetophenone and heptanal for the disk device are greater than 2000 ml. The breakthrough volumes for acetophenone and heptanal are slightly larger for the cartridge device indicating its higher retention capacity, which is probably a property of the differences in the sorbents used to prepare the two sampling devices. This is not important for the present discussion. With the exception of dodecane for the cartridge device the observed mean recovery of the test compounds exceeds 90% for both devices under optimized conditions when the breakthrough volume is not exceeded. The difference in the mean recovery of heptanal and 1,2,4-trichlorobenzene is statistically significant (Student t test at the 95% probability level) but the observed values for both devices would be deemed acceptable for analytical work. For dodecane the difference in mean recovery is significant, 97.9% for the disk device and 63.3% for the cartridge device. For substances like dodecane the disk device is clearly superior. The major contribution to the difference in mean recovery of dodecane is the difficulty of recovering the analyte from the sorbent for the cartridge device. There is no statistically significant difference in the precision of either method after optimization (F test at the 95% probability level).

4. Conclusions

A perusal of the data in Table 1 and Table 10 indicates the importance of optimizing the experimental protocol for SPE using disk and cartridge devices. The narrative of the paper demonstrates the importance of modifying a protocol for cartridges to suit the different sampling conditions characteristic of the particle-loaded membranes. Simply changing the sampling device from a cartridge to a disk and employing the same experimental protocol developed for cartridge devices will likely produce disappointing results.

Analyte recovery from the disks is universally low and the sample flow rate too slow unless the

Table 10
Breakthrough volumes and mean recovery of test compounds under optimized conditions

Compound	Device	Breakthrough Volume (ml)	Mean Recovery (%)	Standard Deviation
Heptanal	disk	750–1000	94.6	2.3 (n = 8)
	cartridge	> 2000	90.3	3.8 (n = 12)
n-Propylbenzene	disk	> 2000	92.6	2.7 (n = 11)
	cartridge	> 2000	95.1	3.8 (n = 12)
1-Bromoheptane	disk	> 2000	91.7	2.6 (n = 11)
	cartridge	> 2000	90.7	4.1 (n = 12)
Acetophenone	disk	100–200	98.6	2.7 (n = 4)
	cartridge	200–350	95.1	3.1 (n = 4)
1,2,4-Trichlorobenzene	disk	> 2000	94.8	1.5 (n = 11)
	cartridge	> 2000	98.5	1.5 (n = 12)
Dodecane	disk	> 2000	97.9	3.0 (n = 11)
	cartridge	> 2000	63.3	4.1 (n = 12)

disk is preconditioned prior to processing the sample. Since preconditioning of the sorbent cartridge has minimal influence on analyte recovery or sample flow rate it is probable that this difference in properties is related to the wetting characteristics of the poly(tetrafluoroethylene) microfibrils used to stabilize the sorbent bed in the construction of the disk device.

The sampling characteristics of the cartridges are more variable than for the disks. This results from significant variation in sorbent packing density for the cartridges concomitantly yielding heterogeneous flow through the sorbent bed. For this reason we report data for single cartridges so that the vacuum could be adjusted to produce a known flow rate. It would be very difficult to obtain similar results with parallel sample processing because of the flow rate variations through individual cartridges. The analyte recovery for cartridges is dependent on the sample flow rate if the sample volume is greater than the breakthrough volume and also depends on the eluent flow rate when a fixed volume of eluting solvent is used to displace the analytes from the sorbent surface, as is normal practice. The disk devices exhibit little flow rate dependence on recovery over the normal accessible flow ranges.

The benefit of employing a drying step between the sample processing and analyte elution steps with either the disk or cartridge device is that it reduces the volume of water co-eluted from the sampling device. This may be desirable for further sample processing steps but does not generally result in an increase in analyte recovery. Most of the water is trapped within the support structures (frits in the case of the cartridges and glass frit support for the disks) as well as in the interparticle sorbent volume. This water is quickly removed by suction so that short drying times are adequate to remove most of the water. Water in the pore volume of the sorbent is presumably removed only slowly and provided that a water miscible eluting solvent is used in sufficient volume there is no evidence that the presence of the pore water influences the recovery of the analytes. If further drying is required it might be better to dry the eluent prior to concentration rather than to use extended drying time to dry the sampling devices by suction. Since the analytes are lost by evaporation from the sorbent surface during the drying step using suction the drying time should be adjusted based on the volatility of the analytes.

The optimized sampling conditions described in the experimental section are applicable to a wide range of neutral, polar semi-volatile compounds [23,25]. The choice of solvents and conditions, of course, must be sensibly related to the properties of individual analytes. The experimental conditions described here can not be considered universal but should prove adequate as a starting point for optimizing the recovery by solid-phase extraction of neutral analytes devoid of specific sorbent interactions. It has been our experience that the experimental parameters identified as critical factors affecting recovery in the above discussion remain the important factors when compounds of a more diverse structure are considered.

References

[1] C.F. Poole and S.K. Poole, Chromatography Today, Elsevier, Amsterdam, 1991, pp. 777–793.
[2] S.K. Poole, T.A. Dean, J.W. Oudsema and C.F. Poole, Anal. Chim. Acta, 236 (1990) 3.
[3] H.C. Hennion, Trends Anal. Chem., 10 (1991) 317.
[4] I. Liska, J. Krupcik and P.A. Leclercq, J. High Resolut. Chromatogr., 12 (1989) 577.
[5] R.D. McDowall, J. Chromatogr., 492 (1989) 3.
[6] K.C. Horne (Ed.), Sorbent Extraction Technology, Analytichem International, Harbor City, CA, 1985.
[7] D.R. Hagen, C.G. Markell, G. Schmitt and D.B. Blevins, Anal. Chim. Acta, 236 (1990) 157.
[8] C. Markell, D.F. Hagen and V.A. Bunnelle, LC–GC Mag., 9 (1991) 332.
[9] G.M. Hearne and D.O. Hall, Am. Lab., (1993) 28H.
[10] A. Kraut-Vass and J. Thoma, J. Chromatogr., 538 (1991) 233.
[11] E.R. Brouwer, H. Lingeman and U.A.Th. Brinkman, Chromatographia, 29 (1990) 415.
[12] E.R. Brouwer, D.J. Van Iperen, I. Liska, H. Lingeman and U.A.Th. Brinkman, Int. J. Environ. Anal. Chem., 47 (1992) 257.
[13] O. Evans, B.J. Jacobs and A.L. Cohen, Analyst, 116 (1991) 15.
[14] A.L. Howard and L.T. Taylor, J. Chromatogr. Sci., 30 (1992) 374.
[15] B.A. Tomkins, R. Merriweather, R.A. Jenkins and C.K. Bayne, J. Assoc. Off. Anal. Chem. Int., 75 (1992) 1091.

[16] T. McDonnell, J. Rosenfeld and A. Rais-Firouz, J. Chromatogr., 629 (1993) 41.
[17] D. Barcelo, G. Durand, V. Bouvot and M. Nielen, Environ. Sci. Technol., 27 (1993) 271.
[18] S. Chiron and D. Barcelo, J. Chromatogr., 645 (1993) 125.
[19] L. Schmidt, J.J. Sun, J.S. Fritz, D.F. Hagen, C.G. Markell and E.E. Wisted, J. Chromatogr., 641 (1993) 57.
[20] I.S. Dean, C.M. Davidson, D. Littlejohn and I. Brown, Analyst, 118 (1993) 1375.
[21] G.L. Lensmeyer, D.A. Wiebe and B.A. Dorsey, J. Chromatogr. Sci., 29 (1991) 444.
[22] W.P.N. Fernando, M.L. Larrivee and C.F. Poole, Anal. Chem., 65 (1993) 588.
[23] M.L. Larrivee and C.F. Poole, Anal. Chem., 66 (1994) 139.
[24] ANSYS (Irvine, CA), SPEC-NEWS, May 1993, Vol. 2, No. 1.
[25] K.D. Miller and C.F. Poole, J. High Resolut. Chromatogr., 17 (1994) 125.
[26] G.A. Junk and J.J. Richard, Anal. Chem., 60 (1988) 451.
[27] C. Carr and J.A. Riddick, Ind. Eng. Chem., 43 (1951) 692.

ELSEVIER

Analytica Chimica Acta 294 (1994) 127–134

ANALYTICA CHIMICA ACTA

Study of the influence of free dissolved amino acids on copper(II) adsorption/remobilization from inorganic fractions of marine sediments using a reversed-phase liquid chromatographic procedure

F. Baffi [a,*], M.C. Ianni [a], M. Ravera [b], E. Magi [a]

[a] *Istituto di Chimica Generale, Cattedra di Chimica Analitica, Università di Genova, Viale Benedetto XV 3, 16132 Genova, Italy*
[b] *ITIS A. Gastaldi, Via Milano, 16126 Genova, Italy*

Received 19th November 1993; revised manuscript received 14th March 1994

Abstract

A reversed-phase liquid chromatographic procedure for the determination of amino acids and copper(II)–amino acid complexes was improved and applied to studies dealing with adsorption and remobilization of copper from sediments in the presence of free and complexed amino acids. In particular, the adsorption by inorganic fractions of a marine sediment was investigated by means of batch equilibration experiments. The results indicate that two adsorption mechanisms, one due to electrostatic interaction and the other one based on hydrophobic characteristics of the considered species, are simultaneously possible. Scanning electron microscopy with electron probe microanalysis was utilized to provide further information.

Key words: Liquid chromatography; Amino acids; Copper; Metal complexes; Sediments

1. Introduction

Adsorption of metallic and organic species by marine sediments and by suspended particulate matter appears to be very important for biogeochemical cycles of trace metals in natural waters [1].

Adsorption behaviour of metal ions on solid phases has been subject of several studies [2–7], but only a small number concerned adsorption in the presence of ligands. In 1979 Elliot and Huang [8] reported a survey of earlier investigations on the influence of several chelating agents (including some amino acids) on the adsorption of various metallic ions by some oxides, in particular γ-Al_2O_3. They also report on results obtained for adsorption by γ-Al_2O_3 of Cu(II) complexes with nitrilotriacetic acid (NTA), glycine and aspartic acid. Later, the same authors [9] studied adsorption of metal–amino acid complexes by two different solids: γ-Al_2O_3, which is relatively hydrophilic, and activated carbon, which is hydrophobic. They also studied the adsorption of

* Corresponding author.

SSDI 0003-2670(94)00133-7

Cu(II) complexes with various ligands by several aluminosilicates with different Si/Al ratios, surface charge and ion-exchange characteristics [10].

The effects of amino acids on the adsorption behaviour of radioactive zinc in sea water using montmorillonite and cation-exchange resins as adsorbents have been studied by Isciyama et al. [11]. The results indicate that it is not possible to isolate a single adsorption mechanism.

Recently, a study on the influence of dissolved ligands and inorganic ions on Co(II) adsorption by silica gel has been published [12]. The silica gel–Co(II) system simply permits to apply the surface complexation model to the adsorption of trace metal ions on particulates in fresh waters. The theory of the surface complexation considers the adsorption sites on a solid as dissolved complex forming species [5], so that specific adsorption of metal ions on solid phase surfaces may be interpreted as a surface coordination reaction [13]. This model can be easily combined with the equilibrium model for dissolved species in aqueous solution [14] and it can predict the effects of anions and chelating ligands in solution on adsorption of metal ions on solid phases.

Finally, an investigation on the influence of a strong, adsorbed ligand, such as polyphosphate, on the distribution of metal ions on ferrihydrite was published by Lin and Benjamin [15].

The purpose of the present work is to study the adsorption of amino acids and their complexes, dissolved in simulated interstitial sea water, by inorganic fractions of marine sediments. The batch equilibration experiments were carried out by adding different solutions, containing amino acids or Cu(II)–amino acid complexes in sea water, to the sediment at the proper pH value for amino acids and complexes adsorption on the sediment studied here.

A reversed-phase liquid chromatographic (RPLC) procedure, optimized in our previous experiments [16–18], was used for amino acids and Cu–amino acid complexes determination. Scanning electron microscopy with electron beam probe microanalysis (SEM-EPMA) was also employed in order to verify the adsorption of copper by the sediment.

2. Experimental

2.1. Instrumentation

The LC system was a Bruker Quaternary Gradient LC-2300 and the data system was an LC-21 Epson QX 10 microcomputer with an FX-85 printer. The temperature control unit for the column was a Violet T55.

The post-column derivatization reaction was performed in a PTFE delay tube (Supelco), immersed in a thermostatic bath.

Amino acids were determined according to a previously described procedure [16,18]. Fractions were collected with a Frac-200 fraction collector (Pharmacia).

The detector was a Bruker LC-315 fluorescence monitor, with a diffraction grating monochromator, a xenon lamp and a 12-μl quartz flow cell. Excitation and emission wavelengths were 360 and 530 nm, respectively.

Copper determination was carried out by electrothermal atomization atomic absorption spectroscopy (ETA-AAS), using Zeeman-effect background correction (Varian Spectra A3000).

The scanning electron microscope was a Model ISI 40 from International Scientific Instruments.

2.2. Reagents and materials

Marine sediment samples were obtained from Dipartimento di Scienze della Terra, Cattedra di Sedimentologia, Università di Genova. The samples were collected offshore Imperia (Ligurian Sea) at a depth of 480 m, and classified as mud. The sediment was certified by x-ray powder diffractometric analysis with the following composition (wt.%): chlorite 12, mica 7, kaolin 10, quartz 22, K-feldspar 5, plagioclase 7, calcite 17, Mg-calcite 2, dolomite 5, amphibole 3, serpentine 10. After treatment with HNO_3 the average Si/Al ratio is about 3.5 (obtained by SEM-EPMA).

Coastal sea water samples were collected from the Ligurian Sea, filtered through 0.45-μm Millipore filters and stored at 4°C.

Glycine, DL-alanine, DL-serine, DL-phenylalanine and L-isoleucine (Serva), basic copper(II)

carbonate and methanol (Carlo Erba, RPE), 85% phosphoric acid and 30% sodium hydroxide Suprapur solutions and acetonitrile for chromatography (Merck), Fluoraldehyde (*o*-phthalaldehyde reagent solution) (Pierce) were used.

The samples and the eluents were prepared using water obtained from a Milli-Q system (Millipore) and filtered with a polycarbonate apparatus (Sartorius, Model SM 165.10) through 0.45-μm Millipore filters.

Sediment treatment was carried out in a PTFE container. Glass test tubes with glass caps were used for batch experiments. The glass material was checked for adsorption and release phenomena. All other containers were made of polyethylene.

2.3. Cleaning procedure

Containers, filtration apparatus, Millipore filters and micropipette tips were treated before use with hydrochloric acid (Carlo Erba, RPE), washed with 1,1,2-trifluoroethane (Carlo Erba, RPE) and stored in polyethylene bags. All chemical procedures were carried out in a laminar vertical flow hood and polyethylene gloves were used.

2.4. Sample preparation

The copper–amino acids complexes were prepared according to the procedure described by Hirson and Barsily [19]. Solid $CuCO_3 \cdot Cu(OH)_2 \cdot nH_2O$ was added, in excess, to a 10 mM solution of the amino acid at 50°C and shaken for a few minutes. After cooling and filtration the sample was prepared for batch experiments by 1 + 9 dilution with sea water.

When only amino acids were used for batch methods, the 10 mM solution was diluted with sea water just like the sample containing the complex.

2.5. Methods

The complete procedure is illustrated in the flow chart of Fig. 1.

Solid phase preparation

The sediment was treated with 8 M HNO_3 for 2 h at 95°C, rinsed with Milli-Q water for several times and subsequently conditioned in sea water (5 days) up to the pH value of 4.5–5, which is the optimum pH for the highest possible adsorption on aluminosilicates with an average Si/Al ratio of about 3.5 [10]. The sediment was then dried at 40°C.

Liquid phase preparation

Solutions in sea water were: ionic copper, 0.5×10^{-3} M; amino acids, 10^{-3} M; Cu(II)–amino acid complexes, 10^{-3} M amino acid and ca. 0.5×10^{-3} M Cu. The solutions were checked for cop-

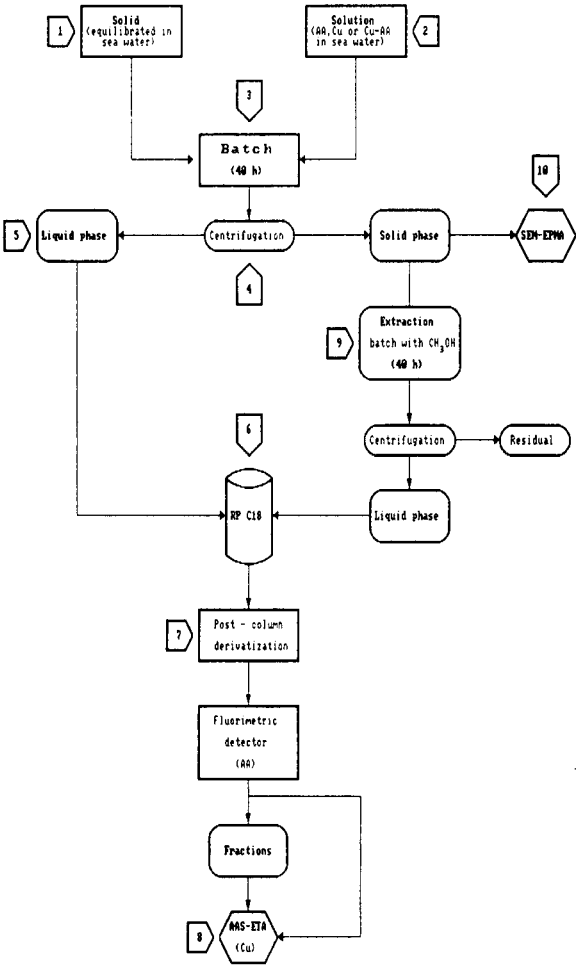

Fig. 1. Flow chart of the complete procedure

per and amino acid content before the batch experiments started.

Batch equilibration procedure

The solid phase to solution ratio was 6 g/15 ml, in order to simulate the interstitial water situation. Batch equilibration was performed at a constant temperature of 20°C (for 40 h) using a rotating shaker.

Centrifugation

The separation of liquid phase from the solid phase was carried out by centrifugation at 10000 rpm for 20 min (16700 *g*). The liquid was filtered through 0.45-μm Millipore filters.

Liquid phase

After batch equilibration the pH value was always 4.5–5.

Improved chromatographic procedure

The column used was a Superpac-Spherisorb ODS-2 (Dual-Bond), 250 mm × 4 mm i.d., with an average particle diameter of 5 μm (Pharmacia LKB). This column gave the best results in our previous experiments [17] when compared with other columns. During the present work we have verified that, after about 50 chromatographic runs, the column performance was seriously reduced (about 30%) due to lower coverage of silanolic groups by the reversed phase. For this reason we optimized a procedure for column presaturation with ionic copper that assures, in our case, a quantitative recovery of injected copper.

The presaturation procedure consists of injecting, under the same chromatographic conditions as for the analytical run, a sample containing ionic copper at a concentration of 60 mg/l. This is about two times the concentration of analytical samples, which will be injected after 30 min (the time, as verified by previous experiments, when the copper band reaches the end). Between the two injections the loop is rinsed with Milli-Q water.

The column temperature was 30°C.

Chromatographic runs were carried out under isocratic conditions. The eluent was 12.5 mM phosphate buffer (pH 7.2)–acetonitrile (90:10). The phosphate buffer was prepared by mixing 0.8

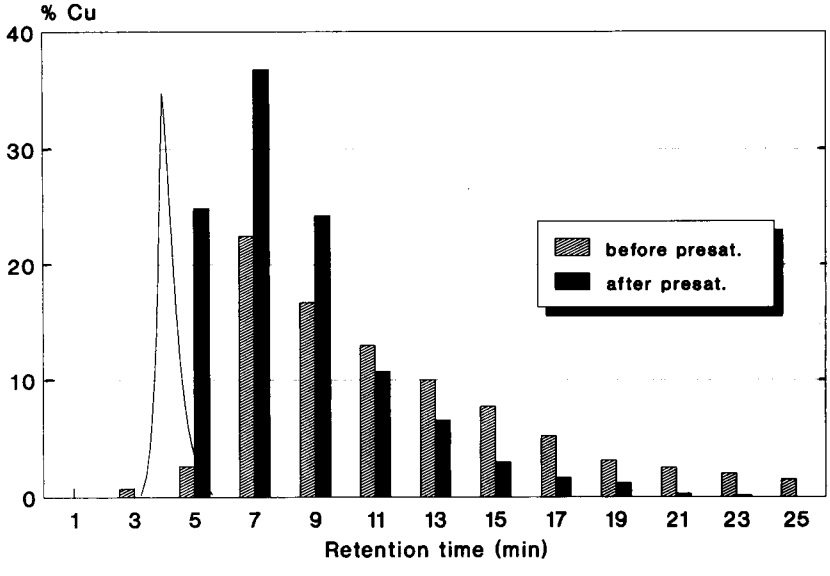

Fig. 2. Recovery of copper in the 1-ml fractions and chromatogram of alanine, obtained by injection of the copper–alanine complex on the column before and after presaturation. Copper total recovery: 86.7 and 102%, respectively; peak area recovery 100% in both cases.

ml of 85% H_3PO_4, and 2 ml of 30% NaOH. Purified Milli-Q water was added up to 1 l and the pH was adjusted, if necessary, to 7.2.

The flow rate and the sample volume injected were 1 ml min^{-1} and 20 μl, respectively.

An example is illustrated in Fig. 2. It is evident that, besides the improvement in the copper recovery yield, there is more overlap between the amino acid and Cu peaks. After a considerable number of chromatographic runs, copper will

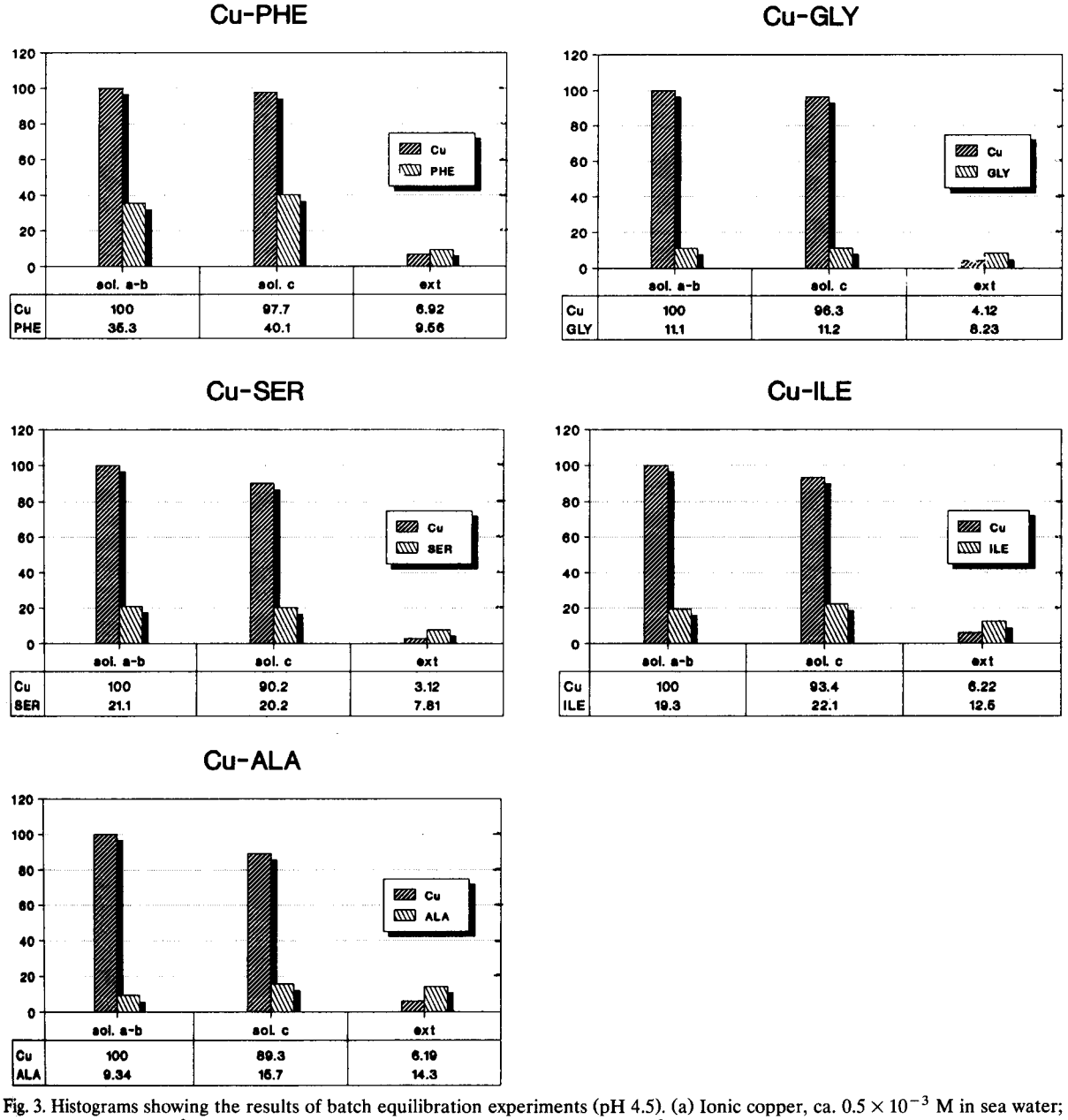

Fig. 3. Histograms showing the results of batch equilibration experiments (pH 4.5). (a) Ionic copper, ca. 0.5×10^{-3} M in sea water; (b) amino acid 1×10^{-3} M in sea water; (c) Cu(II)–amino acid complex 1×10^{-3} M in sea water; (ext) methanolic extract, 6 g of sediment per 15 ml of solution, 40 h in contact.

presumably be eluted as a low and very tailed band.

Post column derivatization procedure and copper determination in eluate

For the derivatization we used a previously optimized procedure [16], in which the flow rate for the derivatization reagent was 0.5 ml min^{-1} and the reaction coil temperature was 50°C. The copper content of the eluate fractions in the pre-batch runs, carried out to check the concentrations, and of the total eluate in the post-batch runs was determined by atomic absorption spectrometry.

Extraction procedure

After batch equilibration the residual sediment was extracted for 40 h with 15 ml of methanol in a rotating shaker. After centrifugation total copper and amino acid content were determined in the liquid phases.

SEM-EPMA

The residual sediment after batch equilibration was analysed by scanning electron microscopy. A small quantity (about 5 mg/l) of wet sediment was suspended in Milli-Q water and 2.5 ml were subsequently filtered through 0.45-μm Millipore filters (14 mm diam.). Doing so, every filter had the same number of deposited particles and was representative to a sufficient degree. Once dried, the filters were graphitized (the layer of graphite was about 160 μm thick) and the morphology and chemical analysis (about 25 particles) were microscopically determined.

3. Results and discussion

The results obtained are shown in Fig. 3 and refer to the total copper and amino acid content. It was not possible to determine copper in the eluate fractions of the post-batch runs because of the low concentrations, caused by the high degree of adsorption.

The pH after batch equilibration was about 4.5–5 for batch experiments with solutions "a" but, in spite of this value [8,9], ionic copper is completely adsorbed, probably because of the high sediment to sea water ratio. Positively charged species are attracted by those sediment fractions (which contain, for example, $Si-O^-$ groups) which can be negatively charged at this pH value. The amino acids are adsorbed in the following order: phenylalanine (PHE) > serine (SER) > isoleucine (ILE) > glycine (GLY) > alanine (ALA). These results are in good agreement with the studies on active carbon reported by Elliot and Huang [9], which state that PHE is much more retained than GLY and ALA. The most important factor seems to be the hydrophobicity of the considered species, as is shown in Fig. 4.

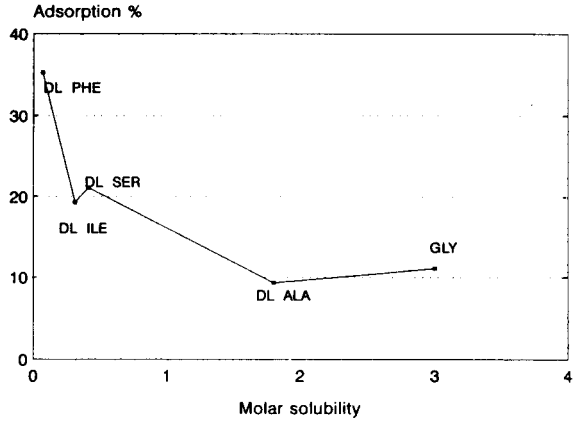

Fig. 4. Total concentration (%) of adsorbed amino acid versus molar solubility at 20°C [20].

During batch experiments with solutions "b" the Cu–AA complexes in sea water decompose in various charged or uncharged species because a pH drop occurs (pH after batch experiments is ca. 4.5).

Cu is always retained to a great extent (from 89.3% for Cu–ALA to 97.7% for Cu–PHE), but not completely as ionic copper. This result is in agreement with the surface complexation model, which predicts that the influence of ligands can lower the rate of adsorption of metal ions.

Presence of free amino acids prevents direct correlation between distribution of complexes and their stability constants, because free amino acids are also adsorbed. Cu is probably adsorbed in all its species. The total free and complexed amino acids are retained in different amounts and in the

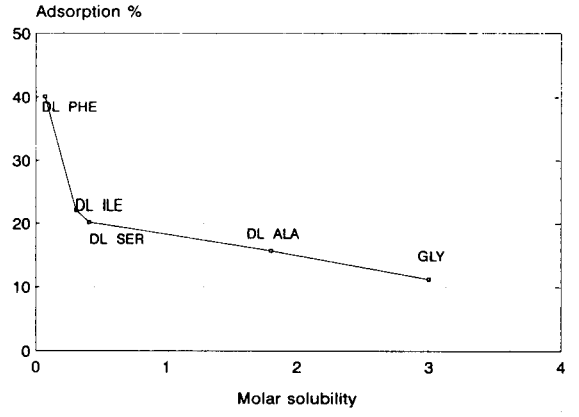

Fig. 5. Total concentration (%) of adsorbed amino acid versus molar solubility at 20°C [20].

following order: PHE > ILE > SER > ALA > GLY. For the PHE, ALA and GLY complexes this sequence is identical to the sequence obtained with active carbon [9]. Again it seems that hydrophobicity is the main retainment factor (see Fig. 5). Further tests must be performed in order to confirm this assumption.

Moreover, complexed ILE, PHE and ALA are retained in a greater amount in comparison with the free amino acids. The increase regarding ALA is also reported in the literature [11].

For batch experiments with solutions "c", the extracted amount of Cu is always much lower than the amount of retained Cu, as might be expected. The extracted amount of amino acids follows the sequence: ALA > ILE > PHE > GLY > SER. The AA to Cu ratio in the extracts is about 2, confirming hydrophobic adsorption of 1:2 complexes, except for Cu–PHE end Cu–SER. In the first case (ratio of 1.4) $CuPHE^+$ is probably present in the extract because of the presence of an aromatic ring.

3.1. SEM–EPMA determination

The SEM-EPMA tests were carried out in order to verify if the copper species are adsorbed on those particles that have an average Si/Al ratio of 3.5.

The analysis concerned three different kind of residual sediment from the batch experiments: a sediment which was in contact with sea water only, a sediment which was in contact with a solution containing ionic copper in sea water and a sediment which was in contact with a solution containing the Cu–ALA complex in sea water. In the first case the tests showed that the residue has the following composition: quartz, 20%; silica, 15%; aluminosilicate, 60% (which may contain Fe and Ti). Only few particles have a negligible Cu level.

The second residue showed several copper-containing particles with an average Si/Al atom ratio of 3.8.

Finally, the last sediment shows several particles (about the same number as in the previous case) with an average Si/Al atom ratio of about 2.6, which have higher copper levels (average value about 1,5%) than in the previous case.

In these tests, copper was always found to be associated to aluminosilicate particles.

Moreover, these results seem to be supported by a preliminary study on SEM-EPMA analysis of a plankton reference sample subjected to selective sequential extraction [21].

4. Conclusions

A chromatographic procedure, which was previously optimized and utilized for separation and determination of copper–amino acid complexes, was improved and extended with column presaturation, in order to apply the procedure to amino acids and copper–amino acid adsorption by marine sediment samples.

These studies have shown that, under the conditions described, the sediment simultaneously exhibits two different adsorption mechanisms involving the species considered. The former consists of a strong electrostatic attraction of positively charged species, while the latter, which is weaker, involves those species that have hydrophobic characteristics.

When only amino acids are present they can be retained with a hydrophobic adsorption mechanism, as pointed out by other authors [9,22]. When only ionic copper is present it is retained with an electrostatic attraction mechanism. How-

ever, when complexes are present too, the adsorption is determined by both mechanisms and there is a global remobilization of copper, which, in all cases, does not exceed 10% (except for PHE). In this case even the positively charged complex is highly hydrophobic.

The SEM-EPMA results pointed out that the aluminosilicate fraction of the sediment is involved in the adsorption mechanism.

Further batch equilibration experiments will be performed in order to confirm these results, in particular hydrophobic adsorption of the Cu(II)–amino acid complexes.

Acknowledgements

This work is a contribution of the Gruppo di Ricerca Oceanologica, Genova (GRO-G) and was financially supported by the Ministero della Università e della Ricerca Scientifica e Tecnologica (MURST), Fondi 40%, Italy.

References

[1] W. Salomons and U. Forstner, Metals in the Hydrocycle, Springer Verlag, Berlin, 1984, p. 63.
[2] J.A. Davis, R.O. James and J.O. Leckie, J. Colloid Interface Sci., 63 (1978) 480.
[3] J.A. Davis and J.O. Leckie, J. Colloid Interface Sci., 67 (1978) 90.
[4] C.P. Huang and W. Stumm, J. Colloid Interface Sci., 43 (1973) 409.
[5] H. Hohl and W. Stumm, J. Colloid Interface Sci., 55 (1976) 281.
[6] S. Osaki, T. Miyoshi, S. Sugihara and Y. Takashima, Sci. Total Environ., 99 (1990) 105.
[7] S. Osaki, T. Miyoshi, S. Sugihara and Y. Takashima, Sci. Total Environ., 99 (1990) 115.
[8] H.A. Elliot and C.P. Huang, J. Colloid Interface Sci., 70 (1979) 29.
[9] H.A. Elliot and C.P. Huang, Environ. Sci. Technol., 14 (1980) 87.
[10] H.A. Elliot and C.P. Huang, Water Res., 15 (1981) 849.
[11] T. Isciyama, T. Matsamura and Y. Takashima, Sci. Total Envir., 99 (1990) 93.
[12] S. Osaki, Y. Kuroki, S. Sugihara and Y. Takashima, Sci. Total Environ., 99 (1990) 93.
[13] H. Hohl, L. Sigg and W. Stumm, Particulates in Water, American Chemical Society, Washington, DC, 1980, p. 1.
[14] J. Westall, Particulates in Water, American Chemical Society, Washington, DC, 1980, p. 1.
[15] C.F. Lin and M.M. Benjamin, Water Res., 26 (1992) 397.
[16] F. Baffi, M.C. Ianni, A.M. Cardinale, E. Magi, R. Frache and M. Ravera, Anal. Chim. Acta, 260 (1992) 99.
[17] F.Baffi, M.C. Ianni, E. Magi and M. Ravera, Anal. Chim. Acta, 278 (1993) 83.
[18] F. Baffi, Int. J. Environ. Anal. Chem., 41 (1990) 173.
[19] B. Hirson and I. Barsily, Bull. Soc. Chim. Fr., (1957) 1336.
[20] J.P. Greenstein and M. Winitz, Chemistry of the Aminoacids, Wiley, New York, 1961, p. 532.
[21] F. Baffi, M.C. Ianni and M. Ravera, in preparation
[22] V. Zutic and J. Tomaic, Mar. Chem., 23 (1988) 51.

ELSEVIER

Analytica Chimica Acta 294 (1994) 135–143

ANALYTICA CHIMICA ACTA

Stationary phase effects on retention behavior of phenols in micellar liquid chromatography: Perfluorooctane vs. C_{18}

Shenyuan Yang, Morteza G. Khaledi *

Department of Chemistry, P.O. Box 8204, North Carolina State University, Raleigh, NC 27695, USA

Received 13th December 1993; revised manuscript received 24th February 1994

Abstract

The usefulness of fluorinated bonded stationary phases is further examined in micellar liquid chromatography (MLC) using cationic micellar eluents. The retention behavior of substituted phenols was investigated in MLC with both a Perfluorooctane (FO) column and a C_{18} column. It has been found that phenols with electron withdrawing groups (e.g., –CN, $-NO_2$ and –COR) have longer retention on the FO column than that on the C_{18} column. This might be due to the larger specific polar interactions between the solutes and the FO column. The functional group selectivity (τ) values of these polar substituents were significantly increased on the FO column. However, phenols with substituted hydrocarbons show shorter retention on the FO column than that on the C_{18} column. This may be due to the smaller hydrophobic interactions between hydrocarbon substituents and fluorocarbon stationary phase. The simultaneous enhancement of solvent strength and selectivity that has been reported in the SDS hybrid system was also observed in the C_{14}TAB hybrid system. This is due to the existence of the competing partitioning equilibria in MLC and because of the interactive nature of the two eluent parameters, micelle concentration and the volume fraction of organic solvents; both of which influence solvent strength and selectivity. The iterative regression strategy was used to optimize these two mobile phase parameters for a group of phenols using the FO column with the cationic micellar eluents. Excellent agreement was obtained between the observed and the predicated optimum chromatograms using only five initial experiments. This indicates that the easily predictable and highly reproducible retention behavior that has been reported in MLC systems with the alkyl bonded phases is also observed with fluorocarbon bonded phases and cationic micellar eluents.

Key words: Liquid chromatography; Micelles; Fluorinated bonded stationary phases; Stationary phase effects; Phenols

1. Introduction

Micellar liquid chromatography (MLC) has received much attention since it was first introduced by Armstrong and Henry in 1980 [1]. It has certain unique advantages, for example: capability of simultaneous separation of ionic and non-ionic compounds, reproducible and predictable retention behavior, and simultaneous enhancement of separation selectivity and solvent strength [2–8]. MLC has been recognized as a powerful

* Corresponding author.

SSDI 0003-2670(94)00130-E

alternative to ion pair chromatography (IPC) for the separation of charged compounds [9].

Perhaps the major shortcoming of MLC is its poor chromatographic efficiency. Several workers have suggested that the adsorption of monomer hydrocarbon surfactants on the alkyl bonded stationary phase in MLC contributes significantly to the additional band broadening as compared to that in conventional reversed-phase liquid chromatography (LC) with hydro-organic eluents. In general, the slow kinetics of mass transfer in both stationary phase and mobile phase have been recognized as the reasons behind the poor chromatographic efficiency [10–13]. Commonly, the use of secondary chemical equilibria in the reversed-phase LC system (such as ion pairing or micelle partitioning) provides enhanced selectivity at the expense of additional band broadening.

Alkyl bonded stationary phases have been used in nearly all of the MLC separations until now. Recently, the usefulness of fluorinated bonded stationary phases was examined in the anionic surfactant (SDS) based MLC system [14]. Higher efficiencies and different selectivities were observed by using a Flurooctyl (FO) column for both nonionic and ionic compounds as compared to those of a C_{18} column in MLC. The unique phenomenon of the simultaneous enhancement of solvent strength and selectivity that often occurs in the MLC systems with alkyl bonded stationary phases was also observed in the SDS based MLC system with the FO column. The iterative regression strategy [8,15] that was developed originally with the alkyl bonded phases in MLC was successfully utilized to optimize the concentration of surfactant (SDS) and the volume fraction of organic solvent (propan-1-ol) for a group of amino acids and small peptides with the FO column. Excellent agreement was obtained between the observed optimum chromatogram and the one predicted by the iterative regression strategy.

In this paper, the usefulness of fluorinated bonded stationary phases is further examined in the cationic surfactant (C_{14}TAB) based MLC system. The retention behavior of phenols with different functional groups was investigated in MLC with both a Flurooctyl (FO) column and a C_{18} column at the same mobile phase conditions. The influence of stationary phase on the functional group selectivity for the substituted phenols is studied.

2. Experimental

2.1. Chromatographic system

The chromatographic apparatus consisted of an HPLC pump (Model 400, Applied Biosystems, Foster city, CA) and a variable wavelength absorbance detector (Model 783A, Applied Biosystems) set at 254 nm for the test phenols. The LC system was controlled by the Chemresearch chromatographic data management system controller software (ISCO, Lincoln, NE) running on a PC-88 Turbo personal computer (IDS, Paramount, CA). A 5-μm particle size Flurooctyl (FO) column (E.S. Industries, Berlin, NJ) 250 × 4.6 mm and a 5-μm particle LiChroCart C_{18} column (Merck, Darmstadt) 12.5 cm × 4 mm were used. The columns were thermostated at 40°C by a water circulator bath (Lauda Model MT-6, Brinkmann Instruments, Westburry, NY). A silica precolumn was used to saturate the mobile phase with silicates and to protect the analytical column. Two 1.5-μm precolumn filters (Rainin Instruments) were placed between the silica precolumn and a VIGI injector (Valco, Houston, TX) and between the injector and the analytical column. The column dead times were measured from the injection point of water samples and the first deviation of the baseline.

2.2. Reagents

The stock solution of tetradecyltrimethylammonium bromide, C_{14}TAB (sigma), was prepared by dissolving the required amount of surfactant in doubly distilled, deionized water and was filtered through a 0.45-μm Nylon-66 membrane filter (Rainin Instruments). All the test solutes were obtained from Sigma. They are identified in Table 1. The sample solutions were prepared by diluting the stock solutions (5 mg/ml in methanol) with the mobile phase. The buffer concentration

Table 1
Stationary phase effect on retention (mobile phase: 0.12 M C_{14}TAB, 3% propan-2-ol, pH 7.0)

Compound	FO column		C_{18} column	
	k'	Elution order	k'	Elution order
(1) 4-Benzamidephenol	4.32	1	1.83	1
(2) 4-Hydroxybenzylcyanide	9.47	2	6.35	2
(3) Phenol	12.10	3	10.14	5
(4) 4-Fluorophenol	12.80	4	11.55	6
(5) 4-Hydroxyacetophenone	17.97	5	8.30	3
(6) 4-Hydroxydiphenylmethane	18.17	6	21.36	10
(7) 4-Hydroxybenzaldehyde	18.91	7	8.52	4
(8) 4-Isopropylphenol	19.42	8	21.69	11
(9) 4-*tert.*-Butylphenol	21.51	9	25.78	12
(10) 4-Nitrophenol	23.28	10	14.88	8
(11) 4-Hydroxypropiophenol	25.24	11	13.46	7
(12) 4-Hydroxybenzophenone	31.47	12	18.13	9

in the final solution was 0.050 M. After adding the required amount of organic solvents, propan-2-ol (Fisher Scientific, Pittsburgh, PA), the pH was adjusted to 7.00.

3. Results and discussion

Retention behavior of charged solutes in MLC separation can be affected by the type of stationary phase and mobile phase parameters such as type/concentration of organic solvent and surfactant, pH, ionic strength, and temperature. In this study, the effects of volume fraction of organic solvent (propan-2-ol) and concentration of surfactant on the chromatographic behavior of the test solutes (phenols) were examined by using a FO column and a C_{18} column; whereas, the other mobile phase conditions were kept constant. The stationary phase effect on functional group selectivity was studied. The usefulness of fluorinated bonded phases in the C_{14}TAB hybrid system was compared to that in the SDS hybrid system.

3.1. Retention behavior of phenols on both FO column and C_{18} column

Simultaneous enhancement of solvent strength and separation selectivity has been previously reported in the anionic surfactant (SDS) MLC system on both the FO column and the C_{18} column [7,14,16]. A similar behavior was also observed in the cationic surfactant (C_{14}TAB) MLC system for phenols on both the FO column and the C_{18} column.

In MLC systems, Eqs. 1 and 2 [7,14,16] describe the dependence of retention factor on the volume fraction of organic solvent and the micelle concentration, respectively.

$$\ln k' = -S\phi_{org} + \ln k'_o \quad (1)$$

$$1/k' = \{K_{mw}[M] + 1\}/(P_{sw}\Phi) \quad (2)$$

Where k' is the retention factor of a solute, ϕ_{org} is the volume fraction of the organic solvent, k'_o is the retention factor in a purely aqueous micellar mobile phase, S is the solvent strength parameter, [M] is the micelle concentration, Φ is the phase ratio, K_{mw} is the binding constant of solute to micelles and P_{sw} is the partition coefficient of a compound from mobile phase into stationary phase.

According to Eqs. 1 and 2, increasing solvent strength in MLC through an increase in the volume fraction of an organic solvent or an increase in the micelle concentration leads to a decrease in retention. This effect has been reported for the SDS micellar eluents. Figs. 1 and 2 show that Eqs. 1 and 2 are also valid for the cationic (C_{14}TAB) micellar mobile phases with both the FO column and the C_{18} column for a group of substituted phenols as test compounds. The pro-

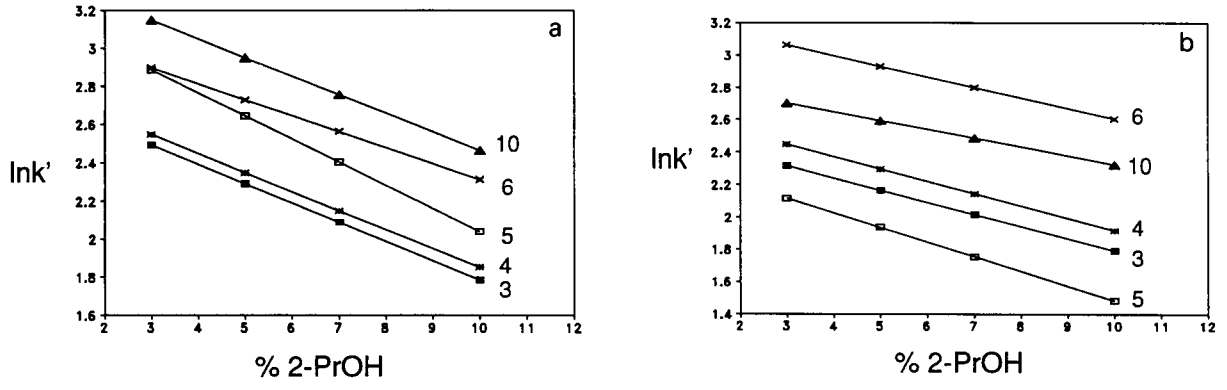

Fig. 1. The stationary phase effect on the retention behavior of phenols with the change of volume fraction of propan-2-ol (0.12 M C_{14}TAB). (a) FO column, (b) C_{18} column.

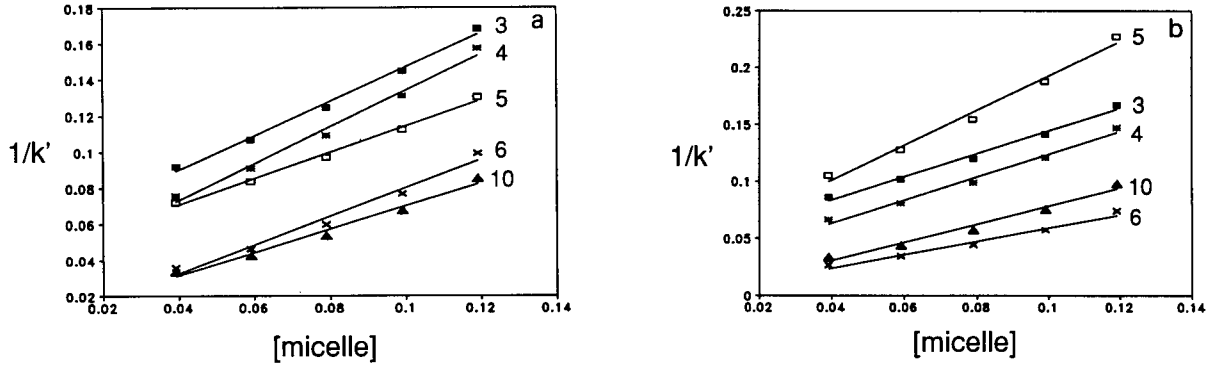

Fig. 2. The stationary phase effect on the retention behavior of phenols with the change of micelle concentration (10% propan-2-ol). (a) FO column, (b) C_{18} column.

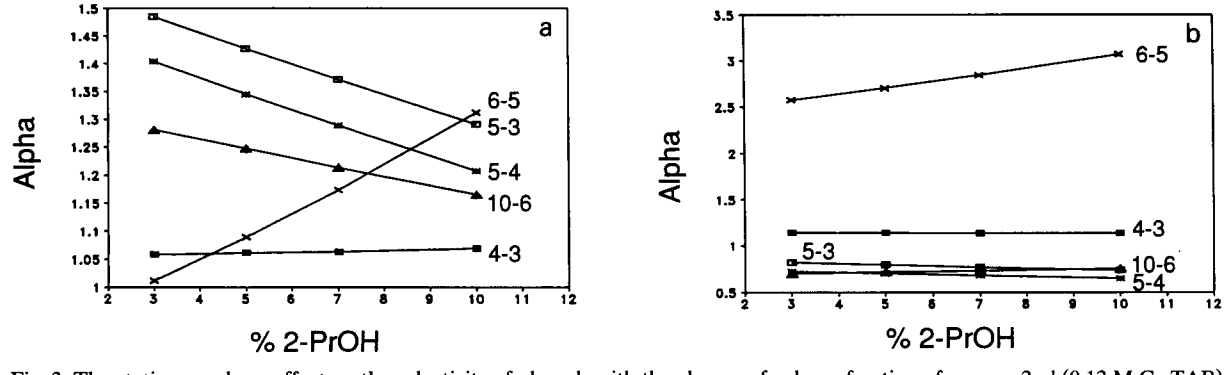

Fig. 3. The stationary phase effect on the selectivity of phenols with the change of volume fraction of propan-2-ol (0.12 M C_{14}TAB). (a) FO column, (b) C_{18} column.

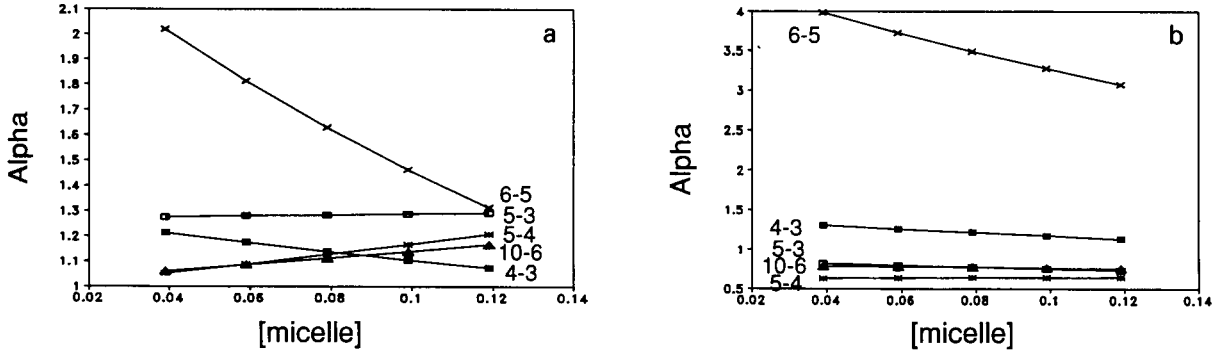

Fig. 4. The stationary phase effect on the selectivity (alpha) of phenols with the change of micelle concentration (10% propan-2-ol). (a) FO column, (b) C_{18} column.

nounced effect of the type of stationary phase on the retention behavior is quite evident in Fig. 1a and b as well as Fig. 2a and b. Different elution order and selectivity are observed on the C_{18} and FO columns.

Eqs. 3 and 4 describe the changes in selectivity between compounds 1 and 2 as a function of the volume fraction of organic solvent or the micelle concentration.

$$\ln \alpha = -(S_2 - S_1)\phi_{org} + (\ln k'_{o,2} - \ln k'_{o,1}) \quad (3)$$

$$\alpha = \frac{(\alpha_{sw})\{[M] + 1/K_{mw,1}\}}{(\alpha_{mw})\{[M] + 1/K_{mw,2}\}} \quad (4)$$

Where α is selectivity between solutes 1 and 2 and defined as $\alpha = k'_2/k'_1$, α_{sw} is the stationary phase partitioning selectivity ($P_{sw,2}/P_{sw,1}$) and α_{mw} is the selectivity of binding to (or partitioning into) micelles ($K_{mw,2}/K_{mw,1}$).

The experimental results for a group of phenols are illustrated in Fig. 3 and Fig. 4 with both the FO column and the C_{18} column. Obviously, the significant selectivity difference should be attributed to the stationary phase effect.

The significantly different retention behavior of phenols on FO column and C_{18} column is further evident in the plot of k'_o on the C_{18} column vs. k'_o on the FO column for all the test solutes as shown in Fig. 5. The correlation coefficient (r^2) of the linear regression was 0.3025 for the set of 12 compounds. Obviously, there are two subgroups of test compounds. The first subgroup consists of mostly alkyl substituted phenols which prefer the C_{18} column ($k'_o(C_{18}) = 1.84k'_o(FO) - 17.16$, $r^2 = 0.9976$, compounds 2, 3, 4, 6, 8 and 9). However, the second subgroup of phenols favor the FO column ($k'_o(C_{18}) = 0.57k'_o(FO) - 2.45$, $r^2 = 0.9488$) and they have polar substituents such as carbonyl or nitro (compounds 1, 5, 7, 10, 11 and 12). This may be due to the smaller hydrophobic interactions between the hydrocarbon substituents and the fluorocarbon stationary phase and the larger specific polar interactions between the polar functional groups and the fluorocarbon stationary phase.

It was previously shown that there is no direct relation between solvent strength and selectivity in the anionic surfactant (SDS) based MLC system [7,9,14,16]. This is in contrast to many situations in RPLC and IPC systems where solvent

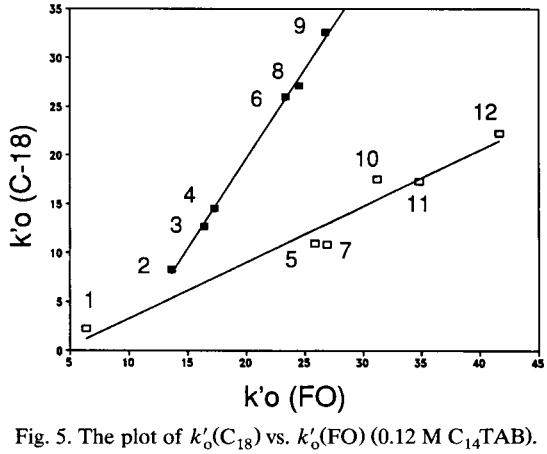

Fig. 5. The plot of $k'_o(C_{18})$ vs. $k'_o(FO)$ (0.12 M $C_{14}TAB$).

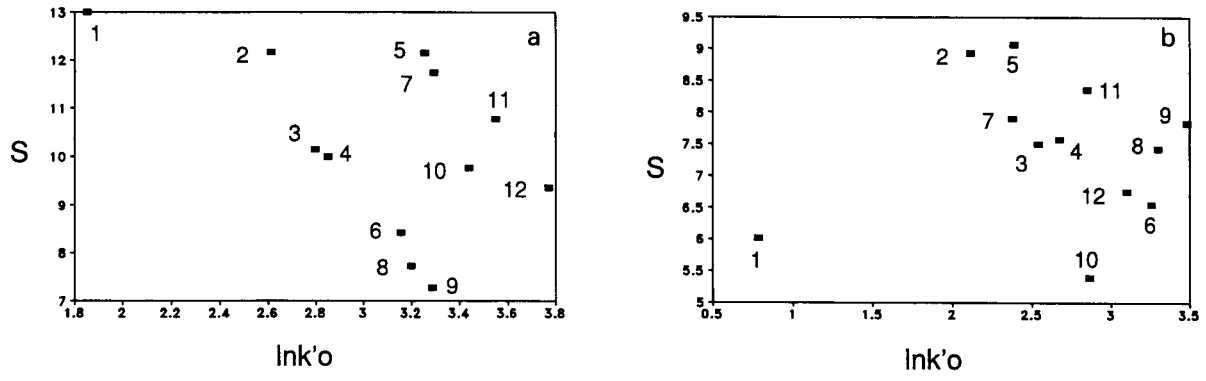

Fig. 6. The stationary phase effect on the S vs. ln k'_o plot (0.12 M C_{14}TAB). (a) FO column, (b) C_{18} column.

strength and selectivity are inversely related because of the direct relationship between solvent strength parameter (S) and retention (ln k'_o, the intercept of Eq. 1) [7,9,17]. In an MLC system, the S values for different compounds would depend on the extent of their interactions with micelles; i.e., S values are no longer linearly related to ln k'_o [7,9,14,16]. This is also observed in the C_{14}TAB based MLC systems with both the FO column and the C_{18} column for phenols as shown in Fig. 6a and b. The overall S vs. ln k'_o patterns as shown in Fig. 6a and b are again very

Table 2
Stationary phase effect on the free energy transfer of functional group

Functional group, FO column	$\Delta\Delta G$ (kJ/mol) [a]			
	5% propan-2-ol\[C_{14}TAB]		0.08 M C_{14}TAB	
	0.04 M	0.12 M	3% 2-PrOH	10% 2-PrOH
-CO-NH_2	3.068	2.831	3.142	3.639
-CN	0.794	0.745	0.714	1.174
-CO-CH_3	−1.114	−0.925	−1.072	−0.647
-CO-H	−1.342	−1.078	−1.252	−0.933
-NO_2	−2.283	−1.722	−1.993	−2.192
-CO-CH_2CH_3	−2.398	−1.880	−2.156	−2.023
-CO-C_6H_5	−3.233	−2.528	−2.861	−3.132
-F	−0.409	−0.154	−0.276	−0.339
-CH_2-C_6H_5	−1.834	−1.147	−1.447	−1.916
-$CH(CH_3)_2$	−1.859	−1.356	−1.547	−2.057
-$C(CH_3)_3$	−2.146	−1.647	−1.822	−2.415
Functional group, C_{18} column				
-CO-NH_2	4.753	4.377	4.349	4.448
-CN	1.395	1.295	1.166	1.618
-CO-CH_3	0.297	0.600	0.289	0.660
-CO-H	−0.087	0.476	0.061	0.243
-NO_2	−0.542	−1.107	−1.615	−1.916
-CO-CH_2CH_3	−1.692	−0.693	−1.040	−0.951
-CO-C_6H_5	−0.042	−1.550	−1.975	−2.281
-F	−0.649	−0.334	−0.470	−0.507
-CH_2-C_6C_5	−2.775	−1.986	−2.109	−2.594
-$CH(CH_3)_2$	−2.525	−1.982	−2.039	−2.353
-$C(CH_3)_3$	−2.938	−2.410	−2.458	−2.736

[a] The free energy of transfer ($\Delta\Delta G$) is defined as $\Delta\Delta G = -RT \ln \tau$ (τ is the *para*-substituted functional group selectivity).

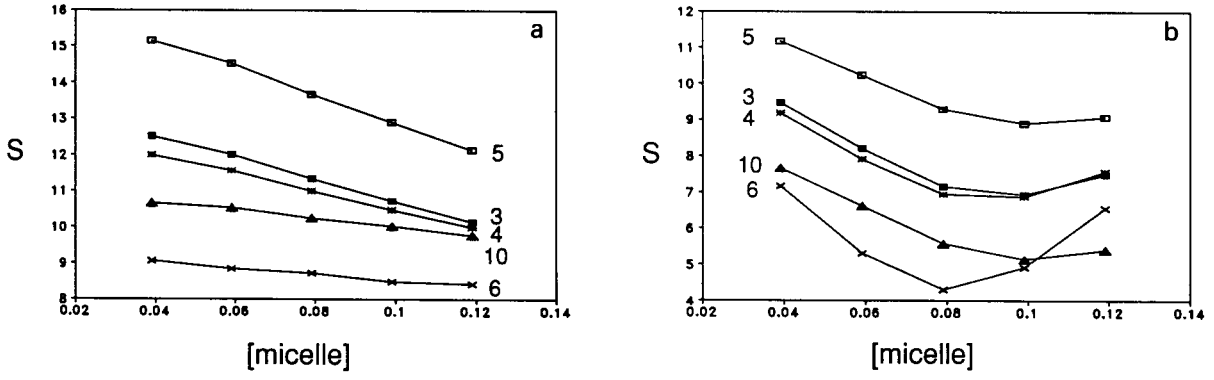

Fig. 7. The stationary phase effect on the solvent strength parameter (S) with the change of micelle concentration. (a) FO column, (b) C_{18} column.

different due to the stationary phase effect, which may be part of the reason behind the significant differences in retention and selectivity behaviors.

The effect of C_{14}TAB concentration on solvent strength parameter (S) of phenols with both the FO column and the C_{18} column is illustrated in Fig. 7a and b. The S values decrease with the increase in CTAB concentration (with the exception of high C_{14}TAB concentration with the C_{18} column). Note that S is a measure of retention sensitivity towards changes in the organic modifier concentration. The dependence of S on micelle concentration is an indication of the influence of micelles on the role of organic modifiers in MLC. It is quite interesting that in MLC, changing micelle concentration at a constant organic modifier composition would influence the chromatographic strength of the organic modifier. A similar behavior has been observed in the anionic surfactant (SDS) based C_{18} MLC system [16]. This is due to the competing partitioning equilibria and the characteristics of micelles acting as organized media.

3.2. Stationary phase effect on functional group selectivity

The retention factor and the elution order of 12 phenols were examined on both the FO column and the C_{18} column at the same mobile phase conditions. The results are listed in Table 1. It is obvious that phenols with electron withdrawing groups (e.g., -CN, $-NO_2$, -COR) have longer retention factors on the FO column than those on the C_{18} column. However, lower retention was observed for alkyl substituted phenols on the FO column as compared to that on the C_{18} column.

Stationary phase effect on retention behavior of phenols was further examined by investigating the functional group selectivity (τ), which is defined as the ratio of capacity factors of the substituted phenols to that of phenol, i.e., k'(PO–R)/k'(PO). Note that the free energy of transfer of a functional group from the mobile phase to the stationary phase is directly related to the group selectivity as: $\Delta\Delta G = -RT \ln \tau$. Table 2 illustrates the influence of surfactant concentration on the free energy of transfer of the *para*-substituted functional groups with different stationary phases (FO vs. C_{18}). It is clear that electron withdrawing groups have stronger interactions with the FO column than those with the C_{18} column. The reversed results were obtained for phenols with substituted hydrocarbons, i.e., they have weaker interactions with the FO column than those with the C_{18} column. These are consistent to the conventional hydro-organic RPLC system with these two columns [17–19].

3.3. Optimization of separation

The iterative regression (IR) optimization design [8,15] was used to optimize the separation of

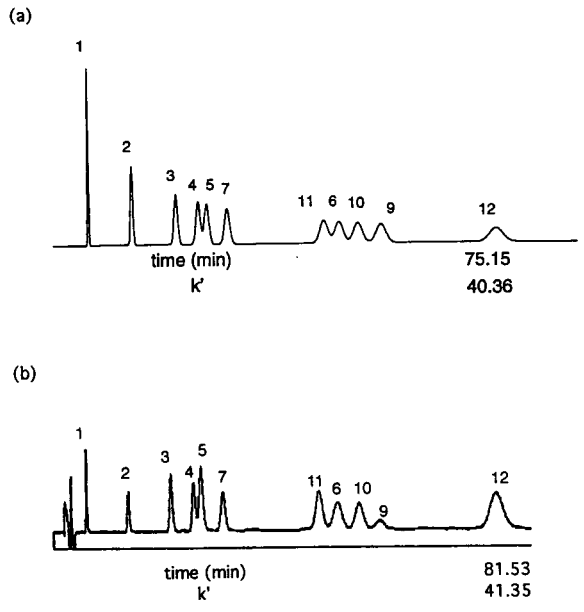

Fig. 8. The predicted (a) and observed (b) chromatograms on the 25 cm FO column at the optimum mobile phase composition (10% propan-2-ol, 0.047 M C_{14}TAB) for 11 phenols.

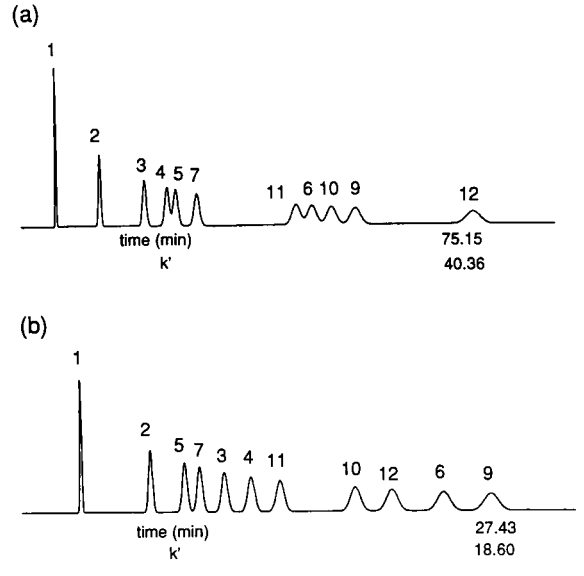

Fig. 9. The stationary phase effect on the predicted optimum separation of eleven phenols. $N = 4500$, (a) 25 cm FO column, 10% propan-2-ol, 0.047 M C_{14}TAB, (b) 25 cm C_{18} column, 7.9% propan-2-ol, 0.11 M C_{14}TAB.

11 phenols in the MLC system with CTAB–propanol eluents and the FO column. Fig. 8 shows an excellent agreement between the predicted and the observed chromatograms under optimum conditions. We have previously reported similar results using a C_{18} column [8]. These results indicate that the retention patterns in MLC with both fluorinated and alkyl bonded stationary phases are easily predictable and highly reproducible. Note that the IR experimental design for the optimization of the two important parameters, the concentration of surfactant (C_{14}TAB) and the volume fraction of organic solvent (propan-2-ol), was based on only five initial experiments, four at the corners of a square and one at the center [8,14]. The stationary phase effect on the optimized separation of 11 phenols is shown in Fig. 9. Again, the stationary phase has significant effect on retention behavior and selectivity.

4. Conclusions

The stationary phase effect (FO vs. C_{18}) on retention behavior of phenols in the C_{14}TAB based MLC system was investigated. It was found that the stationary phase in MLC has a significant impact on the retention behavior of test solutes. The retention factors and elution order of phenols were found to be very different with a FO column and a C_{18} column because of the increased polar interactions and the decreased hydrophobic interactions between the solutes and the flurooctyl phase as compared to those with the C_{18} phase. Further studies on the effect of stationary phase on the retention behavior of different compounds and the mechanism of retention with different stationary phases in MLC are needed.

Acknowledgments

We thank the US National Institutes of Health for the support of this work from a grant to North Carolina State University (First Award GM 38738).

References

[1] D.W. Armstrong and S.J. Henry, J. Liq. Chromatogr., 3 (1980) 657.
[2] L.J. Cline Love, J.G. Habarta and J.G. Dorsey, Anal. Chem., 56 (1984) 1132A.
[3] D.W. Armstrong, Sep. Purif. Methods, 14 (1985) 213.
[4] J.G. Dorsey, Adv. Chromatogr., 27 (1987) 167.
[5] W.L. Hinze, in W.L. Hinze and D.W. Armstrong (Eds.), Ordered Media in Chemical Separation, ACS Symposium Series 324, American Chemical Society, Washington, DC, 1987, Chap. 1, p. 2.
[6] M.G. Khaledi, Trends Anal. Chem., 7 (1988) 293.
[7] M.G. Khaledi, J.K. Strasters, A.H. Rodgers and E.D. Breyer, Anal. Chem., 62 (1990) 130.
[8] J.K. Strasters, E.D. Breyer, A.H. Rodgers and M.G. Khaledi, J. Chromatogr., 511 (1990) 17.
[9] A.S. Kord and M.G. Khaledi, Anal. Chem., 64 (1992) 1901.
[10] J.G. Dorsey, M. DeEchegaray and J.S. Landy, Anal. Chem., 55 (1983) 924.
[11] D.W. Armstrong, J.J. Ward and A. Berthod, Anal. Chem., 58 (1986) 579.
[12] A. Berthod, M.F. Borgerding and W.L. Hinze, J. Chromatogr., 556 (1991) 263.
[13] P. Yarmchuk, R. Weinberger, R.F. Hirsch and L.J. Cline love, J. Chromatogr., 47 (1984) 283.
[14] S. Yang, L.F.R. Kruk and M.G. Khaledi, J. Chromatogr., 664 (1994) 1.
[15] J.K. Strasters, S.-T. Kim and M.G. Khaledi, J. Chromatogr., 586 (1991) 221.
[16] A.S. Kord and M.G. Khaledi, Anal. Chem., 64 (1992) 1894.
[17] P. Varughes, M.E. Gangoda and R.K. Gilpin, J. Chromatogr. Sci., 26 (1988) 401.
[18] P.C. Sadek and P.W. Carr, J. Chromatogr., 288 (1984) 25.
[19] N.D. Danielson, L.G. Beaver and J. Wangsa, J. Chromatogr., 544 (1991) 187.

ELSEVIER

Analytica Chimica Acta 294 (1994) 145–153

ANALYTICA CHIMICA ACTA

Complex equilibria in capillary zone electrophoresis and their use for the separation of rare earth metal ions [1]

C. Vogt *, S. Conradi

Department of Chemistry, Analytical Division, University of Leipzig, Linnéstrasse 3, 04103 Leipzig, Germany

Received 29th November 1993

Abstract

The separation of lanthanides by capillary zone electrophoresis is carried out by addition of a complex forming agent to the separation buffer, thus generating charge and mobility differences between the species. The choice of a suitable ligand and especially the precalculation of the optimum ligand concentration is possible if the stability constants of the complexes are known. In this paper the relation between the calculated concentrations and the quality of separation at these concentrations is demonstrated. Furthermore, the influence of pH on the separation with hydroxyisobutyric acid is investigated as an example.

Key words: Electrophoresis; Complex equilibria; Lanthanides

1. Introduction

Now capillary electrophoresis has become available as a routine technique since a few years, the possibility to separate metal ion mixtures has increased. This technique offers essential improvements to the analysis of metal ions or metal containing compounds under relatively simple conditions because the separation efficiency of this method is extremely high, with ample possibilities of buffer modification. One of the problems observed during the electrophoretic separation of metal ions is caused by the nearly identical electrophoretic mobilities of the hydrated metal ions due to equal charges and similar radii. To achieve a separation of such mixtures it is necessary to introduce additional chemical interactions into the separation system. In this way complex forming equilibria or the formation of host–guest complexes can be used to modify the mobilities of different metal ions to a discriminating extent. Depending on the spectroscopic properties of the ligand, direct or indirect detection is used. Saitoh et al. [1] separated metal chelates of 4-(2-pyridylazo)resorcin by micellar electrokinetic chromatography (MECC) with direct UV detection. The same method is employed for metal β-diketonato complexes [2]. Another example is the direct UV or fluorescence detection of the complexation of metals with 8-hydroxyquinoline-5-sulfonic acid [3,4]. Indirect detection is used

* Corresponding author.

[1] Dedicated to the 60th birthday of our teacher Prof. Dr. G. Werner.

SSDI 0003-2670(94)00126-7

when neither the complex nor the ligand are UV-active. Weston et al. [5,6] reported on the separation of metals by complexation with α-hydroxyisobutyric acid (α-HIBA), oxalate and citrate in different UV-active buffer systems. Bächmann et al. [7] employed crown ethers for the separation of alkali and alkaline earth metals. Therefore, capillary electrophoresis offers many possibilities for the separation of metal ions using mobility modification of the ions with complexation during the sample preparation step or the separation process itself.

Separation of rare earth elements is a well-known example because of their very similar chemical and physico-chemical behaviour. Jokl et al. [8] demonstrated in 1966 that the separation of lanthanide mixtures by paper electrophoresis is possible when hydroxyamino acids are added to the buffer. In further publications hydroxycarboxylic acids [9,10] and aminopolycarboxylic acids [11,12] are used for the complexation of metal ions. Foret et al. [13] reported the separation of all lanthanides by capillary zone electrophoresis with α-HIBA as complexing agent.

In this paper a possible prediction method for the optimum ligand concentration during the capillary electrophoretic separation using the complex forming constants of the rare earth elements is demonstrated.

2. Experimental

All measurements were performed using the P/ACE 2000 capillary electrophoresis system of Beckman (Palo Alto, CA). Indirect detection was carried out at 214 nm. Untreated polyimide-clad fused-silica capillaries of different lengths (30–37 cm and 40–47 cm) and internal diameters (75 μm and 100 μm), obtained from CS-chromatographie Service (Langerwehe), were used.

All chemicals were of analytical-reagent grade. Creatinine was purchased from Serva (Heidelberg), α-hydroxyisobutyric acid was obtained from Riedel-de Häen (Seelze) and lactic acid from Laborchemie (Apolda). The lanthanide nitrate standard solutions were prepared from the nitrates of La, Ce, Pr, Sm, Eu, Gd, Tb, Dy and Er, and the oxides of Nd, Ho, Tm and Yb with nitric acid and triply distilled water from Laborchemie.

For the electrophoretic separation 30 mM creatinine buffer with the appropriate concentrations of the ligands α-HIBA, lactate and acetate in triply distilled water were applied. The pH of the buffer was adjusted with HCl. All standard metal solutions were 1×10^{-4} M. The injection was performed by pressure. For the optimization of the pH and the ligand concentration a mixture of three lanthanides (lanthanum, samarium and dysprosium) was chosen. All other measurements were carried out with a mixture of the thirteen rare earth elements mentioned above. The electroosmotic velocity was measured by means of the UV active β-naphthol.

3. Theory

For the rare earth ions only slight differences in the electrophoretic mobilities of the metal ions (M^{3+}) are to be expected because of the equal charge and the minor differences in ionic radii of the stable oxidation level +3 (from 72.3×10^{-5} $cm^2\ V^{-1}\ s^{-1}$ for La^{3+} to 67.5×10^{-5} $cm^2\ V^{-1}\ s^{-1}$ for Yb^{3+}), as shown in Fig. 1. The differences in the mobilities in a mixture of rare earth metal ions are not sufficient for an electrophoretic separation. A modification of the mobilities by the interaction of the metal ions with complex forming agents is possible, thus generat-

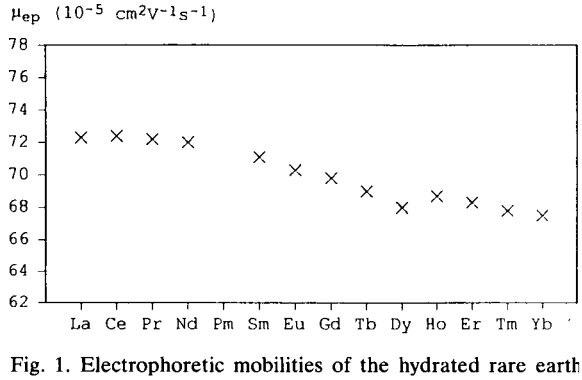

Fig. 1. Electrophoretic mobilities of the hydrated rare earth ions [14].

ing mobility differences between the species which are high enough for the separation.

By addition of a monovalent ligand to the separation buffer the formation of the following complexes is possible:

$$M^{3+} + L^- \rightleftharpoons ML^{2+}$$

$$\beta_1 = \frac{[ML^{2+}]}{[M^{3+}][L^-]} \quad (1)$$

$$M^{3+} + 2L^- \rightleftharpoons ML_2^+$$

$$\beta_2 = \frac{[ML_2^+]}{[M^{3+}][L^-]^2} \quad (2)$$

$$M^{3+} + 3L^- \rightleftharpoons ML_3$$

$$\beta_3 = \frac{[ML_3]}{[M^{3+}][L^-]^3} \quad (3)$$

$$M^{3+} + 4L^- \rightleftharpoons ML_4^-$$

$$\beta_4 = \frac{[ML_4^-]}{[M^{3+}][L^-]^4} \quad (4)$$

Suitable ligands for the complexation often possess acidic and sometimes basic properties. Therefore it has to be taken into consideration that they are subject to protolysis in aqueous solution, e.g.:

$$HL \rightleftharpoons H^+ + L^-$$

$$K_s = \frac{[H^+][L^-]}{[HL]} \quad (5)$$

The concentration of free ligand L^- is determined by:

$$K_s = \frac{[H^+][L^-]}{c_s - [L^-]}$$

and

$$[L^-] = \frac{K_s c_s}{[H^+] + K_s} \quad (6)$$

where c_s is the total ligand concentration. In solution the complexes mentioned in the Eqs. 1–4 are existing in mutual equilibrium caused by stepwise complex formation and moderate stability constants. Due to the fast equilibration between the different complexes it is possible to describe the system by a single complex $ML_{\bar{n}}^{(3-\bar{n})+}$ with the number $\bar{n}$ of ligands, which is equivalent to the average degree of complexation [15]. This degree can be calculated as follows:

$$\bar{n} = \frac{[ML^{2+}] + 2[ML_2^+] + 3[ML_3] + 4[ML_4^-]}{[M^{3+}] + [ML^{2+}] + [ML_2^+] + [ML_3] + [ML_4^-]} \quad (7)$$

$$\bar{n} = \frac{\beta_1[L^-] + 2\beta_2[L^-]^2 + 3\beta_3[L^-]^3 + 4\beta_4[L^-]^4}{1 + \beta_1[L^-] + \beta_2[L^-]^2 + \beta_3[L^-]^3 + \beta_4[L^-]^4} \quad (8)$$

Eq. 8 shows that the average degree of complexation depends only on the concentration of free ligand $[L^-]$, which is variable by the total concentration c_s of ligand or, if c_s is constant, by variation of the pH of the buffer.

If the stability constants of the complexes of different metals with the same ligand are known, it is possible to precalculate the optimum ligand concentration in the separation buffer by means of the average degree of complexation $\bar{n}$. The optimum ligand concentration for the electrophoretic separation is characterized by the highest mobility differences of the metal complexes and with the highest resolution. With increasing $\bar{n}$ the positive charge of the metal complex decreases. Maximum differences of the average degree of complexation $\bar{n}$ and thereby of the gross charges of two metal ions should make the best separation of this two metal ions available.

The mobility (μ) of an ion in capillary electrophoresis is influenced by both electrophoretic (μ_{ep}) and electroosmotic (μ_{eo}) parameters.

$$\mu = \mu_{eo} + \mu_{ep}$$

and

$$\mu_{ep} = \frac{Ls}{tU} - \mu_{eo} \quad (9)$$

where L is the overall length of the capillary, s is the capillary length to the detector and U is the voltage. If a complex forming equilibrium exists it is possible to calculate the electrophoretic mobility from the mobilities of the different complexes and their proportion in the equilibrium.

$$\mu = \mu_{eo} + x_{M^{3+}}\mu_{M^{3+}} + x_{ML^{2+}}\mu_{ML^{2+}} + x_{ML_2^+}\mu_{ML_2^+} + x_{ML_3}\mu_{ML_3} - x_{ML_4^-}\mu_{ML_4^-} \quad (10)$$

The term $x_{ML_3}\mu_{ML_3}$ in this equation can be cancelled because the electrophoretic mobility of

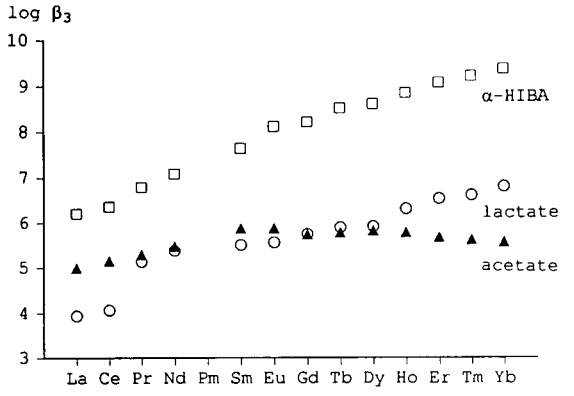

Fig. 2. Overall stability constants (log β_3) of the rare earth complexes [14,16].

the uncharged complex ML_3 is zero. The molar fractions x_i can be expressed in dependence on the total concentration c_0:

$$x_{M^{3+}} = \frac{[M^{3+}]}{c_0}, \quad x_{ML^{2+}} = \frac{[ML^{2+}]}{c_0}, \ldots$$

$$c_0 = [M^{3+}] + [ML^{2+}] + [ML_2^+] + [ML_3] + [ML_4^-] \quad (11)$$

After combining Eqs. 1–4 the following expression for the total concentration c_0 results:

$$c_0 = [M^{3+}]\left(1 + \beta_1[L^-] + \beta_2[L^-]^2 + \beta_3[L^-]^3 + \beta_4[L^-]^4\right) = [M^{3+}]\sum \quad (12)$$

The electrophoretic mobility of the complexed metal ion can be determined by the migration time of the complex at a constant ligand concentration under consideration of the electroosmotic velocity (Eq. 13b).

$$\mu = \mu_{eo} + \frac{1}{\sum}\mu_{M^{3+}}\frac{\beta_1[L^-]}{\sum}\mu_{ML^{2+}} + \frac{\beta_2[L^-]^2}{\sum}\mu_{ML_2^+} - \frac{\beta_4[L^-]^4}{\sum}\mu_{ML_4^-} \quad (13a)$$

$$\mu_{ep} = \mu - \mu_{eo} = \frac{1}{\sum}\left(\mu_{M^{3+}} + \beta_1[L^-]\mu_{ML^{2+}} + \beta_2[L^-]^2\mu_{ML_2^+} - \beta_4[L^-]^4\mu_{ML_4^-}\right) \quad (13b)$$

4. Results and discussion

In this paper three ligands, α-HIBA, lactate and acetate, were chosen for complexation measurements. Fig. 2 shows the stability constants (log β_3) of all rare earth elements with these ligands taken from the literature [14,16].

For acetate, only ML_3 complexes are known. The stability constants only show slight differences with a maximum for samarium. Therefore a good separation should not be expected. Both lactate and α-HIBA form ML_4^- complexes with the heavier lanthanides (starting from samarium) and these ligands possess higher differences in the stability constants, especially the HIB^- complexes. A separation with capillary electrophoresis should be possible by complexation with these ligands.

In this paper the influence and optimization of pH and ligand concentration are discussed. α-HIBA complexes with La, Sm and Dy are described as an example.

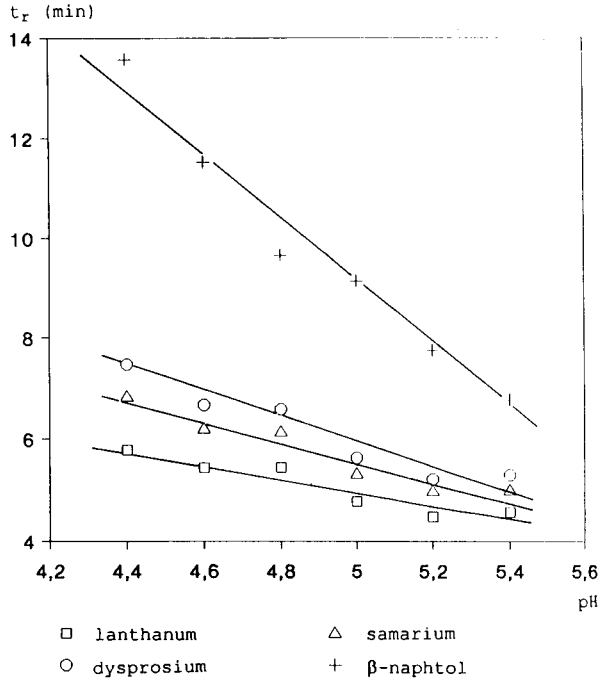

Fig. 3. Dependence on pH of the migration time (t_r) of the rare earth complexes with α-HIBA.

4.1. Influence of pH

The influence of pH on the free ligand concentration and on the migration time (t_r) of the complexes is shown in Fig. 3. The pH range from 4.40 to 5.40 was examined. A lower pH value cannot be used since a sufficient deprotonation of the ligand has to be guaranteed. At pH > 5.40 both the precipitation of the hydroxides and a strong increase of the electroosmotic velocity has to be taken into account. The separation effect reached by the addition of a complex forming agent is lost because of the fast migration of all ions or complexes due to the increased electroosmotic flow (EOF).

With increasing pH the concentration of free ligand increases, which is caused by increasing dissociation. Consequently the degree of complexation of the metal ions increases too. With increasing number of ligands in the metal complex the average degree of complexation ($\bar{n}$) increases and both gross charge and electrophoretic

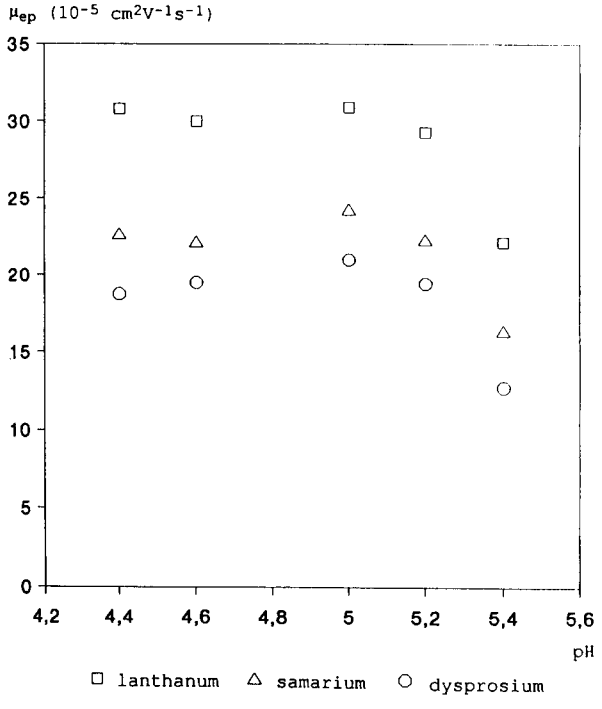

Fig. 4. Dependence on pH of the electrophoretic mobilities of the rare earth complexes with α-HIBA.

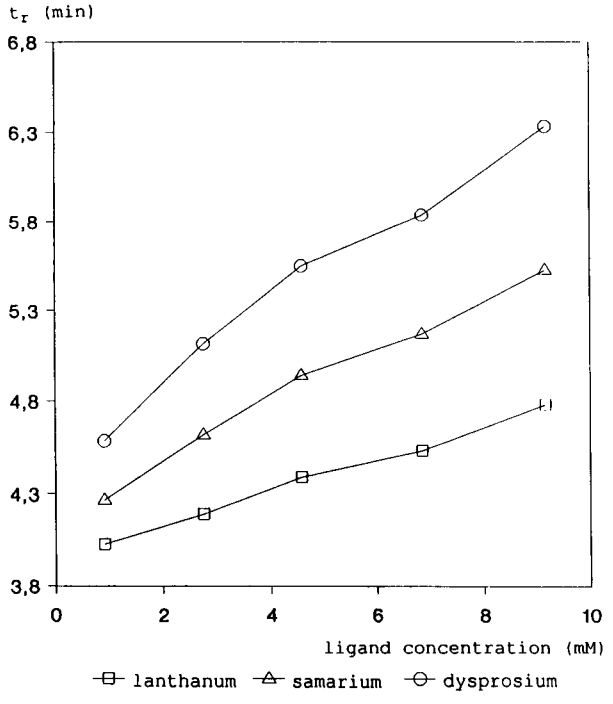

Fig. 5. Dependence on the ligand concentration of the migration times of the rare earth complexes with α-HIBA.

mobility decrease. This should cause a longer migration time, but the effect of pH on the complexation is only secondary. Most important is the increase of the electroosmotic flow due to rising pH, as expressed by the curve of β-naphthol in Fig. 3. The increasing degree of complexation causes the lower slope of the curves for the lanthanides compared with those of β-naphthol. The dependence of the electrophoretic mobilities of the complexes (derived from Eq. 13b) on the pH of the buffer is shown in Fig. 4. As expected, the electrophoretic mobilities decrease with increasing pH.

4.2. Influence of the ligand concentration

For the characterisation of the influence of the ligand concentration on the degree of complexation and resulting migration velocity the α-HIBA concentration was varied from 0 to 10 mM at a constant pH of 5.00. This pH was chosen to guarantee a sufficient dissociation of the ligand.

Table 1
Stability constants of the HIB^- complexes [14]

Metal ion	$\log \beta_1$	$\log \beta_2$	$\log \beta_3$	$\log \beta_4$
La^{3+}	2.99	5.15	6.20	–
Sm^{3+}	3.42	6.00	7.64	8.83
Dy^{3+}	3.66	6.55	8.60	9.82

Fig. 5 shows the dependence of migration time on the free ligand concentration HIB^-, calculated by Eq. 6. With increasing HIB^- concentration the migration times increase, because the charge of the species and thereby their electrophoretic mobilities decrease due to the increasing complexation degree.

The average degree of complexation ($\bar{n}$), calculated by Eq. 8 with the values listed in Table 1, and the electrophoretic mobility (μ_{ep}), both depending on the ligand concentration, are compared in Fig. 6. The experimentally determined values of μ_{ep} are in good agreement with the curves of the calculated average degree of complexation $\bar{n}$ at a ligand concentration > 3 mM.

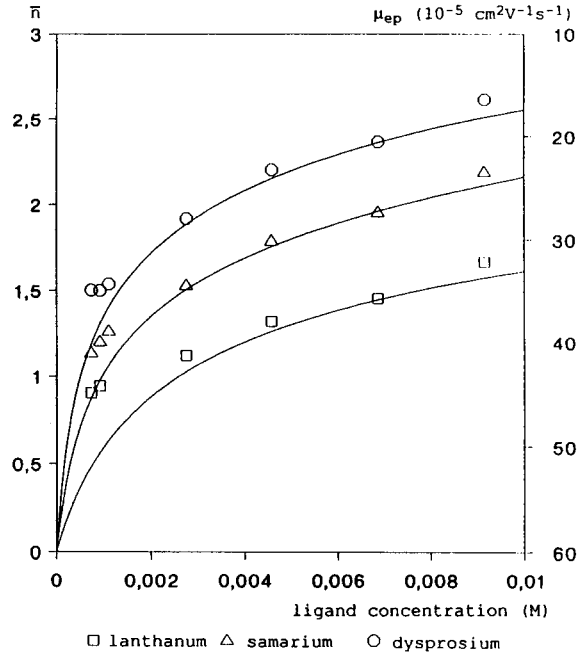

Fig. 6. Dependence on the ligand concentration of the electrophoretic mobilities μ_{ep} and the average degree of complexation $\bar{n}$ (solid lines) of the rare earth complexes with α-HIBA.

No separation is observed in the absence of ligand because of the similar electrophoretic mobilities of the metal ions and the similar average degree of complexation (see Fig. 8A). The values of μ_{ep} determined in the experiments are lower than the values taken from the literature. This may be caused by the adsorption of the non-complexed metal cations to the capillary wall (interaction with the silanol groups). The influence of this wall effect increases with decreasing ligand concentration resulting in differences between μ_{ep} and $\bar{n}$ in the low-ligand concentration range. Furthermore, the lower the concentration of

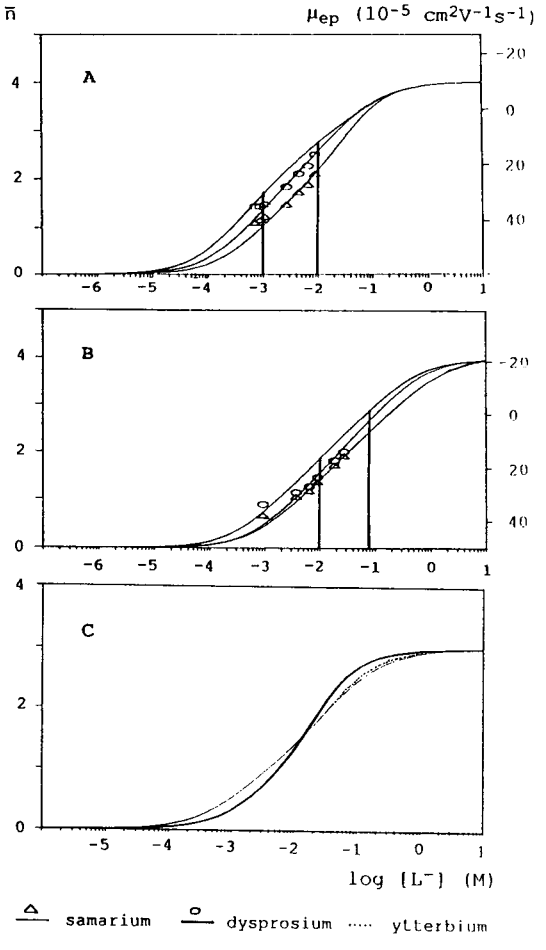

Fig. 7. Dependence of the average degree of complexation $\bar{n}$ on the ligand concentration: (A) α-HIBA with optimum concentration range; (B) lactate with optimum concentration range; (C) acetate.

complex forming agent (for $[HIB^-] < 3$ mM) the higher is the influence of the formation of hydroxo complexes on the experimental data.

In the experimentally examined ligand concentration range the differences of both the average degree of complexation ($\bar{n}$) and the electrophoretic mobilities of the chosen metal ions are increasing with increasing ligand concentration. A good separation of the metal ions is reached in the area of partial complexation ($\bar{n} = 1,\ldots,3$).

4.3. Influence of the ligand

As mentioned above the average degree of complexation ($\bar{n}$) was calculated for all rare earth elements with ligand concentrations up to 10 M. The results for samarium, dysprosium and ytterbium are shown in Fig. 7. These three elements were chosen because for the examined ligands all four (α-HIBA and lactate) or three (acetate) stability constants are known from the literature. For lanthanides lighter than samarium no β_4 constants for the ML_4^- complex of HIB^- and lactate were found in the literature. On the other hand, only acetate is able to form ML_3 complexes. Therefore the calculated average degree of complexation does not exceed $\bar{n} = 3$.

Fig. 7 shows that very high ligand concentrations leading to a maximum complexation with $\bar{n} = 3$ or 4 are not suitable for the separation. In this state the mobility differences of the complexes are lost and separation becomes impossible. For the separations discussed above this state is reached at a ligand concentration of about 0.2 M for α-HIBA and 1 M for lactate in the buffer.

The optimum ligand concentration ranges at which high differences in electrophoretic mobility and a good separation can be achieved are indicated in Fig. 7 for lactate and α-HIBA. In this range the maximum differences in average degree of complexation ($\bar{n}$) and electrophoretic mobility are reached. When acetate is considered as complexing agent no optimum range for the separation of all lanthanides can be observed. No concentration is determined at which all complexation degrees and electrophoretic mobilities differ from each other.

Taken from the theoretical calculation of $\bar{n}$ the optimum ligand concentration should be 7 mM for α-HIBA and 20 mM for lactate. Measurements were carried out at these concentrations. For acetate a separation of all lanthanides at one ligand concentration should be impossible.

Fig. 8 shows the electropherograms obtained under these conditions. Without ligand (Fig. 8A) no separation is achieved and all thirteen rare earth ions have nearly the same mobility.

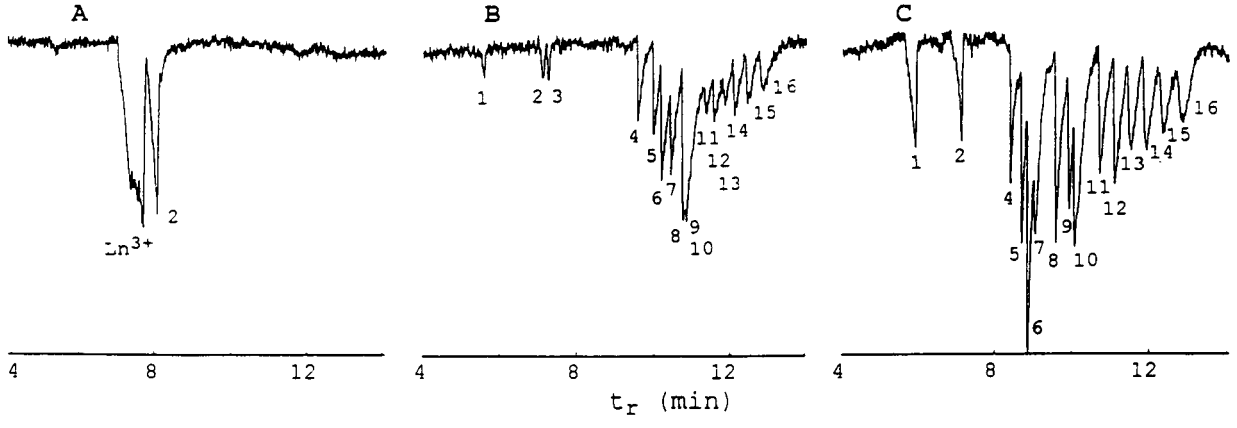

Fig. 8. Separation of the lanthanides with and without different ligands. $l = 40$ cm, i.d = 100 μm, $U = 6$ kV, 214 nm. $1 = K^+$; $2 = Na^+$; $3 = Mg^{2+}$; $4 = La^{3+}$; $5 = Ce^{3+}$; $6 = Pr^{3+}$; $7 = Nd^{3+}$; $8 = Sm^{3+}$; $9 = Eu^{3+}$; $10 = Gd^{3+}$; $11 = Tb^{3+}$; $12 = Dy^{3+}$; $13 = Ho^{3+}$; $14 = Er^{3+}$; $15 = Tm^{3+}$; $16 = Yb^{3+}$. (A) 30 mM creatinine, pH 4.80; (B) 30 mM creatinine, 20 mM lactic acid, pH 4.80; (C) 30 mM creatinine, 7 mM α-HIBA, pH 4.80.

With acetate no satisfactory separation at any concentration of ligand was achieved. Apart from the nearly equal complexation degree of all lanthanides at a known acetate concentration, the poor degree of dissociation (α) of acetic acid at pH 5.00 ($\alpha = 0.562$) caused by the high pK_s value may be one of the reasons for this result.

An increase in pH is not useful because the increasing electroosmotic velocity would cause a loss of the anyhow small differences in migration times.

Fig. 8B shows the separation of the lanthanides using lactate as complexing agent at the calculated optimum concentration of 20 mM. A good resolution of all rare earth ions is obtained except for samarium, europium and gadolinium. Especially samarium and europium have similar stability constants as is shown in Fig. 2. A nearly equal degree of complexation at a given ligand concentration and therefore too small differences in the electrophoretic mobilities are caused, thus making a separation of these three ions with lactate impossible. Potassium, sodium and magnesium are impurities of the lanthanide solutions.

In Fig. 8C the separation of the rare earth ions with α-HIBA as complexing agent is shown. Because of the higher complex stability constants (compared to lactate) a better separation at a lower ligand concentration (7 mM of α-HIBA) can be obtained, but not for all peaks in the

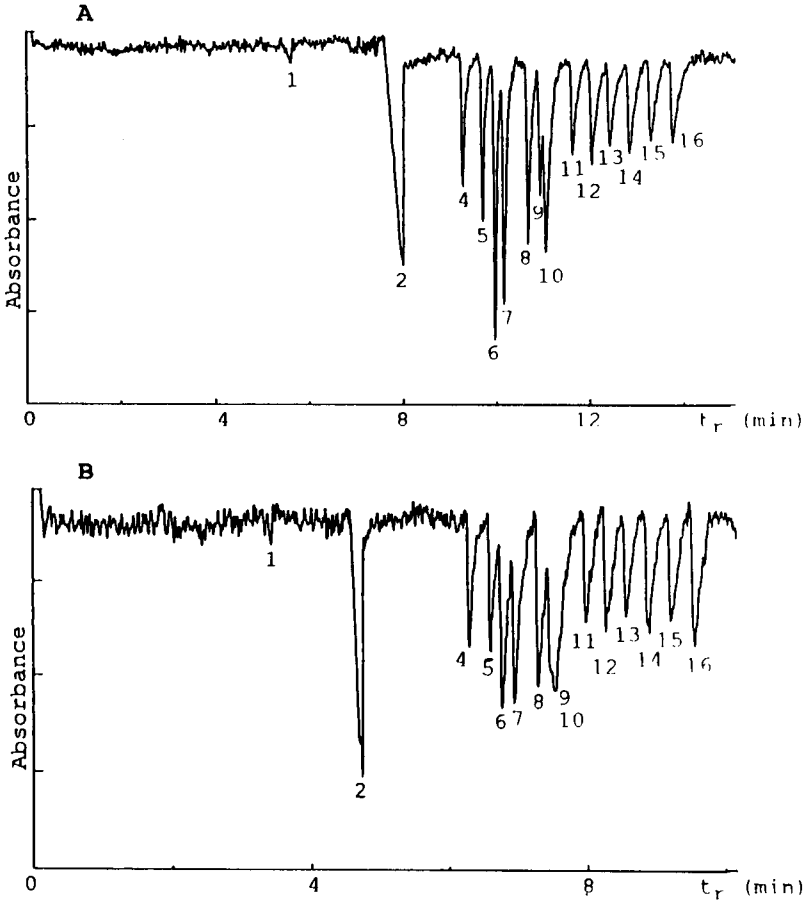

Fig. 9. Separation of the lanthanides with a combination of ligands. $l = 40$ cm, i.d. = 100 μm, 214 nm, numbering as in Fig. 8. (A) 30 mM creatinine, 7 mM α-HIBA, 31 mM acetic acid; (B) 30 mM creatinine, 7 mM α-HIBA, 20 mM lactic acid, pH 4.80, $U = 10$ kV.

electropherogram baseline resolution could be achieved. Europium and gadolinium are not completely separated because of their similar stability constants. Potassium was injected with the sample, sodium originates from rinsing the capillary with sodium hydroxide.

An improvement of the separation can be obtained by the combination of two ligands to achieve higher differences of the complexation and of the electrophoretic mobility. A theoretical consideration of these assorted complexes with different ligands would be too complicated because no stability constants for these complexes could be found in the literature. Fig. 9 shows two electropherograms obtained by the combination of α-HIBA and acetate or α-HIBA and lactate, respectively. With addition of acetate a baseline resolution is achieved for all lanthanides except for europium and gadolinium. Through the addition of lactate no significant improvement of the separation is observed because both ligands show the same complex forming behaviour with samarium, europium and gadolinium. In Fig. 9B is demonstrated that europium and gadolinium are not separated at all and for samarium no baseline resolution is obtained. Therefore a combination of ligands which possess different abilities for the complexation of the metal ions (like α-HIBA and acetate in Fig. 2) leads to a better separation than the combination of ligands with similar complexing behaviour (like α-HIBA and lactate).

In summary it must be pointed out that complex forming equilibria can be used successfully for the separation of metal ions by capillary electrophoresis. If the adjustment of the equilibria is fast, and the stability constants of the formed complexes are known, it is possible to precalculate the optimum ligand concentration for the separation, and the obtained electropherograms at this optimum concentration show a good resolution of the ions analyzed.

References

[1] T. Saitoh, H. Hoshino and T. Yotsuyanagi, J. Chromatogr., 469 (1989) 175.
[2] K. Saitoh, C. Kiyonara and N. Suzuki, J. High Resolut. Chromatogr., 14 (1991) 245.
[3] A.R. Timerbaev, W. Buchberger, O.P. Semenova and G.K. Bonn, J. Chromatogr., 630 (1993) 379.
[4] D.F. Swaile and M.J. Sepaniak, Anal. Chem., 63 (1991) 179.
[5] A. Weston, P.R. Brown, P. Jandik, W.R. Jones and A.L. Heckenberg, J. Chromatogr., 593 (1992) 289.
[6] A. Weston, P.R. Brown, A.L. Heckenberg, P. Jandik and W.R. Jones, J. Chromatogr., 602 (1992) 249.
[7] K. Bächmann, J. Boden and I. Haumann, J. Chromatogr., 626 (1992) 259.
[8] V. Jokl, J. Majer, H. Scharf and H. Kroll, Microchim. Acta, 1–2 (1966) 63.
[9] E. Ohyoshi, Bull. Chem. Soc. Jpn. 43 (1970) 1387.
[10] M. Sakanoue and M. Nakatani, Bull. Chem. Soc. Jpn. 45 (1972) 3429.
[11] V. Jokl and I. Valaskova, J. Chromatogr., 72 (1972) 373.
[12] V. Jokl and Z. Pikulikova, J. Chromatogr., 74 (1972) 325.
[13] F. Foret, S. Fanali, A. Nardi and P. Boček, Electrophoresis, 11 (1990) 780.
[14] T. Hirokawa, N. Aoki and Y. Kiso, J. Chromatogr., 312 (1984) 11.
[15] H.L. Schläfer, Komplexbildung in Lösung, Springer Verlag, Berlin, 1961, p. 75.
[16] H. Deelstra and F. Verbeek, Anal. Chim. Acta, 31 (1964) 251.

ELSEVIER

Analytica Chimica Acta 294 (1994) 155–163

ANALYTICA CHIMICA ACTA

Applicability of capillary zone electrophoresis to study metal complexation in solution

F.B. Erim *, H.F.M. Boelens, J.C. Kraak

Laboratory for Analytical Chemistry, University of Amsterdam, Nieuwe Achtergracht 166, 1018 WV Amsterdam, Netherlands

Received 20th January 1994

Abstract

The suitability of capillary zone electrophoresis for the determination of stability constants of metal complexes was investigated. Three variants were tested viz., the frontal analysis, the Hummel-Dreyer method and the vacancy peak method, in the step-wise complexation between copper(II) and 1,10-phenanthroline as well as 2,2'-bipyridyl. The investigation reveals that CZE has attractive features for the quantitative study of complex formation with neutral ligands. However, the full exploitation requires more sensitive detection systems and application of an automated CZE system.

Key words: Capillary zone electrophoresis; Metal complexes; Stability constants; Neutral ligands

1. Introduction

Metal complexation in solution plays an important role in various areas. In order to understand its role in these areas information about the formation constants of the complexes in solution is indispensable. During the last century numerous analytical techniques have been developed to study metal complexation [1]. Of all these techniques potentiometry and spectrophotometry are by far most applied. Generally the stability constants are calculated from direct or indirect measurement of the concentration of the free or bound ligand in the mixture. For inert, i.e., slowly decomposing complexes, in principle separation techniques like liquid chromatography can be applied to distinguish the free ligand from the complex without significantly influencing the equilibrium [2]. Size exclusion chromatography is frequently applied to determine protein–drug binding constants [3] but not for studying metal complexation in aqueous solutions. This is due to fact that the ligand and complex cannot be separated on basis of their difference in size. In that respect capillary zone electrophoresis (CZE) offers better perspectives [4]. With this recently rediscovered separation technique charged species can be separated, under the influence of an electrical field, according to the differences in the electrophoretic mobilities. The separation is performed in a fused silica capillary and can be considered as a one phase separation system.

* Corresponding author. F.B. Erim, Technical University of Istanbul, Department of Chemistry, Maslak 80626, Istanbul, Turkey

SSDI 0003-2670(94)00134-8

Since CZE has been successfully used by us for studying protein–drug binding [5], we found it worthwhile to investigate the applicability of this technique for the determination of stability constants of metal complexes. For that purpose three different methods to determine the free or bound ligand concentration without disturbing the equilibrium were tested e.g., the Hummel-Dreyer method, the vacancy peak method and the frontal analysis. As model system the stepwise complexation of copper(II) with 1,10-phenanthroline and 2,2′-bipyridyl was selected. The determined stability constants will be compared with values reported in literature and the perspectives of the CZE technique will be discussed.

2. Theory

The extent of complexation is described by the average number of ligands bound to the metal, $\bar{n}$, which is the ratio of the concentration of the bound ligand and total metal concentration. The relationship between $\bar{n}$ and the free ligand concentration according to the theory of successive complex formation is:

$$\bar{n} = \frac{\sum_{j=1}^{N} j\beta_j[L]^j}{1 + \sum_{j=1}^{N} \beta_j[L]^j}$$

All methods to determine stability constants are based on the direct or indirect measurement of the free ligand concentration, calculation of $\bar{n}$, and extraction of the β values from Eq. 1.

The present CZE method exploits the difference in electrophoretic mobility of the ligand and complex to determine the total free and/or bound ligand. The total free ligand is the sum of the protonated ligand, $[HL^+]$ and free ligand [L]. From the total free ligand concentration and the pK_a of the ligand, the free ligand concentration can be calculated.

From computer simulations it appeared that the three applied CZE methods are only applicable when the electrophoretic mobilities of the metal and metal complex are close together and differ from that of the ligand. If this is not the case than the equilibrium during the electrophoresis is not preserved. This restricts the application of the described methods to complexes with neutral ligands because the charge of the metal and complex are the same and their mobilities will differ only slightly.

Therefore in the present study we selected the complexation of copper with 1,10-phenanthroline and 2,2′-bipyridyl. The selection was also done on basis of the following considerations: (i) the complexation of copper and these ligands have been extensively studied and values of stability constants are available in literature; (ii) the pK_a values of the ligands are known; (iii) the molar absorptivities of both ligands are high enough to detect them by on-column UV detection; (iv) both are neutral ligands and protonated forms dissolve in aqueous solutions.

3. Principle of the CZE methods

The various species in the mixture are separated in a fused silica capillary, under the influence of a high electrical field, and detected by using on-column UV detection. Fig. 1 depicts schematically the experimental set-up for the measurements. Two different sample introduction techniques were tested: pressure and electromigration. No significant differences were found between the two techniques but electromigration was selected in this study because of its simplic-

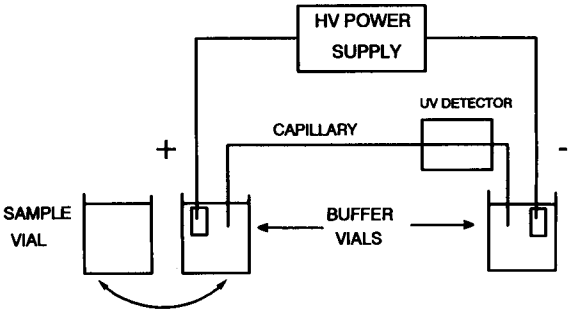

Fig. 1. Schematic representation of the experimental CZE set-up.

ity. With the experimental set-up three different variants to measure the total free or bound ligand were investigated, e.g., the frontal analysis, the Hummel-Dreyer method and the vacancy peak method. These are now briefly discussed, where for the sake of simplicity only a 1:1 complex is considered, although in the actual research higher complexes were also included. A more extensive description of the methods can be found in Ref. 5.

3.1. Frontal analysis

In the frontal analysis, the buffer vials and the capillary are filled with the buffer. Then a large sample plug (60 s, 10 kV), containing buffer + metal + ligand, is injected into the capillary and the voltage applied. Due to the difference in electrophoretic mobilities of the species (in our case $\mu_M \approx \mu_{ML} > \mu_L$) at the front edge of the sample zone free metal is leaving the sample plug while at the rear edge of the sample zone the free ligand leaks out of the sample zone. This finally results in three plateaus in the electropherogram: the first is related to the free metal, the second to the metal complex and the third to the total free ligand. Due to the selected wavelength, the free metal plateau is not visible in the electropherogram and only two plateaus will be found (see Fig. 2A). The height of the third plateau reflects the total free ligand concentration and thus the free ligand concentration can be calculated from the known pK_a value of the ligand and pH of the buffer solution.

3.2. Hummel-Dreyer method

In the Hummel-Dreyer method, the buffer vials and the capillary are filled with a solution containing buffer + ligand. The presence of the ligand in this solution causes a large background detector signal. Then a small amount of a solution of buffer + metal is injected (2.4 s, 10 kV) and the voltage applied. Due to the difference in mobility of the metal and ligand, both species are mixed in the beginning of the capillary and complexation occurs. When the ligand is present in excess the equilibrium is reached after a short distance. However, when the metal is present in excess then the distance will be significantly larger. In the injected plug the total ligand concentration is similar to the ligand concentration in the buffer but part of the ligand is bound to the metal. When the migration proceeds the complex migrates from the sample zone and leaves a local deficiency in ligand concentration. This deficiency causes a negative peak which moves with the mobility of the ligand (see Fig. 2B). The area

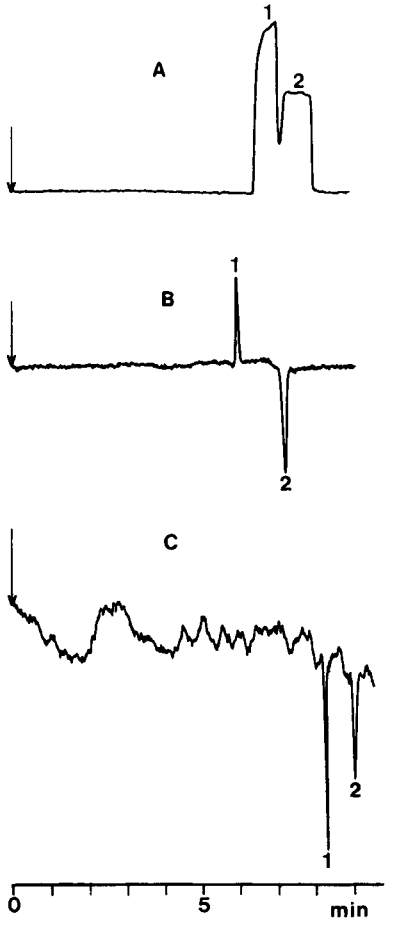

Fig. 2. Typical electropherograms of the copper(II)–1,10-phenanthroline complex obtained with the CZE methods. (A) Frontal analysis method, 20 kV; inj. 60 s, 10 kV, plateau 1: complex; plateau 2: total free ligand. (B) Hummel-Dreyer method, 12 kV; inj. 2.4 s, 10 kV, peak 1: complex; peak 2: deficiency in ligand. (C) Vacancy peak method, 12 kV; inj. 2.4 s, 10 kV, peak 1: deficiency in complex; peak 2: deficiency in ligand.

reflects the amount of ligand bound to metal. The complex moves in the buffer + ligand and is thus always in equilibrium with the ligand. The presence of the complex causes a positive peak on the background.

3.3. Vacancy peak method

The vacancy peak method shows some similarities to the frontal analysis. The buffer vials and the capillary are filled with a solution containing buffer + ligand + metal. This results in a large background detector signal. Then a small volume of only buffer is injected (2.4 s, 10 kV) and the voltage applied.

As a whole the vacancy will move to the cathode since all mobilities are of the same sign. However, at the front edge, ligand is penetrating the vacancy, as its mobility is lowest. At the rear edge metal and complex moves into the vacancy, as its mobility is higher. After some time, dependent on the width of the injected zone, these disturbances will meet, and the complex will be reconstituted according to the equilibrium. From then on the equilibrium is restored but the introduced deficiencies in the total free ligand and complex will be intact during further migration and this will cause two negative peaks in the electropherogram (see Fig. 2C). The first peak is caused by the deficiency of the complex and the area is a measure of the bound ligand. The second negative peak originates from the deficiency of the total free ligand.

4. Experimental

4.1. Apparatus

The measurements were performed on a commercial CZE injection system (Prince, Lauer Labs, Emmen, Netherlands) in combination with on-column UV detection (linear 200, Linear Inst., Fremont, CA). The wavelength was set at 273 or 302 nm depending on the ligand. Platinum wire electrodes were inserted into the buffer vials for connection to the electrical circuit. Sample injection was carried by electromigration (2.4–60 s at 10 kV) at the anodic side. The analysis voltage ranged between 12–20 kV. The used fused silica capillary was 75 cm × 50 μm i.d. and was obtained from Polymicro Technologies (Phoenix, AZ). The detection window was prepared by burning off locally the outer polyimide coating. The distance between the point of injection and the detection window was 41 cm. Before the experiments the capillary was always flushed for 20 min with 1 M KOH, water and buffer, respectively. The measurements were performed at room temperature.

4.2. Chemicals

Chloroacetic acid and 1,10-phenanthroline monohydrate were obtained from Aldrich (Bornem, Belgium). Sodium hydroxide and $CuCl_2 \cdot 2H_2O$ were purchased from Merck (Darmstadt). 2,2′-Bipyridyl was AnalaR grade (BDH, Poole) and recrystallized several times from methanol before use. All ligand solutions were prepared from doubly distilled water and kept in the dark.

4.3. Procedures

Solutions

Chloroacetic acid was chosen as buffer because of its negligible complexation strength with copper(II) and its acid strength. The ionic strength of all buffers was kept at 0.025 M. The pH of the buffer was adjusted with a solution of 0.1 M sodium hydroxide. On the basis of the complexation strength and pK_a value of the ligand, the pH values of the copper–1,10-phenanthroline and copper–2,2′-bipyridyl system were set to 1.96 and 2.85, respectively. At these pH values no copper(II) hydroxide complex is formed.

In all experiments 5×10^{-5} M copper(II) was used except with the frontal analysis of the copper–1,10-phenanthroline system. In this experiment three different copper(II) concentrations, i.e. 4×10^{-5}, 5×10^{-5}, 6×10^{-5} M, were used to study the effect of metal concentration on the determination of the complex formation constants.

The ligand concentrations used range generally between 3×10^{-5} and 1.5×10^{-3} M.

Calculations

For the calculation of the stability constants the relation between of $\bar{n}$, the ratio of the concentration of the bound ligand and total metal, and the free ligand concentration has to be known. The free ligand concentration can be calculated from the total free ligand concentration, pH of the buffer and the pK_a value of the ligand. For 1,10-phenanthroline and 2,2'-bipyridyl the pK_a values are 4.98 and 4.47, respectively [6]. The bound ligand concentration is either directly known, as is the case in the Hummel-Dreyer method, or can be derived from the total free ligand concentration.

In the frontal analysis method the total free ligand concentration was determined from the height of the sample plateau and the height of the plateau obtained when injecting the same total ligand concentration in the buffer as used in the sample. The total free ligand is then calculated according to:

$$C'_L = \left(\frac{sample\ height}{ligand\ height} \right) C_L$$

where C_L is the total ligand concentration and C'_L the total free ligand concentration in the complex solution. The difference between C_L and C'_L is the bound ligand concentration.

In the Hummel-Dreyer method, the bound ligand concentration is determined from two separate injections: the sample, and the buffer only. From the areas of both negative peaks the bound metal concentration, C_b, can be calculated according to:

$$C_b = \left(\frac{A_1 - A_2}{A_2} \right) C_L$$

where A_1 is the area of the sample peak and A_2 the area of the buffer peak. C_L is the total ligand concentration in the solution put in the capillary. Since the ligand is present in a large excess, the free ligand concentration can be directly calculated from C_L.

In the vacancy peak method, the total free ligand concentration was determined by internal calibration. For that purpose increasing concentrations of ligand in the buffer were injected. Depending on the concentration, the peaks can be negative or positive. By plotting the area of the peaks versus the added ligand concentration, the total free ligand concentration can be determined from the intersection on the ligand axis. At this point the added ligand concentration cancels the area of the sample peak. From the total free ligand concentration the free ligand and bound ligand concentration can be calculated.

Fitting of the experimental data

The experimental data were fitted according to Eq. 1, using a non-linear regression curve fitting program based on the Levenberg-Marquardt algorithm [7]. The data were fitted supposing two complexation steps. Since any iterative parameter estimation method has to start with initial values, we used the mean values of β_1 and β_2 from literature as initial values. In order to test whether the selection of the initial values may influence the final values of the stability constants, the fitting was also performed with different initial values (differing a factor 5–50). Varying the initial values in that range did not influence the final values of the stability constants. Furthermore a weighting of the data points with the measurement error was considered. The weighting involves a division of the individual data points by its standard deviation of the replicates. For the frontal analysis and the Hummel-Dreyer method no significant difference in the measurement errors was found and therefore a weighting of the data points is not necessary. However, for the vacancy peak method the measurement errors were different over the pL range and weighting of the data points was essential.

The standard deviations of the calculated stability constants were estimated as described in Ref. [8].

5. Results and discussion

In order to judge the three different CZE methods on their merits, the complexation of copper(II) with 1,10-phenanthroline was extensively investigated. From explorative experiments it appeared necessary to do the measurements

according a stringent time and washing protocol to obtain reproducible data. To get some insight in the reliability of the calculated stability constants, all measurements were replicated at least in duplicate. From the experimental data the complex formation curves were computed by using the non-linear curve fitting program as described in procedures.

5.1. Experimental $\bar{n}$ values

For the calculation of the three stability constants, the experimental data points should cover the whole $\bar{n}$ range. Unfortunately with all three methods it seemed impossible to attain reliable values for high and small $\bar{n}$ values. The reasons for this can be attributed to the limited sensitivity of the detection system and the back ground noise.

Since the coordination of the third ligand to the metal is considerably sterically hindered, a relative high ligand concentration compared to the metal concentration has to be used in order to realise $\bar{n}$ values > 2. This means that under these conditions only a small change in the total free ligand concentration will occur. This change is reflected in the difference of the height or the area of the peak/plateau and the reference peak/plateau. Consequently for the calculation of $\bar{n}$, two large values are subtracted and this appears to give an unacceptable large spreading in $\bar{n}$. Moreover, with the Hummel-Dreyer and the vacancy methods there is a high background detector signal due to the presence of the ligand in the capillary and this background signal causes noise which increases with increasing ligand concentration. With the Hummel-Dreyer method $\bar{n}$ values up to 2.2 were measured but the spreading in replicates was unacceptably large.

For the measurement of $\bar{n}$ values < 1, ligand concentrations smaller than that of the copper have to be used. It can be pointed out that the experimental difficulties in the determination of small $\bar{n}$ values is due to the stability of the first complex and the relative weak formation of the competitive reaction, i.e., the small pK_a value of the acid. The degree of complexation is appreciable even in rather acidic solutions and this makes it difficult to detect the very small total free ligand concentrations with the used detection system. It can be noticed that in principle lowering the pH can circumvent this problem but leads to excessive heat production in the capillary. The very small total free ligand concentration results for the vacancy method in very small peaks and in the frontal analysis in low plateaus. With the Hummel-Dreyer method measurable peak heights were found but the peaks become very broad and at very small ligand/metal concentration ratios even double peaks were monitored. The deformation of the peaks when the copper concentration is larger than that of the ligand, must be attributed to the exhaustion of the amount of ligand. In order to attain an equilibrium, the copper ions have to migrate a longer distance through the ligand zone and this broadens the negative deficiency peak considerably. In principle the area of the deformed negative peak reflects still the amount of bound ligand but it appeared impossible to integrate this area properly with the available integrator.

Due to the absence of ligand in the buffer the background noise with the frontal analysis is small and $\bar{n}$ values down to about 0.6 could be measured with sufficiently small spreading. On basis of the aforementioned limitations to measure $\bar{n}$ values > 2, the experimental data points were fitted assuming only the first two complex formation steps.

5.2. Experimental and computed formation curves

The experimental data points and the computed formation curves of the three CZE methods are reflected in Figs. 3–5. The calculated stability constants, including the standard deviations and literature values, are tabulated in Table 1.

From these figures it can be seen that the experimental points with the Hummel-Dreyer method fall well on the fitted line but with the frontal and vacancy method the experimental points scatter significantly around the fitted line. The reason for the scattering of the experimental points must be partly attributed to the manual operation of the measurements and temperature

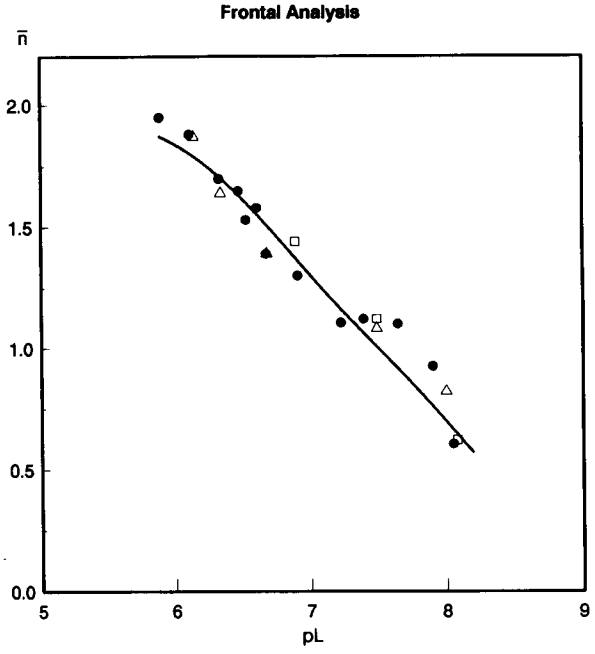

Fig. 3. Experimental datapoints and computed formation curve of copper(II)–1,10-phenanthroline with the frontal analysis method. Copper(II) concentration: □ = 4×10^{-5} ; ● = 5×10^{-5}; △ = 6×10^{-5} M.

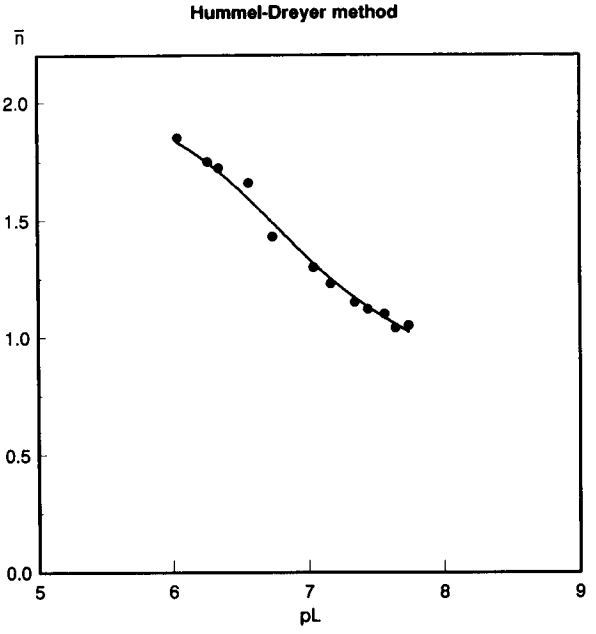

Fig. 4. Experimental datapoints and computed formation curve of copper(II)–1,10-phenanthroline with the Hummel-Dreyer method.

fluctuations in the room. Less scattering can be expected with a completely automated well thermostated CZE system.

From Table 1 it can be seen that the values of the stability constants, calculated with the three methods, fall well within the range of previously reported literature values. The standard deviation is the smallest with the frontal analysis method and is significantly larger with the Hummel-Dreyer and vacancy method. On basis of the good fit of the experimental points with the Hummel-Dreyer method as shown in Fig. 4, the worse standard deviation of the Hummel-Dreyer method might be a surprise for the reader but can be explained by the lack of $\bar{n}$ values below 1 (as is also the case with the vacancy method). This introduces a larger uncertainty in the calculation of the stability constants. It must be noticed that due to the laborious internal calibration, less data points were measured with the vacancy peak method. This certainly leads to larger standard deviations for the stability constants.

In a separate experiment the effect of the copper concentration on the complex formation was investigated with the frontal analysis method

Table 1
Calculated stability constants of the copper(II)–1,10-phenanthroline and copper(II)–2,2′-bipyridyl complexes and reported literature values

Ligand		Frontal Analysis	Hummel-Dreyer Method	Vacancy peak Method	Reported values [6]
1,10-Phenanthroline	$\log \beta_1$	8.3 ± 0.09	8.9 ± 0.17	8.4 ± 0.20	7.4– 9.1
	$\log \beta_2$	15.0 ± 0.10	15.6 ± 0.16	15.0 ± 0.19	15.7–16.0
2,2′-Bipyridyl	$\log \beta_1$	7.5 ± 0.10			6.3– 8.2
	$\log \beta_2$	13.1 ± 0.10			13.6–13.7

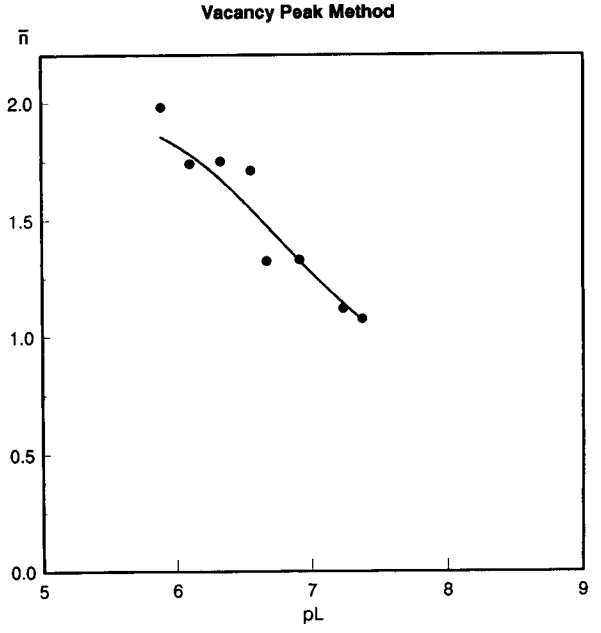

Fig. 5. Experimental datapoints and computed formation curve of copper(II)–1,10-phenanthroline with the vacancy peak method.

and the experimental points are included in Fig. 3. As can be seen all data points fall close to the same line, which largely ensures that under the selected experimental conditions the complex formation is independent of the copper concentration.

In order to demonstrate that the CZE method also works for other complexes the stepwise complex formation of copper(II) and 2,2′-bipyridyl was determined with the frontal analysis. The computed formation curve is shown in Fig. 5 and the values of the calculated stability constants are included in Table 1. The determined values fall well in the range reported in literature.

6. Conclusions

From the results sofar some preliminary conclusions can be drawn. CZE is in principle an attractive and simple technique to determine stability constants of metal complexes. The method is sofar only suited for complexation with neutral ligands. The main drawback is the lack of concentration sensitivity of the applied on-column UV detection. Improvements in concentration sensitivity can be expected when using UV detection cells with a longer lightpath such as a Z- or U-shaped [9] cell or a bubble cell from Hewlett-Packard (Waldbronn, Germany). Also the application of fluorescence and electrochemical detection for certain application looks attractive.

Of the three investigated CZE methods, viz. frontal analysis, Hummel-Dreyer and the vacancy peak methods, at this moment the frontal analysis method appears to be the most reliable method because $\bar{n}$ values < 1 can be determined.

Since all CZE measurements were performed manually it can be expected that more reliable results can be obtained with an automated CZE system. Research in that direction, including an investigation to select the optimal experimental points for the fitting via an experimental design approach, is now undertaken.

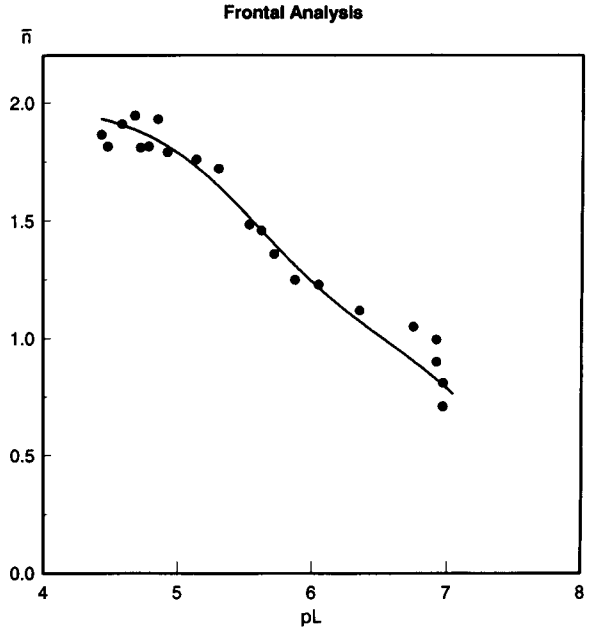

Fig. 6. Experimental data points and computed formation curve of copper(II)-2,2′-bipyridyl with the frontal analysis.

Acknowledgments

The authors thank Prof. Dr. H. Poppe for his valuable remarks during the preparation of the manuscript.

References

[1] F.R. Hartley, C. Burgess and R. Alcock, Solution Equilibria, Ellis Horwood, London, 1980.
[2] H. Veening and B.R. Willeford, in J.C. Giddings, E. Grushka, J. Cazes and P.R. Brown (Eds.), Advances in Chromatography, Marcel Dekker, New York, Vol. 22, 1983.
[3] B. Sebille, R. Zini, C.V. Madjar, N. Thuaud and J.P. Tillement, J. Chromatogr., 531 (1990) 51.
[4] J.W. Jörgenson and K.D. Lukacs, Anal. Chem., 53 (1981) 1298.
[5] J.C. Kraak, S. Bush and H. Poppe, J. Chromatogr., 608 (1992) 257.
[6] R.M. Smith and A.E. Martell, Critical Stability Constants, Vol. 5, Plenum, New York, 1982.
[7] W.H. Press, B.P. Flannary, S.A. Teucholsky and W.S. Vetterling, Numerical Recipes, Cambridge University Press, Cambridge, 1986, pp. 521–538.
[8] N.R. Draper and H. Smith, Applied Regression Analysis, Wiley, New York, 1966, pp. 273–274.
[9] J.P. Chervet, N. van Soest, M. Ursem and J.P. Salzman, J. Chromatogr., 543 (1991) 439.

ELSEVIER

Analytica Chimica Acta 294 (1994) 165–176

ANALYTICA CHIMICA ACTA

Prediction of the migration behaviour of anions in capillary ion analysis

M. Jimidar, D.L. Massart *

Vrije Universiteit Brussel, Pharmaceutical Institute, Department of Pharmaceutical and Biomedical analysis (FABI), Laarbeeklaan 103, B-1090 Brussels, Belgium

Received 21st December 1993

Abstract

The separation of anions in capillary ion analysis below the critical micellar concentration of the modifier (cationic surfactant) is influenced by two chemical equilibria, the ionic dissociation which depends on the pH of the buffer electrolyte and the formation of ion association complexes in function of the concentration modifier. An expression of the mobility in function of the pH and concentration of the modifier is proposed and evaluated using experimental data. The experimental domain is examined with the aid of a central composite design. The model describes the mobility of anions in terms of physical and chemical constants of each ion (acid dissociation constant K_a, ion association constant K_{ia}), the pH of the electrolyte, and the concentration of a modifier ([S]) in the buffer. The model is used to predict the mobility of each solute over a two-dimensional pH/[S] space.

Key words: Capillary ion analysis; Acid dissociation; Ion association; Prediction; Optimization

1. Introduction

Capillary ion analysis (CIA) is widely used for the determination of ions [1–7]. Inorganic ions, which mostly do not show UV absorptivity, are also analysed by CIA. In this technique a background electrolyte is used to give a constant background signal for a stable baseline [3,7]. In anion analysis a modifier is used to make the electroendosmotic flow (EOF) move in the same direction as the anions. This results in shorter analysis time for the anions. In previous studies [1–3] the modifier was ANION-BT®, a substance with an unknown composition supplied by Waters-Millipore (Bedford, MA).

Predictions of the migration behaviour in capillary electrophoresis are of recent date [8–11]. Especially, the description of the behaviour in function of more than one variable simultaneously has not been studied extensively. Khaledi et al. [8–11] described a model for micellar electrokinetic capillary chromatography (MECC) for acidic solutes with pH and the concentration of the surfactant (sodium dodecylsulfate: SDS) as variables. Smith and Khaledi [9] applied this model for the prediction of the migration of 5 chlorophenols.

In the present report it is intended to predict the migration behaviour of 10 inorganic anions in

* Corresponding author.

SSDI 0003-2670(94)00141-8

function of two variables, the pH and the concentration of the modifier below the critical micellar concentration (cmc). Because we prefer to work with known substances, we did not use ANION-BT^R as the modifier but we selected cetyltrimethylammonium bromide (CTAB). A similar cationic surfactant (cetyltrimethylammonium chloride) was used by Kaneta et al. [12] in a study on the migration behaviour in MECC of monovalent inorganic anions in function of the concentration surfactant. According to Kaneta et al. [12] the mobility decreased due to two processes: ion association equilibria of the anions with the monomeric surfactant below the cmc and partitioning into the micelle above the cmc.

The anions which are included in this study were selected on the basis of there ionic charge (monovalent or multivalent) and their pK_a (within the experimental domain or not). These were bromide (Br^-), chloride (Cl^-), sulphate (SO_4^{2-}), nitrite (NO_2^-) and nitrate (NO_3^-), a group of anions which should migrate close to each other, and iodide (I^-), fluoride (F^-), monohydrogenphosphate (HPO_4^{2-}), bicarbonate (HCO_3^-) and iodate (IO_3^-).

2. Theory

From preliminary experiments and from the literature [2,7,10], it appeared that the pH, the concentration of background electrolyte and the concentration of modifier in the buffer had the largest effect on the selectivity in CIA of anions. However, the concentration of the background electrolyte is kept constant. The reason for this is discussed further.

2.1. Mobility in function of pH

The mobility of anions in function of the pH is expected to be a sigmoidal curve, the location of which depends on the pK_a of the conjugated acid of the anion. This was also observed in practice [9,10], in studies of the mobility in function of the pH. When the pK_a lies within the experimental domain, in this case higher than 8.0, then the shape of the curve is sigmoidal. If the pK_a is smaller than 8.0 (by 2 units), then the pH (> 8) does not influence the mobility. The influence of the pH on retention was described by Horvath et al. [13] in chromatography. The same expression is used in CE to describe the mobility [8–11].

Consider the dissociation of an acid HA:

$$HA \Leftrightarrow A^- + H^+ \quad (1)$$

The effective electrophoretic mobility (μ_{eff}) is equal to:

$$\mu_{eff} = F_{HA} \cdot \mu_{HA} + F_A \cdot \mu_{A^-} \quad (2)$$

where F_{HA} and F_A are the mole fractions of the two forms of the acid HA. In terms of the degree of dissociation (α) this can be rewritten as:

$$\mu_{eff} = (1 - \alpha)\mu_0 + \alpha\mu_{A^-} \quad (3)$$

μ_0 is the mobility of the undissociated acid and μ_{A^-} is the mobility of the fully dissociated acid (anion). For a monovalent anion μ_0 is equal to 0 because the mobility of a neutral compound is equal to 0 in CZE. Therefore, one can write the equation for a monovalent ion as follows:

$$\mu_{eff} = \alpha\mu_{A^-} = \frac{K_a \cdot \mu_{A^-}/[H^+]}{1 + K_a/[H^+]} = \frac{K_a \cdot \mu_{A^-}}{K_a + [H^+]} \quad (4)$$

If $[H^+] \ll K_a$, then $\mu = \mu_{A^-}$. If not then the mobility is a function of pH.

2.2. Mobility in function of the concentration of modifier in the buffer

In the reports of Kaneta et al. [12] and of Jones and Jandik [2], linear relationships were observed in function of the modifier concentration. However, Kaneta et al. [12] divided the behaviour in two parts, one under the critical micellar concentration (cmc) and the other above the cmc. They described the mobility in function of the concentration of the modifier for a monovalent anion in both regions.

Under the cmc, the modifier can develop ion association complexes with anions. The stability of these association complexes is a factor in the selectivity of the method.

For a monovalent anion one obtains [12]:

$$\mu_{eff} = \frac{\mu_{ep}}{K_{ia1}[S] + 1} \quad (5)$$

where μ_{eff} stands for the effective mobility of the anion, [S] the concentration of the modifier, K_{ia1} is the ion association constant for a monovalent anion and μ_{ep} is the electrophoretic mobility of the anion, meaning the mobility without the influence of the modifier. However, μ_{ep} can be influenced by the pH.

2.3. Mobility of the anions in function of pH and the concentration of the modifier

By combining the expressions for the effective mobility in function of the pH and the concentration of the modifier one obtains the following expression for an anion (A) with a conjugated acid H_qA:

$$\mu_{eff} = \sum_{i=1}^{q} \left[\frac{\mu_{A^{i-}}}{\left(K\text{ia}_{(i)}[S]^{(i)} + 1\right)} \right] * [(i\text{th term of denominator}) / \left([H^+]^q + K_{a(i)} \cdot [H^+]^{q-i} + \cdots + K_{a(i)} \cdots K_{a(q-i)} \cdot K_{a(q)}\right)] \quad (6)$$

where q is the ionic charge and $\mu_{A^{i-}}$ and $\mu_{A^{q-}}$ are the electrophoretic mobilities of the ith undissociated and the fully dissociated anion, respectively, at initial conditions without the influence of the modifier. For example, for carbonate, $\mu_{A^{i-}}$ represents the mobility of HCO_3^- and $\mu_{A^{q-}}$ the mobility of CO_3^{2-}. $K_{ia(i)}$ and $K_{ia(q)}$ are the ion association constants of the ith undissociated (HCO_3^-) and the fully dissociated (CO_3^{2-}) anion, respectively. It should be noticed that this expression includes anions of different valences.

3. Experimental

3.1. Chemicals

All solutions were prepared using Milli-Q water (Millipore, Bedford, MA). Sodium chromate, sodium fluoride, sodium bromide, sodium chloride, sodium sulphate, sodium nitrite, sodium nitrate, sodium iodide, sodium monohydrogenphosphate, sodium bicarbonate, sodium iodate, sodium and potassium hydroxide and sulphuric acid were purchased from Merck (Darmstadt). Cetyltrimethylammonium bromide was also obtained from Merck.

3.2. Preparation of solutions

Sodium chromate was prepared as a 0.1 M stock solution. All buffers were prepared in 50 ml aliquots and filtered through a 0.45 μm Milex® syringe filter (Millipore, Molsheim, France). The buffers were adjusted to the final pH using sulphuric acid 0.00075 M and sodium hydroxide 0.001 M.

The modifier was prepared as a 50 mM cetyltrimethylammonium bromide solution. The solubility was enhanced with a magnetic stirrer at moderate temperature. After dissolution, it was filtered through the same kind of syringe filter.

Stock-solutions of 1000 mg l^{-1} of each anion were prepared in Milli-Q water and stored in a refrigerator. Standard solutions of each anion were prepared daily in a concentration of 10 mg l^{-1}, except for I^- which had a concentration of 50 mg l^{-1}.

The buffers were adjusted to the pH required using a WTW (pH 537) microprocessor pH meter.

3.3. Instrumentation

The analyses were carried out on a Waters Quanta-4000 capillary electrophoresis system equipped with a negative power supply. The capillaries were ordinary fused-silica capillaries (Waters AccuSep®, 60 cm capillaries) with 75 μm i.d., and 52 cm length from the point of sample introduction to the point of detection. The electrophoretic zones were detected with a fixed-wavelength UV detector at 254 nm. The hydrostatic injection mode (15 s) was used for the injection of the samples. The electropherograms were recorded and integrated with a Waters 810

data workstation equipped with a 'W51-watchdog' interface.

3.4. Preparation of the capillary

Each time before changing a buffer the capillary was purged with 0.5 M potassium hydroxide (KOH) for 5 min, followed by 5 min with Milli-Q water and the buffer electrolyte. Between each run the capillary was flushed with 0.1 M KOH during 1 min, followed by 2 min flushing with milli-Q water and the running buffer. Before shut-down the capillary was flushed for 5 min with 0.5 M KOH and Milli-Q water. The inlet and outlet of the capillary was kept in Milli-Q water.

3.5. Calculations

All calculations were done using spreadsheets in Microsoft Excel (4.0) for Windows. The effective mobility was obtained by applying the expression:

$$\mu_{\text{eff}} = \left(\frac{l^* L}{V}\right) * \left(\frac{1}{T_m} - \frac{1}{T_{\text{eof}}}\right) \quad (7)$$

where l is the length of the capillary from inlet to the point of the detection, L is the total length of the capillary, V is the applied voltage, T_m is the migration time of the anion and T_{eof} is the migration time of the water peak.

The coefficients in the models were determined by non-linear regression methods using the SPSS-PC + Statistics™ version 5.0 for MS-windows (3.1) software package. The Levenberg-Marquardt algorithm procedure was used to estimate the coefficients in the model. The number of iterations was stopped when the relative reduction between successive residual sums of squares was $\leq 1.000 \times 10^{-8}$.

4. Results and discussion

4.1. Influence of the background electrolyte

The background electrolyte (CrO_4^{2-}) has an effect on the selectivity [2], separation efficiency and on the sensitivity [14]. The concentration of the background electrolyte should be as high as possible for obtaining the highest separation efficiency [14], but is limited by the linear dynamic range of the detector response. This characteristic was first evaluated. It was observed that for concentrations higher than 10 mM CrO_4^{2-} the response of the detector deviated from a linearity. Therefore, the concentration of 10 mM was

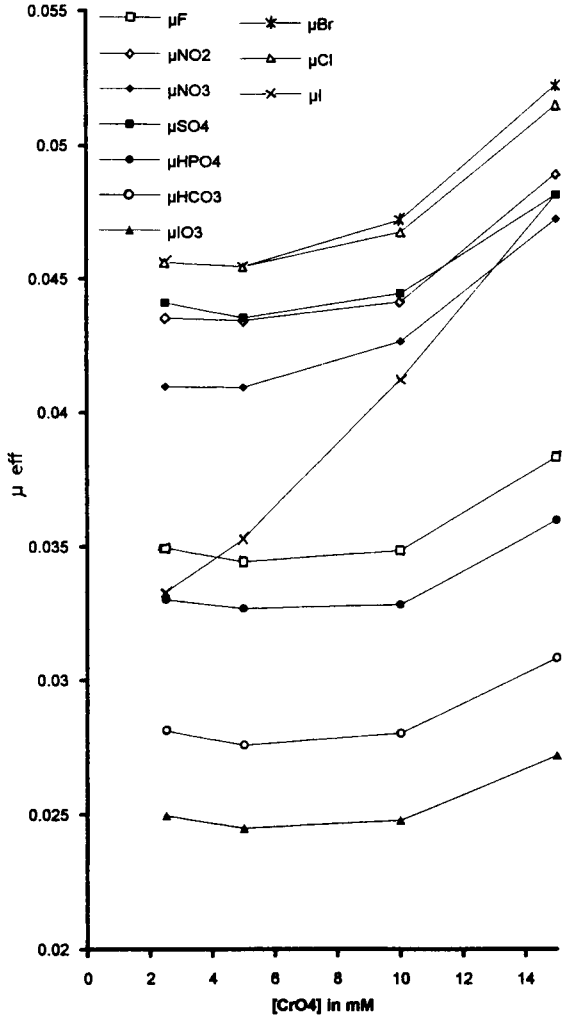

Fig. 1. Effect of the concentration of the background electrolyte on the mobility of the anions. A 10 mg l^{-1} (I^-: 50 mg l^{-1}) mixture of the anions was injected hydrostatically for 15 s. The buffer consisted of 0.5 mM CTAB and CrO_4^{2-} (2.5–15 mM). The running voltage was 20 kV.

selected for further experiments. The effect on the selectivity is shown in Fig. 1. As can be seen the mobility of the anions increases with the concentration of CrO_4^{2-}. This can be understood as a case of ion exchange partitioning. When the concentration of CrO_4^{2-} is increased, there is a competition between the CrO_4^{2-} ions and the other anions for the positive site on the modifier. Apparently, CrO_4^{2-} has a stronger affinity for the cationic modifier and thus releases the anions from the modifier, leading to an overall increase of charge for these anions. This overall increase in charge explains the increase in mobility. Compared to the other anions, the mobility of I^- is strongly affected. The peak of I^- crosses-over F^-, NO_3^- and SO_4^{2-}. As is discussed further, I^- has the strongest affinity for the modifier compared to the other anions. Therefore, even a slight increase in the concentration of CrO_4^{2-} already leads to an important increase in mobility of I^-. At higher concentration SO_4^{2-} crosses-over the peak of NO_2^-, while Br^- separates from Cl^- at CrO_4^{2-} concentration higher than 5 mM. At the selected 10 mM CrO_4^{2-}, the migration order is the following: Br^-, Cl^-, SO_4^{2-}, NO_2^-, NO_3^-, I^-, F^-, HPO_4^{2-}, HCO_3^- and IO_3^-.

The effect on the sensitivity (expressed in peak height) is shown in Fig. 2. The peak heights of the anions increase with increasing concentrations of CrO_4^{2-}, reaching a plateau between 5 and 15 mM. The separation efficiency ($N = 16(T_m/W)^2$, where T_m is the migration time and W is the peak width) appeared to reach an optimum at the selected concentration of CrO_4^{2-}. From these experiments it is clear that the selected concentration of 10 mM CrO_4^{2-} is optimal concerning sensitivity and separation efficiency.

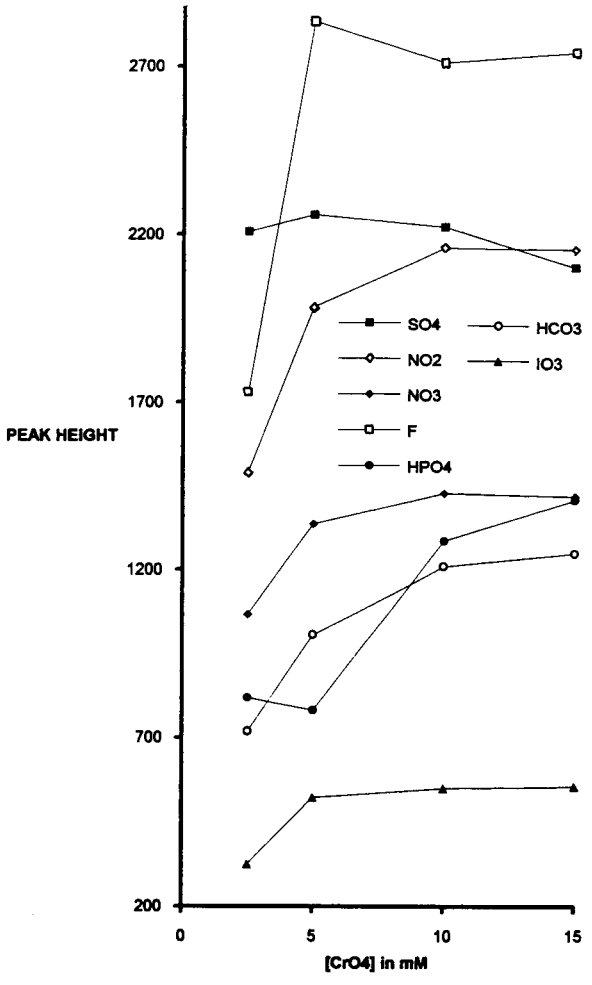

Fig. 2. The effect of the concentration of the background electrolyte on the sensitivity (peak height in 10^{-6} V). For the experimental conditions see Fig. 1.

4.2. Experimental set-up

The experiments were selected using a central composite experimental design. In this way the experimental domain could not only be evaluated completely, but one also has the opportunity to model the responses if necessary. Further, one has the advantage of calculating initial starting conditions for the non-linear regression method. By using the factorial part of the central composite design, one can obtain initial values of K_{ia} and μ_A. The slope and intercept of the function relating mobility to the modifier concentration at low (runs 1 and 3) and high (runs 2 and 4) pH level can be used as initial values of K_{ia} and μ_A for the undissociated and the fully dissociated anions, respectively. The experimental design is presented in Table 1. Runs 1 and 3 are experiments which are done at one (low) pH level, but at low and high levels of modifier concentration. As a linear relationship is expected for the mobility in function of the modifier concentration, one can use the slope of the line between the mobili-

Table 1
Central composite design under the CMC

Run	X_1	pH	X_2	[CTAB]
1	−1	8.60	−1	0.45
2	+1	11.40	−1	0.45
3	−1	8.60	+1	0.85
4	+1	11.40	+1	0.85
5	$-\sqrt{2}$	8.02	0	0.65
6	$+\sqrt{2}$	11.98	0	0.65
7	0	10.00	$-\sqrt{2}$	0.37
8	0	10.00	$+\sqrt{2}$	0.93
9	0	10.00	0	0.65
10 [b]	−1.29	8.20	−1.29	0.39
11 [a]	−0.57	9.20	−0.57	0.54
12 [a]	+0.57	10.80	+0.57	0.76
13 [b]	+1.29	11.80	+1.29	0.91

[a] Within the experimental domain.
[b] Out of the experimental domain.

ties at low and high concentration of the modifier as an initial value for the $K_{ia(i)}$. The intercept of this line can be used as an initial value of the $\mu_{A^{i-}}$. The same procedure can be used at high pH level (runs 2 and 4) to obtain $K_{ia(q)}$ and $\mu_{A^{q-}}$. The central composite design for two variables consisted of 9 runs (run 1–9). However, 13 runs were carried out, four of which were extra points to enable model evaluation. Two of these four extra points were selected within the experimental domain and the other two were selected out of but close to the experimental domain (Table 1).

4.3. Calculation of the coefficients for the models

The coefficients of the models were estimated using non linear regression methods. The monovalent anions such as Br^-, Cl^-, NO_2^-, NO_3^-, I^-, F^-, and IO_3^-, are anions of strong acids. Therefore, the pH has little influence on the mobility of these anions in the selected experimental domain. Expression 6 can be reduced to expression 5. This expression was fitted to the observed mobilities for these anions. To start the procedure of non-linear regression for the estimation of the coefficients in the model, initial values of the coefficients were obtained as described above. However, because of the small pH influence, the mean of the slopes and intercepts calculated for the lines at low and high pH level between the mobility at low and high modifier concentrations were used as the initial K_{ia} and initial $\mu_{A^{q-}}$, respectively. The obtained coefficients are presented in Table 2. As can be seen the ion association constants are different for each anion, leading to the observed difference in selectivity. Of these monovalent anions I^- appears to have by far the strongest affinity for the modifier to form ion association complexes. As was mentioned before, this led to the observed effect of the concentration of CrO_4^{2-} on I^-.

For the divalent anion sulphate, the mobility is also unaffected by the pH in the experimental

Table 2
Estimated coefficients for the models of the anions

Anion	μ_{eff}	K_a	K_{ia}	pK_a(exp) [a]	pK_a(theo) [b]
F^-	0.03454		0.000167		
HPO_4^{2-}	0.032594	0.003605	0.000801	2.44	2.15 (pK_{a1})
		5.67×10^{-7}		6.25	7.2 (pK_{a2})
IO_3^-	0.02447		0.001339		
Cl^-	0.04644		0.010936		
SO_4^{2-}	0.04356		0.020000		
NO_2^-	0.04440		0.024253		
HCO_3^-	0.02855	4.828×10^{-7}	0.031349	6.32	6.35 (pK_{a1})
Br^-	0.04722		0.035125		
PO_4^{3-}	0.034076	4.4160×10^{-12}	0.055327	11.35	12.33 (pK_{a3})
NO_3^-	0.04296		0.056685		
CO_3^{2-}	0.043036	8.4386×10^{-12}	0.087709	11.07	10.33 (pK_{a2})
I^-	0.04474		0.286933		

[a] Experimentally obtained pK_a.
[b] pK_a found in the literature.

domain. The model for sulphate can be reduced to the following expression:

$$\mu_{eff} = \frac{\mu_{A^{2-}}}{\left(K_{ia(2)}[S]^2 + 1\right)} \quad (8)$$

Initial values of the coefficients were obtained as described above. The experimentally obtained coefficients for this model are also presented in Table 2. While the mobility of sulphate is not affected by the pH, this is not the case for the other divalent anion, namely carbonate. For this anion, which has a pK_a value ($pK_{a2} = 10.33$) within the experimental domain, one has to apply expression 6 ($q = 2$) in its complete form. The initial values for μ_{HA^-}, K_{ia1} and $\mu_{A^{2-}}$, K_{ia2} required for the procedure of non-linear regression were also obtained as described above in the experimental set-up section. For the K_{a1} and K_{a2} initial values were obtained from the literature. The calculated coefficients for this model are shown in Table 2.

Phosphate has a pK_a which is slightly higher than the upper pH limit of the experimental domain ($pK_{a3} = 12.33$). Eqn. 6 ($q = 3$) was fitted to the experimentally obtained data. The initial values of the coefficients were selected as for carbonate. The three K_a values were obtained from the literature and were used as initial conditions in the Levenberg-Marquardt agorithm. The coefficients calculated for phosphate are also presented in Table 2. Here too the ion association

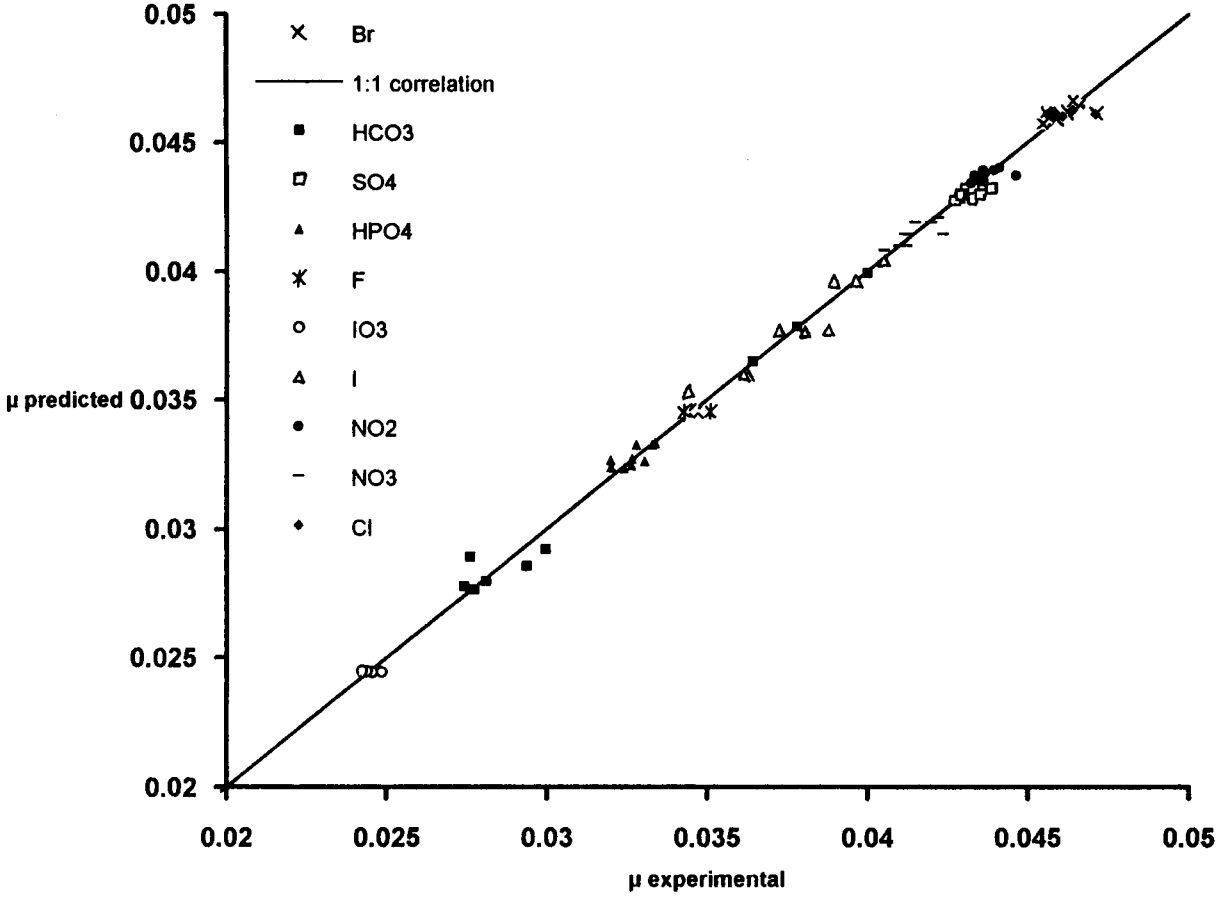

Fig. 3. Correlation between the predicted and experimentally obtained mobilities of the anions. The straight line represents the ideal 1:1 correlation.

constant increases with ionic charge of the anions. This characteristic is comparable to ion exchange chromatography, where the retention of an anion on a resin depends on the charge and the radius of the hydrated ion [15].

The calculated pK_a values of carbonate and phosphate (Table 2) are slightly different from the values in the literature. This difference is probably due to the composition of the buffer, which is not totally aqueous but also contains a fraction of organic compounds, namely the modifier, and/or the inaccuracy of measuring the pH > 10. Khaledi and Smith [8–11] observed a similar pK_a shift in MECC, which was ascribed to the micelles in the buffer. The shift in pK_a depends on the difference in the binding constants of an acid and its conjugated base to micelles. Probably one has a similar kind of effect for the anions and the modifier. The difference in association constants (K_{ia}) of an acid and its conjugated base with the modifier, could have caused the observed shift in pK_a. However, as will be discussed in the following section, the obtained models fitted the experimental data quite well.

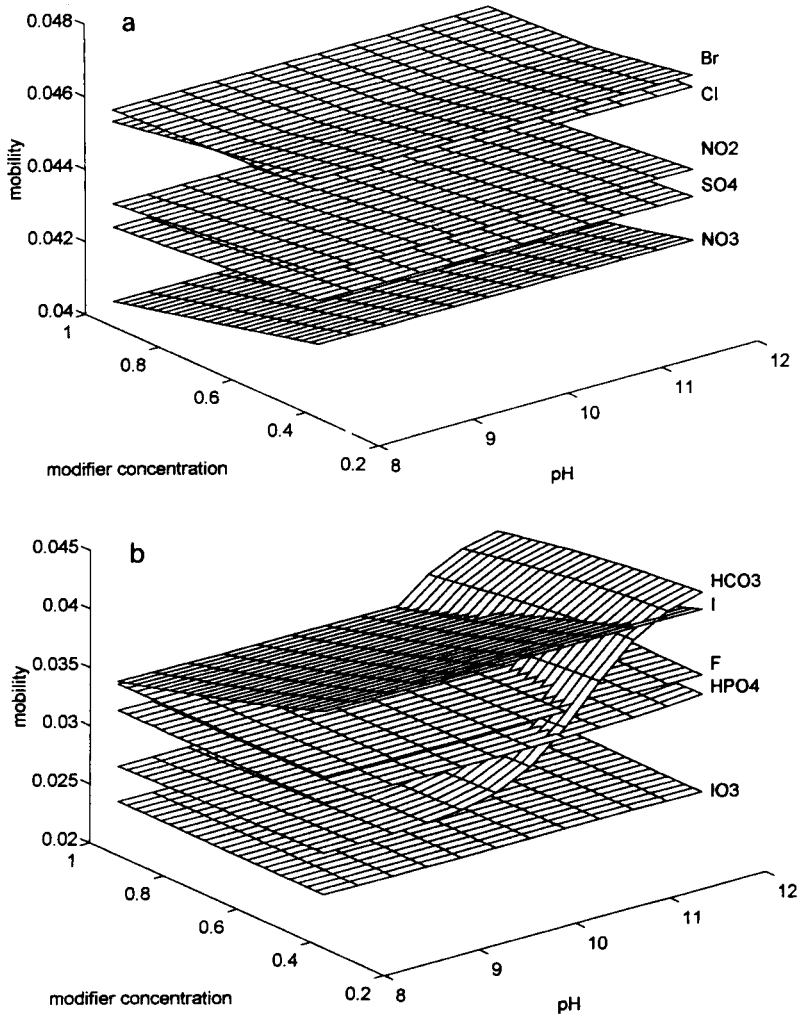

Fig. 4. The calculated response surfaces for the mobility (in $cm^2/V\ s$) of the ten anions in function of the concentration of modifier and the pH. (a) for Cl^-, Br^-, NO_2^-, SO_4^{2-} and NO_3^-, and (b) for F^-, I^-, HPO_4^{2-}, HCO_3^- and IO_3^-.

4.4. Quality of the predictions

The quality of the predictions was evaluated by comparing the predicted values of the mobility with the observed experimental results. The average relative deviations in percentage (A.R.D.%) were generally lower than 1%. In Fig. 3 it can be observed that the predicted values are very well correlated with the experimental results. The continuous line represents the ideal case of 1:1

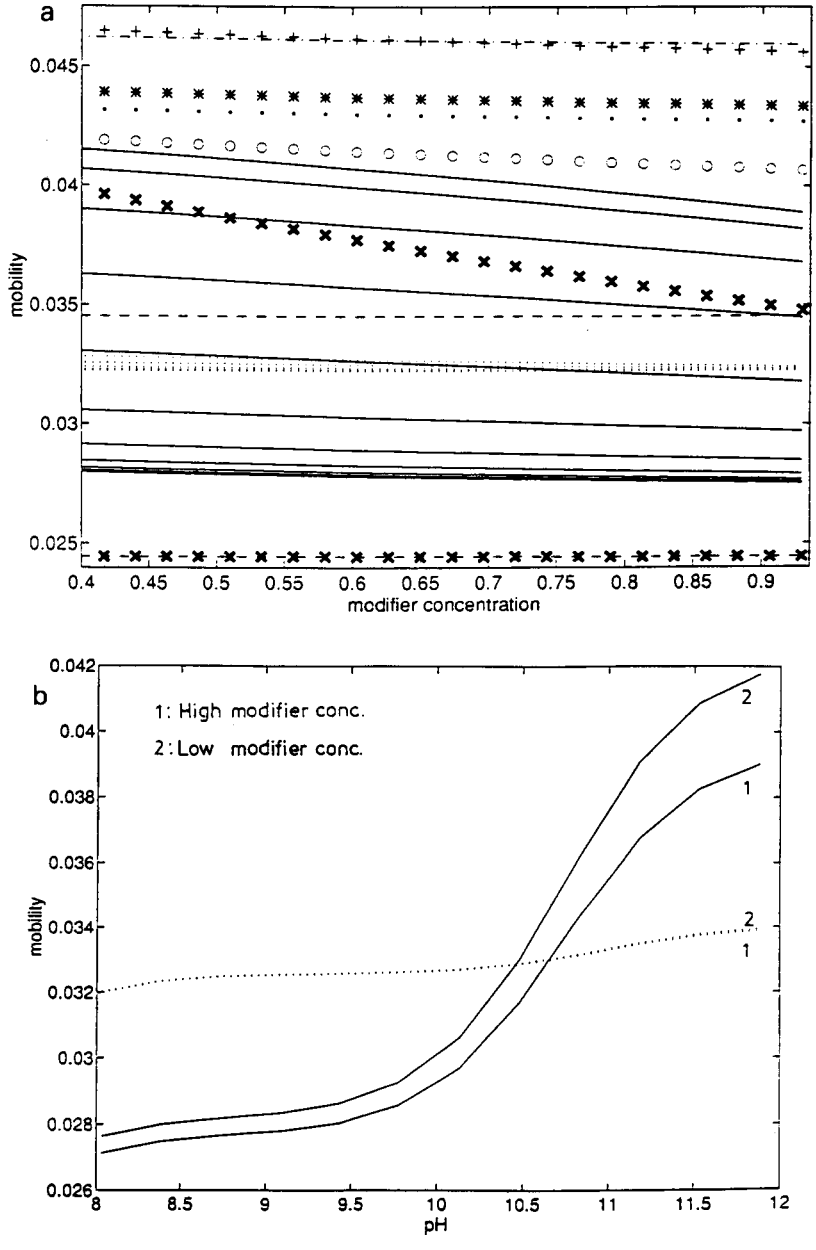

Fig. 5. Two-dimensional plots of the response surfaces of the mobility (in cm^2/V s) as a function of the concentration of the modifier (a) and of the pH (b). Br^-, +; Cl^-, –·–; NO_2^-, *; SO_4^{2-}, ···; NO_3^-, O; F^-, – –; I^-, ×; HPO_4^{2-}, :::; HCO_3^-, —; IO_3^-, -x-.

correlation. The line that fits best through the points has a slope which is not significantly different from 1 [0.99338 (0.983233–1.003527)] and an intercept which is not significantly different from zero [0.000243 (−0.000151–0.000199)]. Therefore, one can accept that the obtained models adequately represent the experimental results.

The response surfaces of the anions are shown in Fig. 4a, for Cl^-, Br^-, NO_2^-, SO_4^{2-}, NO_3^-, and in Fig. 4b for F^-, I^-, HPO_4^{2-}, HCO_3^- and IO_3^-. As can be seen all the anions have a linear surface, except phosphate and carbonate (Fig. 4b). These two anions have a sigmoidal surface, because of the influence of the pH. All the surfaces of the anions show a decline in mobility in function of the concentration of modifier. The steepness of this decline is proportional to the ionic association constant.

The influence of the pH and the concentration of modifier is perceived better if the mobility of the anions is plotted against each variable separately. Fig. 5a is a plot of the mobility in function of the concentration of modifier. As can be seen the mobility of the ions decrease with increasing concentrations of the modifier, except for fluoride and iodate. In this plot it is clear that Br^- crosses-over Cl^- and that carbonate depending on the pH can cross-over phosphate, fluoride, iodide and approaches nitrate. The anions which are affected by the pH (carbonate and phosphate) are represented by different lines in these plots. The steepness of these lines are higher when the mobilities of the anions are high. Higher mobilities are caused by higher pH values. It is evident that the pH only influences the carbonate and phosphate anions. The mobility of these anions shows the expected sigmoidal curvature (Fig. 5b).

4.5. Selectivity optimization

When one is able to predict the mobility of each anion over the experimental domain, one can optimize selectivity. The optimization procedure then requires an optimization criterion. Different criteria can be used to describe the extent of separation in CZE. One often uses the resolution or the separation coefficient (α), which is the ratio of the migration time of two peaks [13]. Kheladi et al. [8–11] used the difference in mobility between two peaks, because this difference is proportional to resolution in CZE. One can model

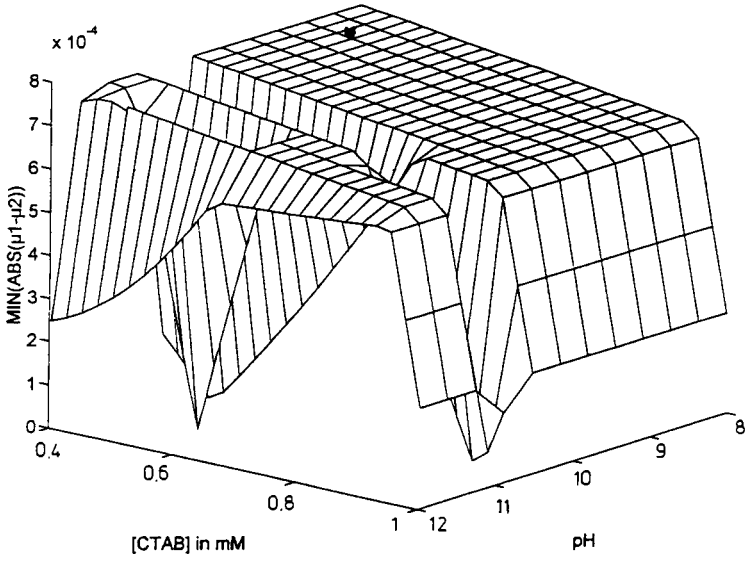

Fig. 6. The calculated minimum absolute difference between the mobilities (in cm^2/V s) of the anions over the experimental domain. The selected point for optimum separation conditions is indicated with a star (*).

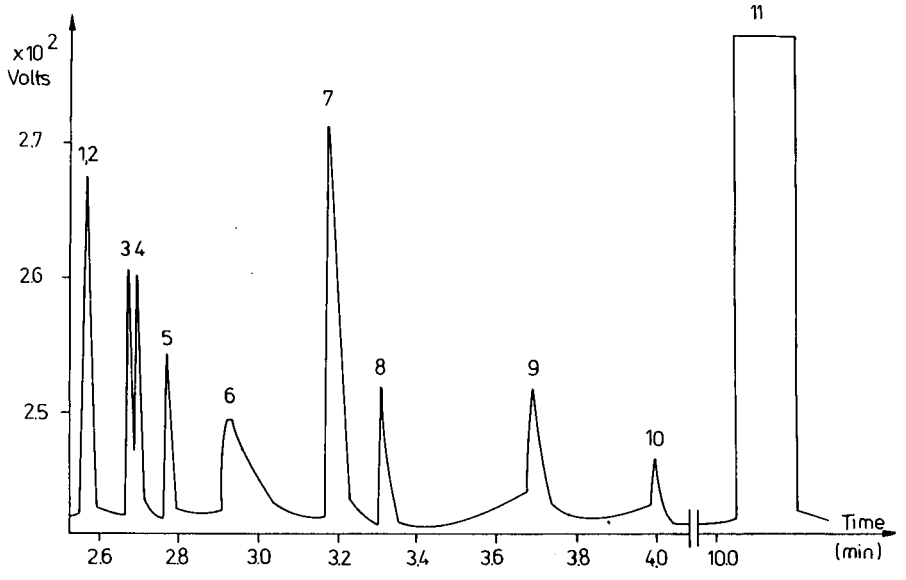

Fig. 7. Electropherogram obtained at the predicted optimal conditions: $[CrO_4^{2-}] = 10$ mM, pH 8.50 and [CTAB] = 0.45 mM. A 10 mg l^{-1} (I^-: 50 mg l^{-1}) mixture of the anions was injected by 15 s hydrostatic injection, the running voltage was 20 kV (with a current of ± 30 μA). Peaks: 1 = Cl^-, 2 = Br^-, 3 = NO_2^-, 4 = SO_4^{2-}, 5 = NO_3^-, 6 = I^-, 7 = F^-, 8 = HPO_4^{2-}, 9 = HCO_3^-, 10 = IO_3^-, 11 = water (EOF-marker).

the mobility of each ion separately over the experimental domain and then select the optimum conditions by determining the highest minimum difference of two peaks. However, one should be aware that this procedure does not consider the width of the peaks.

In this study the latter procedure is applied with a slight adjustment. Instead of selecting the minimum difference between two peaks, the absolute value of the difference of the mobilities of two peaks is calculated. In this way the negative value of the difference at cross-overs is avoided. Afterwards, the minimum absolute difference of each peak pair is determined and used for selection of the optimal conditions. The worst resolved pair of peaks, which in this study is the Br^-–Cl^- peak pair, will determine the outcome of this procedure. In fact, in none of experiments in this experimental domain, a baseline separation was observed for this pair. Therefore, this peak pair was not considered in the selection of the minimum absolute difference in mobility between two peaks. The separation of Br^- from Cl^- is possible at higher concentrations of the modifier, i.e., above the cmc of CTAB. We will report on this in a follow-up article. Other peak pairs which can be important are the NO_2^-–SO_4^{2-}, the I^-–F^- peak pair and the movement of carbonate. The minimum absolute difference of all the peak pairs (except Br^-–Cl^-), over the whole experimental domain is presented in Fig. 6. As can be noticed the minimum absolute difference is high and slightly affected in the region with the following limits: pH between 8.00 and 10.00 and [CTAB]

Table 3
Predicted and experimental migration times of the anions at optimum conditions

Anion	T_m predicted	T_m experimental	A.R.D.%
Br^-	2.589	2.570	0.53
Cl^-	2.556	2.570	0.73
I^-	2.907	2.920	0.46
F^-	3.211	3.180	0.97
NO_2^-	2.691	2.680	0.42
NO_3^-	2.789	2.770	0.68
SO_4^{2-}	2.716	2.700	0.60
HPO_4^{2-}	3.358	3.310	1.44
HCO_3^-	3.623	3.690	1.84
IO_3^-	4.052	4.000	1.29

between 0.40 and 0.90 mM. The optimum separation, however, is situated at low modifier concentration. As discussed before the worst separated peak pair determines the outcome of this procedure. Here, it is the NO_2^-–SO_4^{2-} peak pair. However, in function of the pH and the modifier concentration, one has to deal with crossing-overs of other peak pairs. At concentrations of the modifier higher than 0.90 mM the I^- peak approaches the F^- peak, resulting in a drop of the response surface. At pH > 10 the carbonate peak first crosses–over HPO_4^{2-}, leading to the first decrease and increase of the response surface (Fig. 6). When the pH is further increased carbonate crosses–over F^-, I^-, and approaches the NO_3^- peak, resulting in the down and upward movement of the response surface.

A separation condition was selected in the optimum region: pH 8.50 and [CTAB] = 0.45 mM. The predicted migration times were calculated using the mobility of the EOF (which was calculated using the migration time of the water peak in the electropherogram), experimentally obtained at these conditions. The predicted and experimentally observed migration times are presented in Table 3. There is a good agreement between the predicted and observed migration times. An electropherogram obtained at these conditions is shown in Fig. 7. As can be seen bromide and chloride are not separated (which was expected), the NO_2^-–SO_4^{2-} peak pair is almost baseline separated.

5. Conclusion

The ability to predict the mobility of anions in function of pH and the concentration of the modifier can be helpful in method development and optimization in CIA. The required coefficients (the dissociation constant and the ion association constant) can be determined by non-linear regression methods.

The usefulness of predictions in selectivity optimization was clearly demonstrated for the separation of 10 anions. The overall optimum of the separation was predicted and agreed very well with the experimental results.

Acknowledgments

The authors would like to thank M. Van Bever for the skilful technical assistance and F. Cuesta-Sánchez for the assistance with software in order to draw Figs. 4–6.

References

[1] P. Jandik and W.R. Jones, J. Chromatogr., 546 (1991) 431.
[2] W.R. Jones and P. Jandik, J. Chromatogr., 546 (1991) 445.
[3] P. Jandik, W.R. Jones, A. Weston and P.R. Brown, LC–GC, 5 (1992) 20.
[4] A. Weston, P.R. Brown, P. Jandik, W.R. Jones and A.L. Heckenberg, J. Chromatogr., 593 (1992) 289.
[5] A. Weston, P.R. Brown, P. Jandik, A.L. Heckenberg and W.R. Jones, J. Chromatogr., 593 (1992) 395.
[6] G. Bondoux, P. Jandik and W.R. Jones, J. Chromatogr., 602 (1992) 79.
[7] M. Jimidar, M.S. Khots, T.P. Hamoir and D.L. Massart, Quim. Anal., 12 (1993) 63.
[8] M.G. Khaledi, S.C. Smith, and J.K. Strasters, Anal. Chem., 63 (1991) 1820.
[9] S.C. Smith and M.G. Khaledi, J. Chromatogr., 632 (1993) 177.
[10] P.F. de Aguiar, M. Jimidar and D.L. Massart, Application of the logistic transformation for the prediction of anion mobility in capillary ion analysis, submitted for publication.
[11] S.C. Smith and M.G. Khaledi, Anal. Chem., 65 (1993) 193.
[12] T. Kaneta, S. Tanaka, M. Taga and H. Yoshida, Anal. Chem., 64 (1992) 798.
[13] Cs. Horvath, W. Melander and I. Molnar, Anal. Chem., 49 (1977) 142.
[14] M. Jimidar, T. Hamoir, W. Degezelle, D.L. Massart, S. Soykenç and P. Van de Winkel, Anal. Chim. Acta, 284 (1993) 217.
[15] O.A. Shpigun and A. Zolotov, Ion Chromatography in Water Analysis, Ellis Horwood, London, 1988, pp. 40–41.

ELSEVIER

Analytica Chimica Acta 294 (1994) 177–184

ANALYTICA CHIMICA ACTA

Effect of sample pressure on membrane inlet mass spectrometry

István Futó [a], Hans Degn [b,*]

[a] *Institute of Nuclear Research of the Hungarian Academy of Sciences, Debrecen, Hungary*
[b] *Institute of Biochemistry, Odense University, DK-5230 Odense, Denmark*

Received 1st February 1994

Abstract

The effect of sample pressures up to 6 bar on the signal of a membrane inlet mass spectrometer was studied with supported and unsupported membranes of silicone rubber. In both cases we found undesirable pressure effects. With a supported membrane increasing sample pressure causes a reduction of the signal. This is because lateral diffusion of analyte in the interstitial space between the membrane and the membrane support contributes to the transport of analyte to the mass spectrometer, and the space available for this diffusion is increasingly compressed by increasing sample pressure. With an unsupported membrane increasing sample pressure causes an increasing signal, which is caused by the fact that an unsupported membrane bulges increasingly with increasing sample pressure. The consequently increased area and decreased thickness of the membrane results in increased flux of analyte. Bulging depends strongly on the diameter of the unsuppported membrane area and on the thickness of the membrane. With a 0.185 mm thick membrane spanning a circular hole of 1 mm diameter the bulging is minimal and there is no significant aberration due to sample pressure up to 2 bar. With a larger diameter, a larger pressure or a thinner membrane, significant aberrations occur including change of relative selectivity to polar and unpolar analytes and hysteresis when the pressure is changed up and down. These effects are due to non-linear elastic deformation of the membrane. The effects described should be taken into account in the design of membrane probes for systems where pressure changes may occur.

Key words: Mass spectrometry; Membrane inlet mass spectrometer; Sample pressure effects

1. Introduction

In membrane inlet mass spectrometry (MIMS) the sample to be analyzed is separated from the vacuum by a thin polymer membrane through which analyte diffuses from the sample into the vacuum of the mass spectrometer [1,2]. Under normal laboratory conditions the sample is under atmospheric pressure and no significant pressure changes occur during the measurement. However, if a flow-through cell is used or the membrane probe is inserted into a large scale reactor the pressure experienced by the sample may differ from atmospheric pressure and it may vary considerably during the measurement. Although MIMS is currently used under such conditions, for example monitoring of bioreactors [3–5], the

* Corresponding author.

SSDI 0003-2670(94)00138-C

effect of pressure on MIMS seems not to have been studied before.

Theoretically, the signal of a membrane inlet mass spectrometer is expected to depend upon the sample pressure. The theoretical effect of pressure depends on whether the sample is a gas mixture or a solution. If the sample is a gas mixture the rate of transport of a component of the mixture through the membrane is proportional to the difference between the partial pressures of that component at the two sides of the membrane. Since all partial pressures are practically zero in the vacuum, the rate of transport of a component of a gas mixture is proportional to the partial pressure of the component outside the membrane. The partial pressure, p_i, of a component of an ideal gas mixture depends on the total pressure, p_{tot}, according to the equation

$$a_i = p_{tot} x_i \quad (1)$$

where x_i is the mole fraction of the component. Therefore the signal of a component of a gas mixture is expected to be proportional to the total pressure. On the other hand if the sample is a liquid mixture the rate of transport through the membrane of a component of the mixture is proportional to the activity (relative partial pressure) of that component. The activity, a_i, of a component of a liquid mixture obeying Raoult's law depends on the total pressure according to the approximate equation

$$a_i = x_i \exp[(p_{tot} - 1)V_i/RT] \quad (2)$$

where V_i, R and T are the molar volume, the gas constant and the temperature, respectively. By substitution of relevant numeric values into Eq. 2 it is found that the activity of a component of an ideal liquid mixture is only weakly dependent on the hydrostatic pressure. For example it takes a total pressure of 10 bar to increase the activity of water by 1% [6]. Therefore, the signal of a component of a liquid sample is expected to be practically independent on the hydrostatic pressure within the range covered by the present study (1–6 bar).

In the course of our work with MIMS we have noticed that the signal from a liquid sample may be sensitive to small changes of the sample pressure and the effect depends on the design of the inlet. In order to find the source of this problem we have tested different inlet designs with respect to pressure sensitivity. In most published designs of membrane inlets the membrane is supported by a porous disk or a disk perforated with small holes (< 1 mm). It is a common feature of these designs that some of the membrane area which is exposed to the sample is supported by a solid surface. Analyte which penetrates the membrane

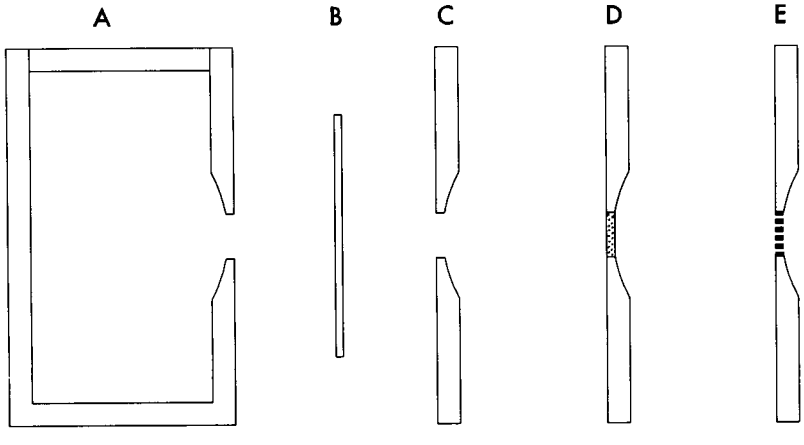

Fig. 1. Schematic representation of membrane inlet made for the investigation of pressure effects. The membrane (B) is clamped between a plane side of the sample cell (A) and a modified blind flange (C, D or E) mounted on the mass spectrometer adjacent to the ion source. The membrane can be mounted without support (C), with a porous disk support (D) or a perforated disk support (E).

at such locations may diffuse laterally through the interstitial space between the membrane and the supporting surface to the porous disk or a hole leading into the mass spectrometer. The reason for the pressure sensitivity of the signal is that the space available for lateral transport of analyte depends on how hard the membrane is pressed against the support. Our finding indicates that the membrane inlet should be designed such as to minimize lateral diffusion. An unsupported membrane is preferable if the signal is sufficiently large with a small membrane area.

2. Experimental

Three different versions of an inlet with a flat membrane were made as shown schematically in Fig. 1. The membrane (B) is clamped between a plane side of the sample cell (A) and a plane surface of a blind flange mounted on the mass spectrometer. The side of the sample cell has a hole which is matched by a hole (C) a perforated disk (D) or an area perforated with several small holes (E) in the blind flange. The version with unsupported membrane (C) was made with three different diameters of the matching holes, 1, 1.5 and 2 mm. The two versions with supported membrane (D and E) had a 2.5 mm diameter hole in the sample cell wall. The porous disk had the same diameter as the hole in the cell wall and the supporting area in version (E) was perforated with seven holes of 0.4 mm diameter. The volume of the sample cell was 5 ml and all parts were made of stainless steel. The sample cell was thermostated and fitted with a magnetic stirrer. All measurements were done at 30°C. Liquid samples were stirred during the measurement in order to avoid concentration gradients adjacent to the membrane surface. The membrane was made of silicone rubber film of 0.186 mm (Dow Corning, Midland, MI) or 0.125 mm (Technical Products, Decatur, GA) thickness as stated. The measuring cell had a cover which could be fixed with screws. It was pressurized by compressed nitrogen or other gas as stated. The pressure was made to increase or decrease linearly with time at a rate of 0.2 bar/min by the help of a computer controlled feed back device based on a pressure transducer (Honeywell type 242PC100G).

A tubular inlet of the catheter type [5] was constructed from a stainless steel capillary with an internal diameter of 2 mm and several holes of 0.5 mm drilled trough its wall near the closed tip. The perforated tip of the probe was covered with silicone rubber tubing serving as the permeable membrane. The tip of the catheter was inserted into a steel cylinder which was pressurized as described above. The measurements were done with a quadrupole mass spectrometer (VG-Micromass Model SX200) equipped with a turbomolecular pumping unit (Balzers Model TPH060) and a cold cathode vacuum gauge (Balzers Model IKR020). Measurements were done at the following mass/charge ratios: nitrogen 28, oxygen 32, argon 40, ethyl acetate 61 and 1,4-dioxane 88.

3. Results and discussion

3.1. Unsupported flat membrane

We have used a sample cell with an unsupported membrane (E in Fig. 1) of 1 mm diameter and a total pressure of up to 2 bar to verify Eq. 1. Fig. 2 shows the effect of pressurizing gaseous

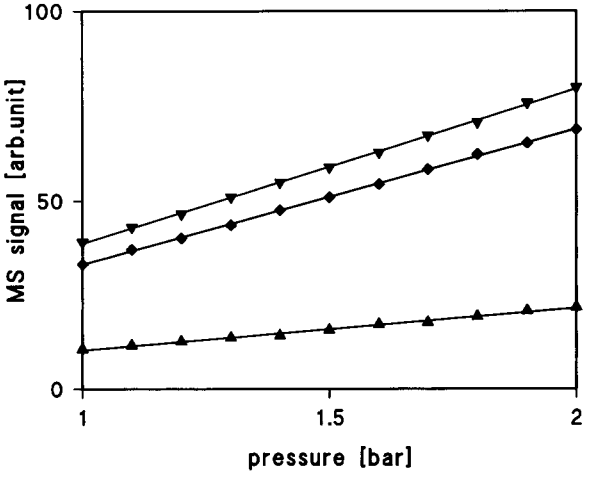

Fig. 2. Pressure dependence of mass spectrometric signals of gaseous samples measured with unsupported membrane. Oxygen (◆) and nitrogen (▼) were measured simultaneously in an air sample. Argon (▲) was measured in a pure gas sample.

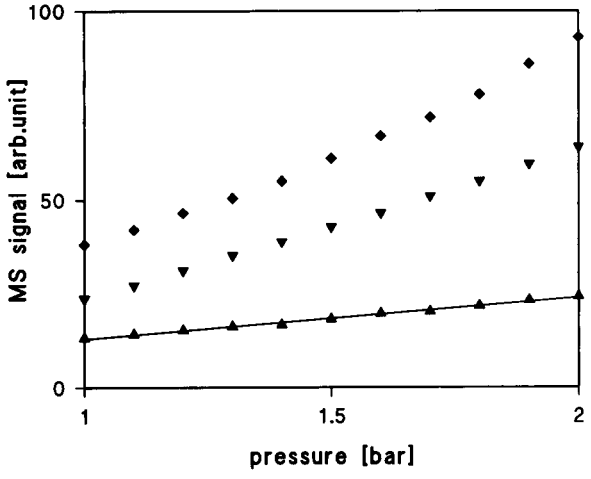

Fig. 3. Pressure dependence of mass spectrometric signal from pure nitrogen measured with unsupported membrane and different diameters of the membrane. The diameters were 1 (▲), 1.5 (▼) and 2 mm (◆).

samples, namely atmospheric air and argon, in such a cell. It is seen that within this pressure range the signals increase linearly with the pressure and the lines intersect at the absolute pressure of zero bar as expected from Eq. 1. In order to investigate the effect of the diameter of the unsupported membrane area the experiment was repeated with three different diameters and pure nitrogen as the sample (Fig. 3). It is seen that the signal shows an increasing positive deviation from the theoretically expected linear dependence on the pressure as the diameter of the unsupported membrane area is increased. This effect is due to a bulging deformation of the unsupported membrane. The deformation results in an increased area and a decreased thickness of the membrane. Both effects cause the transport rate of analyte through the membrane to increase. An unsupported silicone rubber membrane covering a hole of 1 mm diameter can withstand a pressure difference of several bar, although increasing pressure causes increasing deformation of the membrane. Below 2 bar of total pressure the deformation is negligible and there is no significant deviation from Eq. 1. However the deformation caused by the pressure and hence the positive deviation of the signal increases very rapidly with the diameter of the unsupported area.

Similar experiments as shown in Figs. 2 and 3 were done with liquid samples in order to verify Eq. 2. Fig. 4 shows an experiment where the effect of pressure on the signal from pure water was measured with three different diameters of the unsupported membrane. With the 1 mm hole the signal is practically constant as predicted by Eq. 2. With holes of larger diameters the signal increases significantly with the pressure. The explanation is the same as for the positive deviations found in similar measurements on a gaseous sample (Fig. 3).

It is concluded from the experiments shown in Figs. 2–4 that within the range of total pressure up to 2 bar there is no significant deviation from the results predicted by Eqns. 2 and 3 for gaseous and liquid samples, respectively, when measurements are done with an unsupported membrane of 1 mm diameter. With a membrane of 1.5 mm diameter or more there are significant aberrations caused by deformation of the membrane. The practical implication for the design of membrane inlets is that an unsupported membrane of 1 mm diameter is recommendable because pressure sensitivity is insignificant up to a total pressure of 2 bar. Since the signal of a membrane

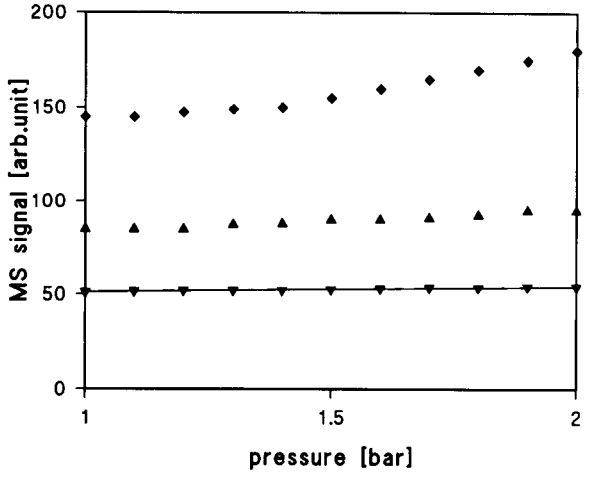

Fig. 4. Pressure dependence of mass spectrometric signal of pure water sample measured with unsupported membrane and different diameters of the membrane. The diameters were 1 (▼), 1.5 (▲) and 2 mm (◆).

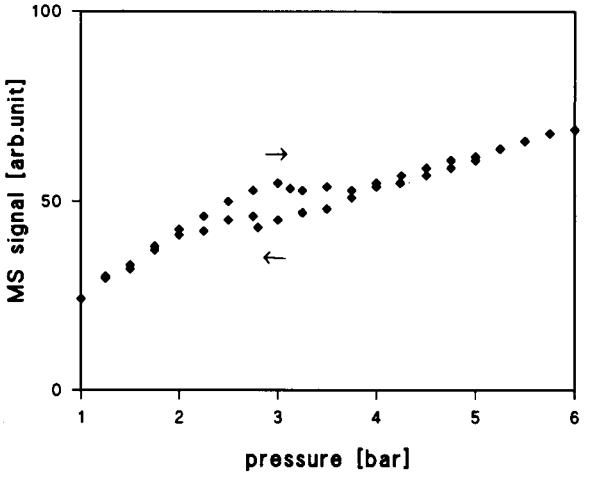

Fig. 5. Hysteresis in pressure dependence of mass spectrometric signal of pure nitrogen sample measured with membrane supported by a perforated surface. The traces were produced with increasing and decreasing pressure as indicated by arrows.

inlet mass spectrometer is proportional to the area of the membrane there is much to be gained with respect to sensitivity by increasing the diameter. However, a large membrane must be supported. In most published designs the support is a porous disk or a solid surface perforated with several small holes.

3.2. Supported flat membrane

Measurements on gas and liquid samples with a solid membrane support perforated with small drilled holes are shown in Figs. 5 and 6 respectively. The two traces in each figure are the results of first increasing and then decreasing the pressure with time. It is seen that the signals are always smaller than expected. At a total pressure of 5 bar the signal is in both cases about 50% of the expected. Hysteresis occurs when the pressure is increased and decreased. Similar but smaller effects of pressure are observed (not shown) when the membrane is supported by a porous disk.

The main difference between the pressure effects on measurements with unsupported and supported membranes is that in the former case the signal is increased above the expected value by pressure and in the latter case it is decreased. The positive aberration found with unsupported membranes can be ascribed to bulging of the membrane. When the membrane bulges, its area increases and its thickness decreases. Both mechanical effects result in increased rate of transport of analyte through the membrane provided that the deformation of the membrane material does not decrease its permeability. The negative aberration obtained with a supported membrane can be ascribed to compression of the interstitial space between the membrane and the support. Analyte which passes the membrane at a place where the membrane rests on a supporting surface will find its way to a hole or a pore leading into the mass spectrometer by lateral diffusion through the interstitial space. Increased sample pressure causes the membrane to be pressed harder onto the support and the interstitial space available for lateral diffusion is narrowed.

3.3. Hysteresis

In the experiments with a supported membrane shown in Figs. 5 and 6 hysteresis was observed. This phenomenon was even more pronounced, in measurements with unsupported membranes when the pressure was increased

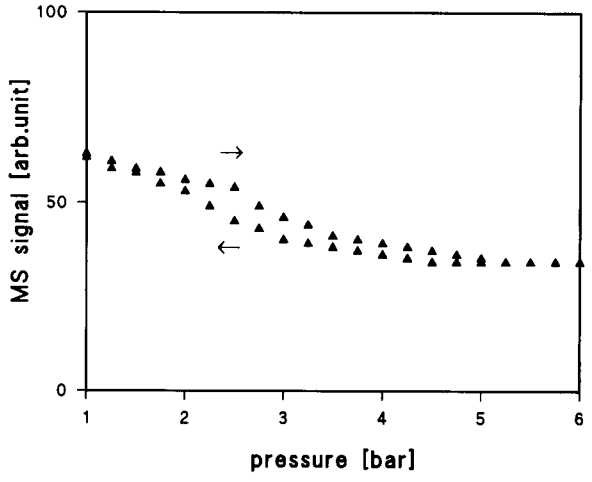

Fig. 6. Hysteresis in pressure dependence of mass spectrometric signal of pure water sample measured with membrane supported by a perforated surface. Arrows show direction of change of pressure.

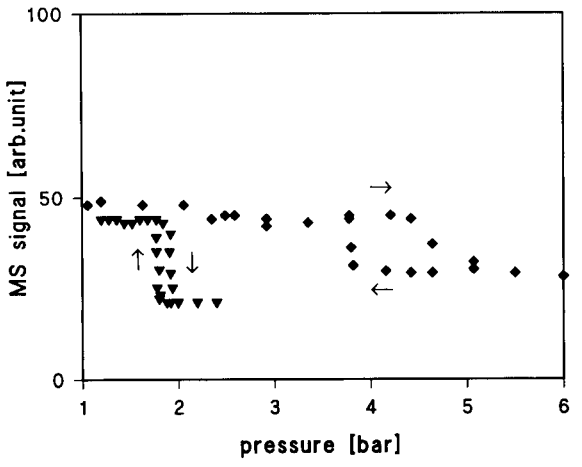

Fig. 7. Hysteresis in pressure dependence of mass spectrometric signal of 0.34 M ethyl acetate dissolved in water measured with unsupported membrane of 1 mm diameter and membranes of different thickness. The membranes were 0.125 (▼) and 0.186 mm (◆) thick. Arrows show direction of change of pressure.

above the the limit of 2 bar which was used in the experiments shown in Figs. 2–4. Fig. 7 shows an experiment where ethyl acetate in aqueous solution was measured in a cell with an unsupported membrane of 1 mm diameter. The measurements were done with two membranes of different thickness and the total sample pressure was taken up to 6 bar. It is observed that the signal of dissolved ethyl acetate is practically independent on the pressure until a certain critical point beyond which the signal falls rapidly to about one half of its initial value. When the pressure is reduced below this critical point the signal returns abruptly to the initial level. Since the two events do not take place at the same pressure a hysteresis loop appears. The hysteresis loop occurs at a much lower pressure with the thinner membrane than with the thicker one.

We think that the hysteresis phenomenon is due to non-linear elastic properties of the membrane material. The elastic deformation of a 0.186 mm thick membrane covering a hole of 1 mm diameter is small and within the linear domain as long as the pressure does not exceed 2 bar. When the pressure is increased to about 4 bar the membrane is strongly deformed and the elastic response of the material is no longer linear. Unfortunately we have found no published data on the mechanical properties of silicone rubber which could be used to substantiate our explanation of the observed hysteresis. The few data available are produced by stretching strips of the material. Such data are not easily applied to a system of a different geometry.

Since the pressure where hysteresis occurs decreases with increasing diameter of the membrane it is possible to adjust the diameter so that the pressure where hysteresis occurs is equal to or lower than the actual sample pressure. It would not seem advisable to use an unsupported membrane under the exact conditions where hysteresis occurs because the signal might jump up and down as a result of small pressure changes. It cannot be excluded that an unsupported membrane inlet can be used under conditions where the sample pressure is higher than the hysteresis range. This seems to be the case with some published inlet designs [7]. However, under such conditions the membrane is bulging so much that a deep cavity exist, at the sample side of the membrane. Such a cavity is difficult to stir efficiently and a concentration gradient of analyte near the membrane surface may invalidate the measurement.

3.4. Pressure effect on relative membrane permeabilities for analytes

The determination of pressure effects on measurements on aqueous solutions of different organic compounds gave seemingly contradictory results. Fig. 8 shows measurements with an unsupported membrane of 1 mm diameter on a solution of ethyl acetate and 1,4-dioxane in water. It is seen that the signal of dioxane was increasing markedly while the signal of ethyl acetate was decreasing slightly with increasing pressure. In both cases there was a simultaneous rapid transition to a lower signal when a certain critical pressure was reached. Similar measurements with different organic compounds indicate that, as a rule, the signal from a non-polar compound responds as exemplified by ethyl acetate and the signal from a more polar compound responds as

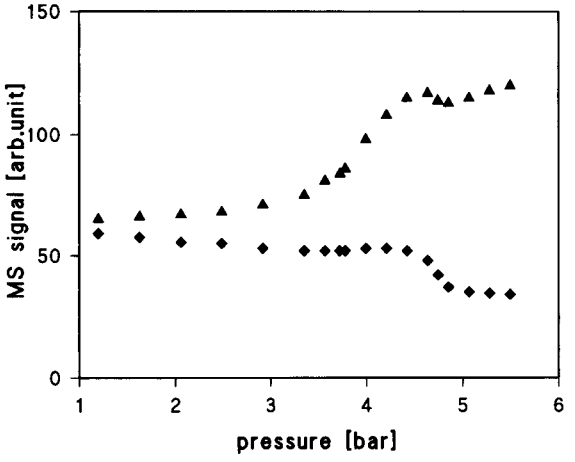

Fig. 8. Pressure dependence of mass spectrometric signals of different organic compounds dissolved in water. 0.34 M ethyl acetate (♦) and 0.34 M 1,4-dioxane (▲) were measured simultaneously at increasing pressure.

exemplified by dioxane in Fig. 8. These results indicate that the permeability properties of the membrane are altered as a result of stretching of the membrane material. The permeability to polar compounds increases and the permeability to non-polar compounds decreases as the material is stretched.

3.5. Tubular membranes

Although the scope of the present work was on pressure effects on flat membranes we have also performed an experiment with a supported tubular membrane. The results (not shown) were similar to those obtained with a flat membrane supported by a perforated surface as shown in Fig. 6. This is not surprising because a supported tubular membrane inlet suffers from the same flaw as a supported flat membrane inlet, namely that lateral interstitial diffusion of analyte may contribute significantly to the signal and this contribution is very pressure sensitive.

Unsupported tubular membranes (hollow fibers) have been employed in many inlet designs. Such inlets may be divided into two classes, those with the sample inside [8] and those with sample outside [9]. One would think that a tubular membrane with sufficient wall thickness to prevent collapse under pressure would be less affected by compression from an outside pressure than by expansion from an inside pressure. This remains to be tested.

4. Conclusion

Our results indicate that pressure sensitivity is an important factor to be taken into account in the design of membrane probes for used in systems where pressure changes may occur. Designs where significant areas of membrane are in contact with the sample on the outside and supported by a solid surface on the vacuum side should be avoided because lateral diffusion of analyte in the interstitial space between the membrane and the supporting surface will give a significant and very pressure sensitive contribution to the signal. If the total sample pressure is below 2 bar the optimal design is a flat membrane clamped between two plane surfaces with matching holes of no more than 1 mm diameter for contact with the sample and the vacuum, respectively. With higher sample pressure, larger membrane area or thinner membrane, an unsupported membrane may not burst but it will be so strongly deformed that it exhibits non-linear elastic properties resulting in hysteresis and its selectivity properties for analytes are changed. When a large membrane area is needed in order to obtain sufficient signal or when the sample pressure is high the membrane must be supported. A support consisting of a solid surface perforated with small holes is the most unfavourable because of pressure sensitive lateral diffusion of analyte. A porous disk support is preferable but it does not entirely prevent aberrations due to pressure sensitive lateral diffusion of analyte. It should be emphasized that all our experiments were done with silicone rubber membranes which are the most frequently used. Since different membrane materials have different mechanical properties our results cannot be applied directly when other membrane materials are used.

References

[1] H. Degn, R.P. Cox and D. Lloyd, Methods Biochem. Anal., 31 (1985) 165.
[2] T. Kotiaho, F.R. Lauritsen, T.K. Choudhury, R.G. Cooks and G.T. Tsao, Anal. Chem., 63 (1991) 875A.
[3] E. Heinzle, Adv. Biochem. Eng./Biotechnol., 35 (1987) 1.
[4] E. Heinzle and M. Reuss (Eds.), Mass Spectrometry in Biotechnological Process Analysis and Control, Plenum, New York, 1988.
[5] S. Bohátka, I. Futó, I. Gál, G. Langer, J. Molnár, A. Paál, G. Pintér, M. Simon, J. Szádai, G. Székely and J. Szilágyi, Vacuum, 44 (1993) 669.
[6] P.A. Rock, Chemical Thermodynamics, University Science Books, Mill Valley, CA, 1983.
[7] M.E. Bier, T. Kotiaho and R.G. Cooks, Anal. Chim. Acta, 231 (1990) 175.
[8] M.A. LaPack, J.C. Tou and C.G. Enke, Anal. Chem., 63 (1991) 1631.
[9] L.E. Dejarme, S.J. Bauer, R.G. Cooks, F.R. Lauritsen, T. Kotiaho and T. Graf, Rapid Commun. Mass Spectrom., 7 (1993) 935.

ELSEVIER

Analytica Chimica Acta 294 (1994) 185–193

ANALYTICA CHIMICA ACTA

Flame atomic absorption spectrometric determination of silver in geological materials using a flow-injection system with on-line preconcentration by coprecipitation with diethyldithiocarbamate

Shiqiao Pei [1], Zhaolun Fang *

Flow Injection Analysis Research Center, Institute of Applied Ecology, Academia Sinica, Box 417, 110015 Shenyang, China

Received 14th December 1993; revised manuscript received 11th March 1994

Abstract

Trace amounts of silver in geological samples were determined by flame atomic absorption spectrometry. The analyte was preconcentrated and separated from the bulk of the matrix by on-line coprecipitation with the iron(II)–diethyldithiocarbamate complex in the presence of 1,10-phenanthroline in a flow-injection system. The precipitate was collected in a knotted reactor without using a filter. The precipitate was dissolved in isobutyl methyl ketone and introduced directly into the nebulizer-burner system of an atomic absorption spectrometer. 1,10-Phenanthroline was added to the sample solution to mask large concentrations of iron(II). The tolerance of the method for iron was thus increased to 4 g l^{-1}. An enhancement factor of 26 and a concentration efficiency of 28 min^{-1} were obtained for a coprecipitation time of 45 s, resulting in a sampling frequency of 62 h^{-1}. The detection limit (3σ) in the sample solution was 0.5 $\mu g\ l^{-1}$. The relative standard deviation at the 30 $\mu g\ l^{-1}$ level was 2.1%. The analytical results obtained for geological reference materials were in good agreement with the certified values.

Key words: Flow injection; Atomic absorption spectrometry; Coprecipitation, on-line; Silver in geological materials; Iron interference

1. Introduction

Silver often occurs in geological materials at extremely low concentration levels (10^{-1}–10^{-2} mg kg^{-1}). Such background levels are sometimes below the quantitation limit of methods based on flame atomic absorption spectrometry (AAS), in which case a time-consuming preconcentration step, involving solvent extraction [1], ion-exchange [2] or coprecipitation [3] has to be implemented. Although electrothermal AAS may provide better sensitivity, a pre-separation is nevertheless unavoidable in order to remove the bulk of the interfering matrices. Neutron activation analysis and inductively coupled plasma mass spectrometry are sufficiently sensitive for measurements at these background levels. However, such facilities are not available in most geological laboratories.

[1] On leave from Institute of Rock and Mineral Analysis, Ministry of Geology and Mineral Resources, Beijing, China.

* Corresponding author.

SSDI 0003-2670(94)00132-6

Recently, flow-injection (FI) on-line separation and preconcentration techniques were shown to be very effective in enhancing the sensitivity and selectivity of AAS methods for the determination of trace constituents in samples with complex matrices [4,5]. Among the various separation approaches reported, coprecipitation methods seem to offer the highest tolerance to sample matrices with high transition metal contents. Fang et al. [6] developed a flame AAS method for the determination of lead in biological samples using FI on-line coprecipitation, based on a batch process involving coprecipitation with hexamethyleneammonium hexamethylenedithiocarbamate (HMA-HMDTC) using an iron(II) carrier [3]. The method exhibited high efficiency and sensitivity as well as high tolerance to matrix constituents in biological samples, achieving a tolerable level of 400 mg l^{-1} for iron. Later this approach was successfully extended to the determination of other trace metals in a large variety of biological and clinical samples by Welz et al. [7]. However, the tolerance capacity of the FI coprecipitation procedure was significantly lowered compared to the original batch procedure, which was used to determine trace elements in pure iron metal and iron compounds [8]. Although the batch procedure has been used successfully for the determination of trace elements in soils and sediments, when adapted into a FI system, the selectivity of the procedure is no longer sufficient for such determinations. These disabilities are the consequence of the limited capacities of on-line precipitate collectors.

Recently our group developed a novel FI preconcentration method for FAAS, collecting the soluble diethyldithiocarbamate (DDC) complexes of trace metals on the walls of a knotted reactor (KR) by sorption [9]. The method was successfully applied to the determination of cadmium in water samples, but with samples containing high concentrations of transition metals, precipitation was observed in the reactor, and strong interferences were encountered. However, this phenomenon stimulated further studies on using DDC and a suitable carrier as a coprecipitation agent to improve the selectivity of the preconcentration procedure. Iron(II) was used as a carrier, and 1,10-phenanthroline was used as a masking agent to further enhance the selectivity. These measures resulted in an on-line preconcentration AAS system for trace silver which significantly enhanced the sensitivity and which tolerated iron contents up to 4 g l^{-1}. The method was used to determine silver in geological materials at the 10^{-1}–10^{-2} mg kg^{-1} level.

2. Experimental

2.1. Equipment

A Model WFX-1D (Beijing Second Optical Instrument Factory) atomic absorption spectrometer, equipped with a silver hollow cathode lamp and a model X1 chart-recorder (Shanghai Dahua Instruments) was used without background corrector. The lowest possible acetylene flow-rate of 1 l min^{-1} was used with an air flow-rate of 10 l min^{-1} to produce a lean flame so that flame conditions were close to optimum when isobutyl methyl ketone (IBMK) was introduced into the flame during the precipitate dissolution. The lowest damping level of 0, slit width 0.2 nm and uptake rate 7 ml min^{-1} were used.

A Model LZ-2000 computerized FI processor (Zhaofa Institute of Laboratory Automation, Shenyang) was used for on-line preconcentration. The instrument was equipped with two separately programmable peristaltic pumps, and an 8-channel, 16-port rotary injector valve. The actuation times of the injector valve and pumps were controlled automatically through the computer program. Since IBMK is incompatible with PVC pump tubes, a solvent displacement bottle was used to deliver the solvent. Water was pumped through the inlet tube which extended to the bottom of the sealed displacement bottle, and IBMK (Beijing Chemicals) was displaced from the top layer through the outlet tube at an identical flow-rate.

Knotted reactor precipitate collectors were made by tying interlaced knots in 0.5 mm i.d., 1.2 mm o.d. PTFE tubing as described in Ref. 6. All connections in the FI manifold were made using 0.5 mm i.d. PTFE tubing.

2.2. Reagents and standard solutions

All reagents were of analytical-reagent grade unless specified otherwise and deionized water was used throughout.

1% (m/v) DDC (Beijing Chemicals) was prepared by dissolving the appropriate amount of sodium diethyldithiocarbamate in a buffer of pH 9.2 (0.01 mol l^{-1} acetic acid–0.02 mol l^{-1} ammonia in water); the solution was filtered when necessary.

1% (m/v) 1,10-phenanthroline (Shenyang Reagent Co. No. 3) was prepared in water containing 2% ethanol.

10% (m/v) ascorbic acid (Northeast Pharmaceutical Co., Shenyang) was freshly prepared each day.

Hydrochloric, nitric, hydrofluoric and perchloric acid (Beijing Chemicals) were of ultrapure grade.

10.0 g l^{-1} iron(III) solution was prepared by dissolving the appropriate amount of iron(III) chloride in water.

Standard solutions containing 50, 40, 30, 20, 10 and 5 μg l^{-1} silver were prepared by multi-stage dilutions of a 100 mg l^{-1} stock solution. The standard solutions were made to contain 2 g l^{-1} iron(III) by adding the appropriate amount of 10.0 g l^{-1} iron(III) solution. The standards were made to contain 0.05 mol l^{-1} nitric acid in the final solution. A few drops of 3% (m/v) sulphosalicylic acid solution were added, and the iron was reduced to its divalent state using 10% ascorbic acid, indicated by a fading of the red colour. A few more drops of the reductant were then added.

2.3. Procedures

Decomposition of geological materials was carried out according to Ref. [10]: 0.5–1 g of ground geological materials were accurately weighed into PTFE crucibles. 15 ml of hydrofluoric acid (48%), 3 ml of hydrochloric acid (37%) and 1 ml of perchloric acid (70%) were added and the crucibles were placed on a sand bath and heated at low boiling temperature to near dryness. After cooling, 10 ml of freshly prepared aqua regia were added and again the samples were heated to dryness. 2.5 ml of 1 mol l^{-1} nitric acid and 20 ml of water were added for complete solubilization. The samples were filtered when necessary, and 100 μl 3% sulphosalicylic acid and 7.5 ml of 10 g l^{-1} of iron(III) were added. 10% ascorbic acid was added dropwise until the red colour had faded completely. An additional 3 drops of the reductant were then added. Finally 2 ml of 1% phenanthroline were added, and the digests made up to 50 ml with water. When the iron contents were known to be higher than 2 g l^{-1} in the sample digests, the addition of iron carrier was omitted.

The FI manifold for on-line precipitate collection and dissolution is shown in Fig. 1, together with the optimized operating parameters. Sample and precipitant were introduced by pump B and the solvent by pump A, respectively. Pump B was activated and pump A was stopped during the loading (preconcentration) stage, which lasted for 45 s, except specified otherwise Fig. 1 (a). Sample and reagent merge at a point about 10 mm upstream of the KR collector. The reaction after merging is assumed to be almost instantaneous, but nothing could be collected until the solvent from the previous run had been expelled from the collector. The time required to expel the solvent completely was dependent on the length of the collector conduit and the sample flow-rate. For a collector length of 150 cm, and a sample flow-rate of 4.2 ml min^{-1}, the expulsion lasted approximately 4 s, after which one could observe a gradual increase of black precipitate adhering to the walls of the collector. The effluent emerging from the collector was discarded and simultaneously water was aspirated into the nebulizer by suction to define the baseline. The loading stage was terminated when the injector turned to dissolution position (Fig. 1b). The dissolution (injection) stage was set to 13 s, during which pump B (sample) was stopped; the IBMK solvent was pumped into the collector, whereupon the sorbed complex and precipitate adhering to the walls of the collector was dissolved and analyte was transported into the nebulizer preceded by a small volume of waste sample which had occupied the collector at the initiation of the dissolution stage.

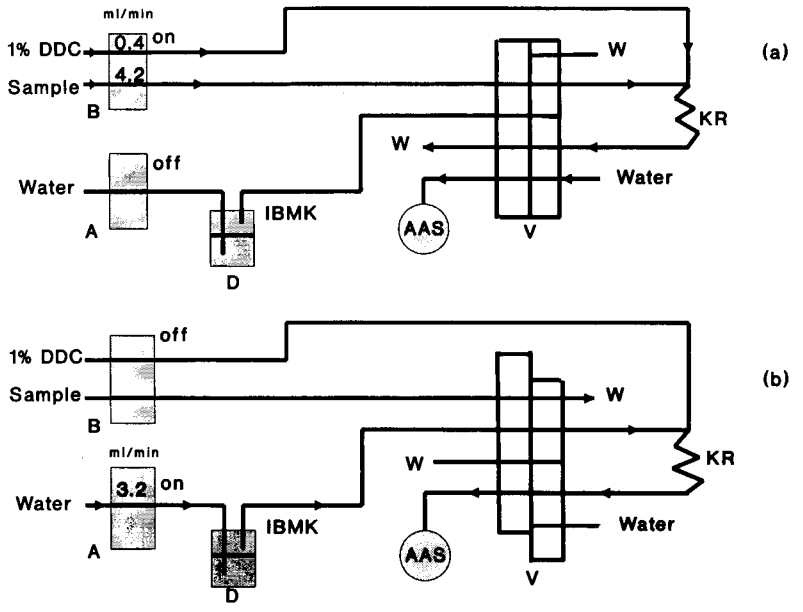

Fig. 1. Flow-injection manifold for on-line coprecipitation-dissolution. V, injector valve; A and B, peristaltic pump; D, displacement bottle; KR, knotted reactor; W, waste; and FAAS, flame atomic absorption spectrometer. (a) Precipitation stage; (b) dissolution stage.

The peak absorbance of the dissolution signal was used for quantification.

The system was calibrated by making triplicate measurements of each standard solution of the standard series mentioned previously, using a 45 s sample loading period. Peak heights were measured manually from the recordings, and average height was used for the construction of calibration curves.

2.4. Method development

The chemical and FI parameters were optimized mainly using an univariate approach, taking sensitivity (peak absorbance) as the principle figure of merit, but with concurrent considerations on reproducibility and efficiency. Parameters used successfully in previous studies for on-line coprecipitation employing Fe(II)–HMDTC [6] were used as a starting point for further optimizations. The variables studied included sample loading and dissolution flow-rates, sample loading time, knotted reactor length, DDC, iron, and phenanthroline concentrations and pH. Two or three cycles of preliminary experiments were required to establish the fixed parameters for each univariate study, so that they approach optimum values.

3. Results and discussion

3.1. Preliminary studies on the preconcentration system

Initially, attempts were made to adapt the preconcentration approach involving sorption of soluble DDC metal complexes on a knotted reactor [9] to preconcentrate silver from geological matrices. Although high enrichment factors were obtained using standard solutions, serious interferences were encountered from coexisting copper and, particularly, iron. Under high iron(III) concentrations, large amounts of precipitates were formed with DDC which cannot be effectively collected in the knotted reactor. The situation is further complicated owing to the fact that the mechanism of analyte collection was at least par-

tially changed to coprecipitation, bringing difficulties into the optimization. Reduction of the iron(III) to iron(II) decreased the amount of precipitate formed but not the extent of interference. Various masking agents, including EDTA, 1,10-phenanthroline, tartaric, sulphosalicylic, and citric acids, were tested under different acidities to keep the iron in complexed form. None of the masking agents prevented precipitation. However, phenanthroline was found to produce a decreased amount of precipitate which was easily collectable in the knotted reactor. This prompted us to optimize the preconcentration system based on coprecipitation principles, using Fe(II)–DDC as a carrier, and phenanthroline as masking agent.

In order to further study the analyte collection mechanism of the system, silver was collected after adding DDC but without introducing the iron carrier. A preconcentration effect was also observed under similar operational parameters without precipitation, although the enhancement factor was about a factor of two worse than that with a coprecipitation carrier. This demonstrated that the Ag–DDC complex could also be retained on the walls of the knotted reactor through sorption. Since the reaction time before collection is extremely short, it is quite probable that the collected analytes were retained through a combination of sorption and coprecipitation processes.

3.2. Optimization of chemical variables

The chemical variables of the on-line preconcentration system were optimized as described under method development. The results on the effects of DDC, phenanthroline and iron, nitric acid concentrations on peak absorbance of silver are shown in Figs. 2–5, respectively.

The effects of the concentration of DDC in the final reaction mixture on silver peak absorbance, in the presence of 2.0 g l^{-1} Fe and 0.04% phenanthroline, are shown in Fig. 2. The absorbance remained almost constant from 0.5 to 1.5% DDC, within which concentration range a fine precipitate was produced which was easily collected on the reactor walls. The decrease in peak height at lower concentrations implies insufficient reagent for complexing the carrier and

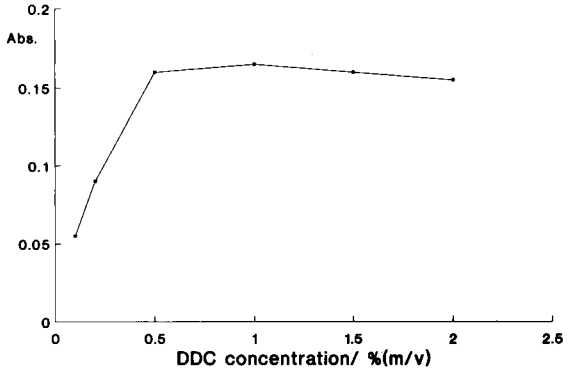

Fig. 2. Effect of DDC concentration on the peak absorbance of 30 μg l^{-1} silver [with 2 g l^{-1} iron(II) and 0.04% phenanthroline]. FI conditions as in Fig. 1.

analyte. However, high concentrations of DDC induce the production of large precipitate volumes which are more difficult to manipulate. The gradual decrease of sensitivity at the higher concentrations was probably due to failure in collecting the larger amount of precipitate formed. Therefore, a medium DDC concentration of 1.0% was used in further studies.

The effect of 1,10-phenanthroline masking agent on the coprecipitation of silver with 1.0% DDC and 2 g l^{-1} Fe is shown in Fig. 3. An almost steady response was obtained above a concentration of 0.02% in the sample digest. However, a concentration of 0.04% was adopted to provide a safety margin for higher iron concentrations.

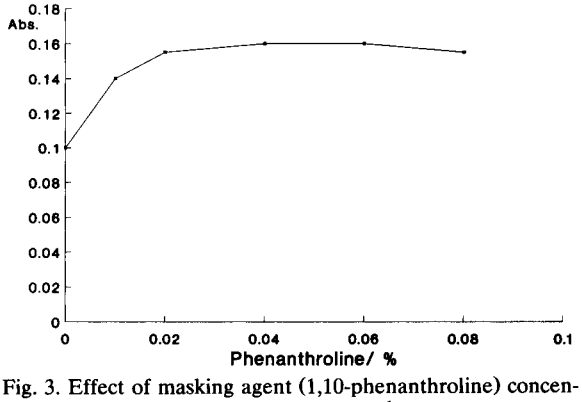

Fig. 3. Effect of masking agent (1,10-phenanthroline) concentration on peak absorbance of 30 μg l^{-1} silver in a solution containing 2 mg l^{-1}, 1% DDC. FI conditions as in Fig. 1.

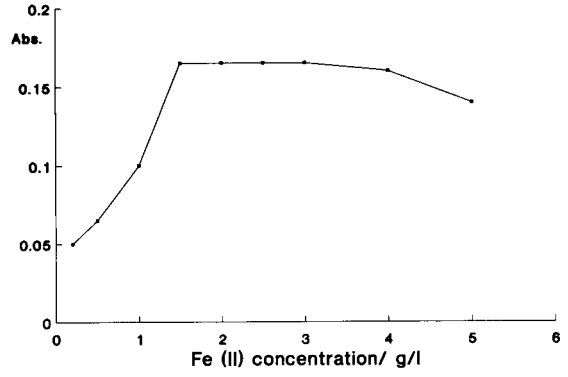

Fig. 4. Effect of iron(II) concentration on peak absorbance of 30 μg l^{-1} silver, containing 0.04% phenanthroline, 1% DDC. FI conditions as in Fig. 1.

Since the Fe(II)–DDC complex acted as a carrier for the coprecipitation of silver, it is essential that a minimum concentration of iron be present in the sample. This is demonstrated by the significant decrease in peak absorbance in the presence of less than 1.5 g l^{-1} of iron(II) in Fig. 4. The absorbance remained almost constant up to about 4.0 g l^{-1} iron(II), above which a gradual decrease in the absorbance of silver was observed owing to large precipitate particles being dislodged from the reactor walls. According to these results, 2.0 g l^{-1} iron were added to all standard solutions. The addition of 1.5 g l^{-1} iron is recommended for most geological samples, since iron present in the sample should be sufficient to bring the concentration well within the tolerable range of 1.5 – 4 g l^{-1} Fe. Obviously, addition of iron should no more be necessary when iron concentrations in the sample are known to exceed 2 g l^{-1} in the digest.

The influence of nitric acid concentration on the coprecipitation of silver using Fe(II)–DDC as precipitant and phenanthroline as masking agent is shown in Fig. 5. The sensitivity decreased above an acid concentration of 0.1 mol l^{-1}, but remained quite stable within 0.01–0.1 mol l^{-1}. The acidity was readily controlled at 0.05 mol l^{-1} HNO_3 for further studies.

3.3. Optimization of FI variables

With very short reactor lengths of below 120 cm an almost linear relationship between the peak response and reactor length was observed (Fig. 6). For longer lengths of tubing the absorbance gradually approached a constant value, which seemed to imply the completeness of precipitate collection at such lengths. In order to evaluate the retention efficiency under such conditions, the waste solution emerging from the outlet of a 150 cm knotted reactor was collected and analyzed for residual silver by extracting the solution with IBMK and determining silver in the organic phase by conventional flame AAS. The

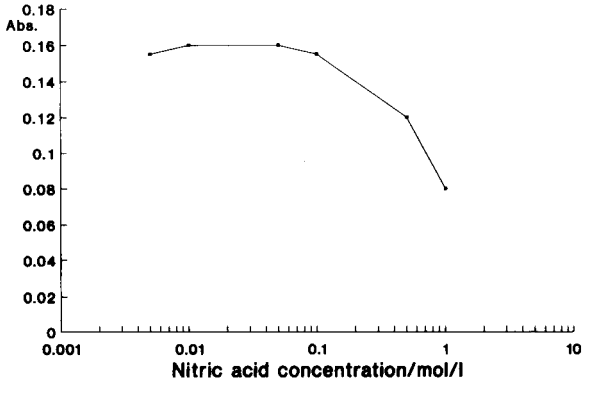

Fig. 5. Effect of nitric acid concentration on peak absorbance of 30 μg l^{-1} silver in a solution containing 2 g l^{-1} iron(II) and 0.04% phenanthroline, 1% DDC. FI conditions as in Fig. 1.

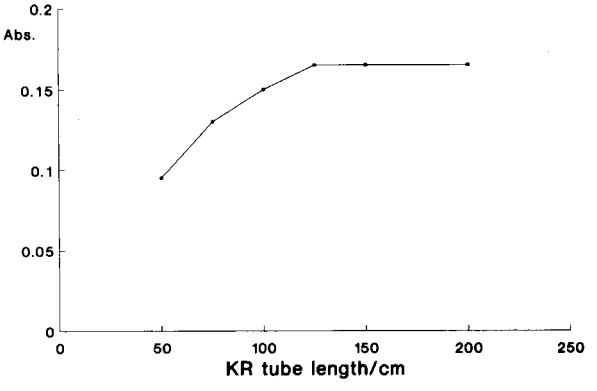

Fig. 6. Effect of length of 0.5 mm i.d. PTFE knotted reactor on peak absorbance of 30 μg l^{-1} silver in a solution containing 2 g l^{-1} iron (II) and 0.04% phenanthroline. Other FI conditions as in Fig. 1.

silver in the waste was less than 54% of the original concentration, which demonstrates the incompleteness of the coprecipitation. This may be explained by the short reaction time of about 4–5 s experienced by the on-line coprecipitation, in contrast to 15 min standing time for the batch coprecipitation procedures [3]. However, the incompleteness of mass transfer does not affect the precision or accuracy of determinations, as demonstrated in another FI on-line coprecipitation procedure [7]. On the contrary, this feature might be one of the reasons for the relatively high selectivity of the procedure.

In on-line preconcentration systems with time-based sampling the sample delivery rate determines the amount of sample to be processed in a given period of time. This rate is often limited by the flow resistance of the reactor and the rate of the reaction. The effect of sample flow-rate on peak absorbance of silver in a solution containing 2 g l^{-1} iron(II) and 0.04% phenanthroline using a 150 cm reactor is shown in Fig. 7. A non-linear relationship between peak response and flow-rate was observed, with the slopes of the graphs levelling off somewhat at flow-rates below 2 ml min^{-1} and above 4.2 min ml^{-1}. The decreased retention observed at low flow-rates may be explained by the smaller centrifugal force created in the knotted reactor under these conditions. Such forces were considered to be an important factor in retaining the precipitate [11]. The decreased retention efficiency observed at higher flow-rates was attributed to insufficient time for completion of coprecipitation. Although better sensitivities may be obtained using higher flow-rates, a moderate flow-rate of 4.2 ml min^{-1} was used in further studies for long term trouble-free operation. Excessive back-pressures built up occasionally under high sample flow-rates, leading to leakage and deterioration in precision.

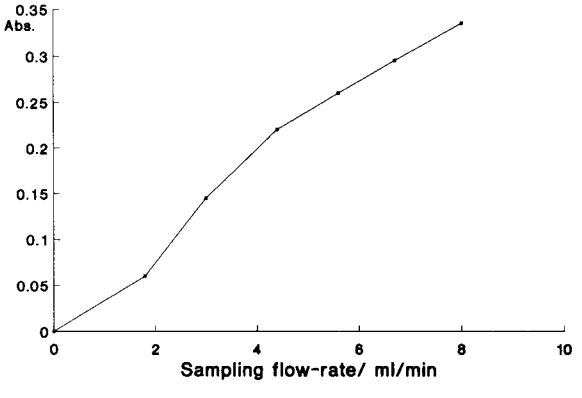

Fig. 7. Effect of sampling flow-rate on peak absorbance of 30 μg l^{-1} silver in a solution containing 2 g l^{-1} iron(II) and 0.04% phenanthroline. Other FI conditions as in Fig. 1.

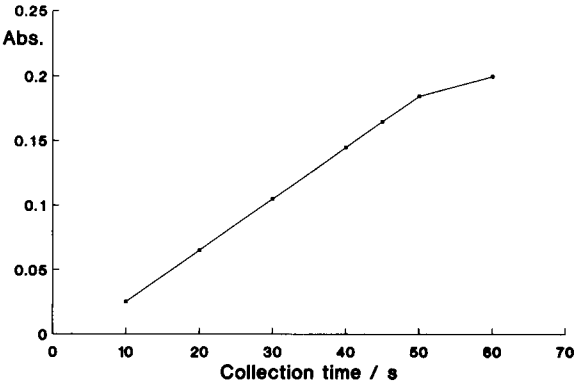

Fig. 8. Peak absorbance of 30 μg l^{-1} silver [with 2 g l^{-1} iron(II) and 0.04% phenanthroline] for different collection (sampling) periods; other FI conditions as in Fig. 1.

Within certain limits, the enhancement factor increases with the duration of the sampling (precipitation) period. The precipitate collection time is limited by the capacity of the collector and the amount of precipitate produced within a preconcentration cycle. The results obtained using different collection times with samples containing 2 g l^{-1} iron(II) and 0.04% phenanthroline are shown in Fig. 8. The relationship between collection time and peak absorbance was almost linear between 10 s and 50 s, with an interception on the time axis at approximately 4 s, which was the time required to expel the residual IBMK from the reactor at the beginning of the precipitation stage. A precipitate collection period of 45 s was used to achieve better concentration efficiency.

The flow-rate of the IBMK dissolution solvent was found to be an important parameter among the variables of the on-line coprecipitation-dissolution system (Fig. 9). A gradual decrease in the peak absorbance for silver was observed at flow-rates lower than 2.5 ml min^{-1}, apparently

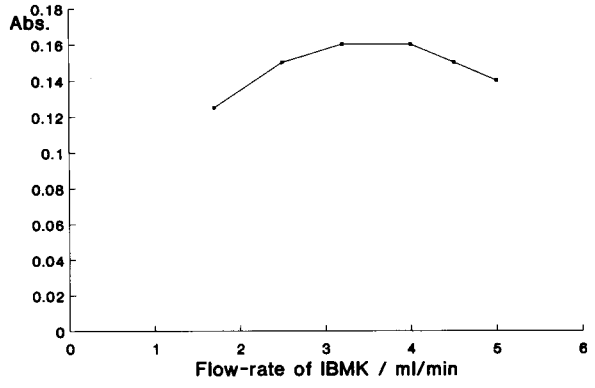

Fig. 9. Effect of solvent flow-rate on peak absorbance of 30 μg l^{-1} silver in a solution containing 2 g l^{-1} iron(II) and 0.04% phenanthroline. Other FI conditions as in Fig. 1.

Table 1
Interference of coexisting ions (30 μg l^{-1} Ag)

Ions	Conc. (mg l^{-1})	Recovery (%)	Ions	Conc. (mg l^{-1})	Recovery (%)
Cd(II)	20	94	Zr(IV)	1	95
Co(II)	10	91	Ni(II)	20	90
Zn(II)	20	100	Sn(IV)	1	94
Cu(II)	10	93	Pb(II)	1	92
Se(IV)	2	100	La(III)	1	100
Sb(III)	2	98	Pd(II)	1	94
Bi(III)	2	98	Hg(II)	0.1	92
As(III)	2	96	Au(III)	1	100
Mo(V)	4	91	Mn(II)	100	95
V(V)	1	100	Cr(III)	10	93
Ba(II)	20	95	Be(II)	0.4	95
Sr(II)	20	98	Fe(III)	2000	94

owing to flow starvation in the nebulizing system. A similar decrease in the peak absorbance was found at flow-rates higher than 4.0 ml min^{-1}, presumably owing to insufficient dissolution time for the solvent. The relatively wide plateau of maximum response, which extended from 2.5 to 4.0 ml min^{-1}, should imply good tolerance of flow-rate fluctuations. An optimized dissolution flow-rate of 3.2 ml min^{-1} was used in the final procedure.

3.4. Interference studies

Effects of potential interferents occurring in geological samples on the determination of silver were investigated using the optimized FI coprecipitation system. The results in Table 1 generally show good tolerance to the species studied. Iron may be tolerated up to a concentration of 2 g l^{-1} Fe(II) in the presence of the same amount of carrier. The tolerable level may be increased to 4 g l^{-1} when the precipitation carrier is omitted, and the iron in the sample is used as carrier.

3.5. Performance of the on-line coprecipitation–dissolution system

Characteristic performance data for the on-line coprecipitation–dissolution preconcentration system are presented in Table 2. For a precipitate collection (sampling) time of 45 s and a sampling frequency of 62, an enhancement factor of 26 was obtained for silver compared to the sensitivity

Table 2
Performance of the on-line coprecipitation-dissolution preconcentration flame AAS system

Linear calibration range	0–50 μg l^{-1} silver
Regression equation (y = abs., $x = [Ag^+]$ in μg/l, $n = 6$)	$y = 0.00176 + 0.00549x$
Correlation coefficient	$r = 0.9996$
Sampling frequency	62 h^{-1}
Enhancement factor [a]	26
Concentration efficiency	28 min^{-1}
Detection limit (3σ) in digest	0.5 μg l^{-1}
R.S.D. (30 μg l^{-1} silver, $n = 11$)	2.1%
Sample consumption	3.2 ml
IBMK consumption	0.7 ml
1% DDC solution consumption	0.2 ml
Percentage of analyte retained on KR collector	46%

[a] Compared with conventional sample introduction of an aqueous solution with nebulizer uptake rate at 7 ml min^{-1}.

Table 3
Results for the determination of silver in geological reference materials. All values in $\mu g\ g^{-1}$ silver

Reference Material	Certified	Found ($n = 6$)
GSS-1	0.35	0.34 ± 0.016
GSS-5	4.4	4.3 ± 0.15

obtained at 7 ml min^{-1} uptake by conventional aspiration. This corresponded to a concentration efficiency of 28 min^{-1}.

The accuracy of the method in the analysis of geological materials was tested using two standard reference soil samples. The results are shown in Table 3. The agreement between the results obtained with the proposed method and the certified value was good.

4. Conclusions

FI on-line preconcentration using Fe(II)–DDC as coprecipitation agent and phenanthroline as masking agent is capable of significantly enhancing the sensitivity and selectivity for the determination of silver in geological materials by flame AAS while maintaining the high efficiency of AAS procedures. The proposed method may be applicable to the determination of other trace elements in geological materials and even iron-based metal samples with minor modifications.

Acknowledgments

This study is supported by a research funding from the Technical Support Department, Academia Sinica. One of us (S.P.) expresses his gratitude to the Instrumental Analysis Centre of Academia Sinica, Shenyang Branch for supporting his stay in FIARC. The authors express their gratitude to Shukun Xu and Lijing Sun for useful discussions and technical assistance.

References

[1] Q. Jiang, Shaanxi Dizhi Shiyan, 2 (1980) 47.
[2] Y.-Z. Li, Z. Rao and Y.-L. Zhu, Yankuang Ceshi, 9(3), (1990) 47.
[3] R. Eidecker and E. Jackwerth, Fresenius' Z. Anal. Chem., 328 (1987) 469.
[4] Z.-Y. Tang, Z.-X. Jin, Q. Lu and F.-Y. Tian, Yankuang Ceshi, 12(1) (1993) 15.
[5] S.-Q. Pei and Z.-L. Fang, Yankuang Ceshi, in press.
[6] Z.-L. Fang, M. Sperling and B. Welz, J. Anal. At. Spectrom., 6 (1991) 301.
[7] B. Welz, S.-K. Xu and M. Sperling, Appl. Spectrosc., 45 (1991) 1433.
[8] R. Eidecker and E. Jackwerth, Fresenius' Z. Anal. Chem., 331 (1988) 401.
[9] Z.-L. Fang, S.-K. Xu, L.-P., Dong and W.-Q., Li, Talanta, submitted for publication.
[10] L.-Z. Li (Ed.), Rock and Mineral Analysis, Vol. 1, Geology Press, Beijing, 3rd edn., 1991, p. 862.
[11] Z.-L. Fang, Flow Injection Separation and Preconcentration, VCH, Weinheim, 1993, p. 186.

ELSEVIER

Analytica Chimica Acta 294 (1994) 195–199

ANALYTICA CHIMICA ACTA

Stopped-flow injection kinetic determination of multicomponent samples: Simultaneous determination of mercury(II) and silver(I)

Jianhua Wang *, Ronghuan He

Chemistry Department of Yantai Teacher's College, Yantai, China

Received 6th July 1993; revised manuscript received 9th March 1994

Abstract

A catalytic method is proposed for the simultaneous determination of mercury(II) and silver(I) based on their catalytic effect on the ligand substitution reaction rate between hexacyanoferrate(II), $[Fe(CN)_6]^{4-}$ and α,α'-bipyridyl. The reaction was monitored with a stopped-flow injection method and detected spectrophotometrically at 536 nm. Most of the commonly coexisting foreign ions do not interfere with the determination, except for Fe^{3+}, Co^{2+} and Zn^{2+}. The calibration graphs are linear in the ranges 0–75 ng ml^{-1} Hg(II) and 0–64 ng ml^{-1} Ag(I), and the detection limits are 0.5 ng ml^{-1} Hg(II) and 1.0 ng ml^{-1} Ag(I), respectively. Mercury(II) and silver(I) content in tap water, wastewater and a synthetic sample has been determined with the proposed procedure, the relative standard deviations being 3.52–5.20% for mercury (II) and 3.20–4.39% for silver(I).

Key words: Flow injection; Kinetic methods; UV–visible spectrophotometry; Catalysis; Mercury(II); Multi-component analysis; Silver(I)

1. Introduction

The determination of trace amounts of mercury(II) and silver(I) is of growing importance in environmental analytical chemistry. Among the methods most commonly used, kinetic procedures have successfully been applied [1–5]. However, there are serious interferences and in most cases the reproducibilities are poor. The mercury(II) and silver(I) content in wastewaters have been determined with a catalytic procedure based on their catalytic effect on the ligand substitution reaction between hexacyanoferrate(II) and α,α'-bipyridyl with thiourea as an activator [6,7], but suitable separation procedures must be introduced due to serious interferences of other compounds.

In a previous paper [8], we proposed a stopped-flow injection kinetic method for the simultaneous determination of a ternary mixture based on the principles of induced reactions. In this paper, we demonstrate that it is feasible to determine several components simultaneously without separation with a similar kinetic method based on catalytic reactions of any type, i.e. redox reactions or ligand substitution reactions. The

* Corresponding author.

SSDI 0003-2670(94)00125-6

content of mercury(II) and silver(I) in wastewater is determined with the proposed procedure.

2. Experimental

2.1. Reagents

Mercury(II) stock solution (5 μg ml^{-1}). Dissolve 0.0427 g $Hg(NO_3)_2 \cdot 3H_2O$ in 250 ml water to obtain a stock solution of 100 μg ml^{-1}. Working solutions were prepared by appropriate dilution with water of pH 3.2.

Silver(I) stock solution. Dissolve 0.0787 g $AgNO_3$ in 100 ml water to give a 500 μg ml^{-1} stock solution. Working solutions of 5 μg ml^{-1} were prepared by dilution with water of pH 3.2. The solution was stored in a brown flask.

Hexacyanoferrate(II) solution. Dissolve 4.220 g of $K_4[Fe(CN)_6] \cdot 3H_2O$ in 250 ml water to get a stock solution of 4.0×10^{-2} mol l^{-1}. Working solutions were prepared by appropriate dilution with distilled water of pH 3.2.

α,α′-Bipyridyl solution (5.0×10^{-3} mol l^{-1}). 0.1953 g of α,α′-bipyridyl were dissolved in 5 ml alcohol, filled to 250 ml with water and adjusted to pH 3.2.

Thiourea solution. 3.0×10^{-2} mol l^{-1}, pH 3.2.

Buffer solution (pH 3.2). Prepared by mixing appropriate volume of sodium acetate (1 mol l^{-1}) and HCl (1 mol l^{-1}); the pH was checked with a pH meter.

All solutions were prepared with analytical reagent grade chemicals and twice distilled water.

2.2. Apparatus

All absorbance measurements were made using a Model 721 spectrophotometer at 536 nm, which is connected to a Syntone FIA-2400 analyzer with two peristaltic pumps of 10 channels and controlled by a computer. The sample solutions were introduced via a 16-way injection valve with a sample loop of 30 μl. The temperature was controlled with a Syntone FIA-T01 and a JY-501B thermostat, and the pH was measured with a PXS-5 pH meter.

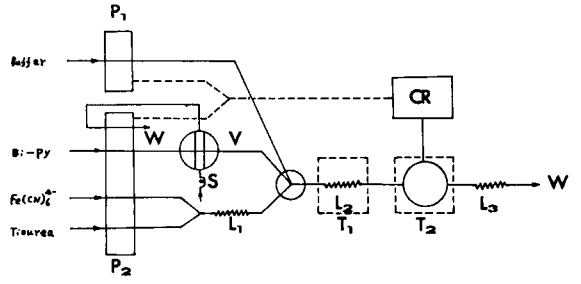

Fig. 1. The manifold used in the determinations. P_1, P_2 = peristaltic pumps controlled by computer; V = injection valve; L_1, L_2 = mixing coils; L_3 = back pressure coil; W = waste liquor; S = sample; CR = controlling and data processing unit; T_1, T_2 = thermostats.

Fig. 1 shows the manifold. The inner diameter of the PTFE tube is 0.5 mm, and that of the back pressure coil is 0.25 mm. The length of mixing coils L_1, L_2 and back pressure coil L_3 are 150, 200 and 3000 mm, respectively. The flow-rate of the buffer solution was 2.4 ml min^{-1}, and those of α,α′-bipyridyl, hexacyanoferrate(II) and thiourea were both 2.0 ml min^{-1}.

2.3. Principles of determination

To illustrate the principle, a kinetically determined reaction: A + B → P, is considered. Suppose that the ions C_1, C_2, $\cdots$ C_i are catalysts for this reaction, and that there are no interactions between catalysts or between intermediates of these catalyzed reactions. In most cases, the catalyst C_i reacts first with one of the reagents A (or B), and an intermediate (M) is formed. Then M reacts with another reagent producing the final product, P:

$$A + C_i \underset{k_{-1}}{\overset{k_1}{\rightleftharpoons}} M \xrightarrow[B]{k_2} P$$

the intermediate concentration, and the product formation rate at time t are:

$$[M]_{it} = k_1[A][C_i]/(k_{-1} + k_2[B])$$

$$R_{it} = d[P_i]/dt = k_2[M]_{it}$$

Suppose that A and B are present in great excess, and that C_i immediately reverts to its original

form as soon as it has participated in the reaction, then the changes of A and B can be neglected, i.e. $[A] \approx [A]_0$, $[B] \approx [B]_0$, $[C_i] = [C_i]_0$, and $k_2[B] \gg k_{-1}$, and

$$[M]_{it} \approx k_1[A][C_i]/k_2[B]$$

$$R_{it} = k_2[M]_{it} = k_1[A]_0[C_i]_0/[B]_0$$

$$= k_{it}[C_i]_0, \ (k_{it} = k_1[A]_0/[B]_0).$$

The concentration of product P, arising from each catalyzed reaction after a given time t ($t \ll t_\infty$), is:

$$[P_i]_t = \int_0^t R_{it}\, dt = k_{it}\int_0^t [C_i]_0\, dt = k_{it}[C_i]_0 \cdot t$$

$$= K_i[C_i]_0, \ (K_i = k_{it} \cdot t).$$

Assume that the product shows an absorbance at a certain wavelength, then the total absorbance at a certain time t_j should be: $\Sigma A_{tj} = \Sigma K_{ij}[C_i]_0$.

The parameters K_{ij} are determined in the reaction system catalyzed by a single catalyst C_i only, with the aid of the graph of absorbance versus catalyst concentration at time t_j, and the concentration of catalysts in the samples could be calculated by solving the above equations.

In the experiments, the flow was stopped for $t = 200$ s, and absorbances were determined at 100 s and 200 s after injection of the sample solutions.

3. Results and discussion

3.1. Maxium absorbance wavelength

The red solution in the presence of Hg(II) and Ag(I) at pH 3.2 showed a maxium absorbance at 536 nm. At this wavelength, thiourea, α,α'-bipyridyl and potassium hexacyanoferrate(II) solution showed negligible absorbance at lower concentrations. The determinations were therefore made at 536 nm.

3.2. Effect of pH

Determinations were made in different acidic media. It was shown that HCl interacted with

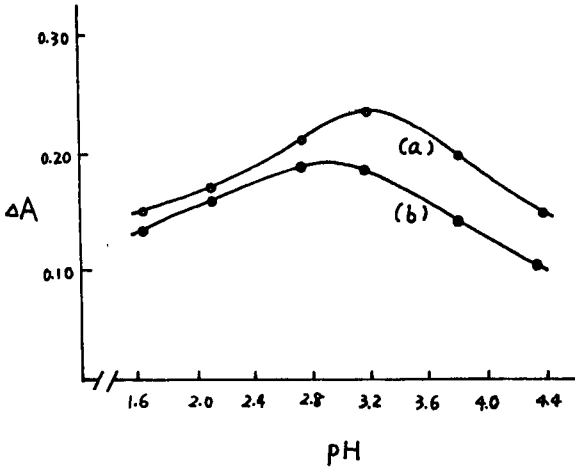

Fig. 2. The effect of pH. $[Fe(CN)_6]^{4-} = 5.0 \times 10^{-4}$ mol l^{-1}; [bipy] $= 7.5 \times 10^{-4}$ mol l^{-1}; [thiourea] $= 6.0 \times 10^{-3}$ mol l^{-1}. (a) [Hg(II)] = 50 ng ml^{-1}; (b) [Ag(I)] = 60 ng ml^{-1}.

Ag(I), but that HNO_3 or H_2SO_4 are acceptable. In this work, H_2SO_4 is chosen. The changes of absorbance differences with pH are shown in Fig. 2; pH 3.2 is chosen to get the highest sensitivities possible for both Hg(II) and Ag(I).

3.3. Effect of temperature and stopping time

The experimental results showed that the rates of both catalyzed and uncatalyzed reactions were enhanced significantly with temperature, and the absorbance differences increased. But higher back pressure must be provided in order to prevent formation of bubbles in the tube, which are difficult to control. The reaction was carried out at 90°C.

It was also shown that the absorbance differences increase with the time interval during which the flow was stopped, and that the sensitivities were improved. A time interval of 200 s was chosen with the aim of increasing the sampling rate, because the sensitivities were high enough under the conditions established. The absorbance differences were determined at 100 s and 200 s after injection of the sample solution.

Table 1
The influence of reagent concentrations (50 ng ml^{-1} Hg(II); 60 ng ml^{-1} Ag(I))

No.	$Fe(CN)_6^{4-}$ ($mol\ l^{-1}$)	Bipy ($mol\ l^{-1}$)	Thiourea ($mol\ l^{-1}$)	ΣA_{tj} Hg(II) (Ag(I))	No.	$Fe(CN)_6^{4-}$ ($mol\ l^{-1}$)	Bipy ($mol\ l^{-1}$)	Thiourea ($mol\ l^{-1}$)	ΣA_{tj} Hg(II) (Ag(I))
1	0.25	0.50	2.00	0.176 (0.0915)	9	0.75	0.50	6.00	0.185 (0.100)
2	0.25	0.75	4.00	0.219 (0.096)	10	0.75	0.75	8.00	0.254 (0.105)
3	0.25	1.00	6.00	0.220 (0.098)	11	0.75	1.00	2.00	0.185 (0.098)
4	0.25	1.25	8.00	0.210 (0.098)	12	0.75	1.25	4.00	0.235 (0.202)
5	0.50	0.50	4.00	0.203 (0.128)	13	1.00	0.50	8.00	0.087 (0.038)
6	0.50	0.75	6.00	0.235 (0.182)	14	1.00	0.75	2.00	0.100 (0.102)
7	0.50	1.00	8.00	0.257 (0.174)	15	1.00	1.00	4.00	0.152 (0.128)
8	0.50	1.25	2.00	0.227 (0.146)	16	1.00	1.25	6.00	0.205 (0.131)

Concentrations of reagents were multiplied by 10^2.

3.4. Effect of reagent concentrations

In order to determine the optimal conditions for the determinations, a series of experiments was made at fixed temperature (90°C), stopping time (200 s) and pH (3.2). From these experiments the optimal concentration ranges of α,α'-bipyridyl, hexacyanoferrate(II), and thiourea were obtained. Another experiment was then carried out under these conditions; the results are summarized in Table 1.

It is obvious that higher sensitivities for both mercury(II) and silver(I) determinations will be obtained under the experimental conditions of No. 6, 7 and 12. It was also shown that the blank of No. 12 was too high to give good reproducible results. The conditions of No. 6 were then chosen for further determinations, i.e. $[Fe(CN)_6]^{4-} = 5.0 \times 10^{-4}$ mol l^{-1}, [bipy] $= 7.5 \times 10^{-4}$ mol l^{-1}, and [thiourea] $= 6.0 \times 10^{-3}$ mol l^{-1}.

3.5. Calibrations and interferences

Mercury(II) and silver(I) solutions of different concentrations were introduced into the reaction systems, and the absorbance differences ΣA_{tj} were determined 100 s and 200 s after injection. The following linear relationship between ΣA_{tj} and Hg(II) or Ag(I) concentrations were obtained.

Table 2
The influence of foreign ions on the determination of 25 ng ml^{-2} Hg(II) and 25 ng ml^{-1} Ag(I)

Ion	Tolerance concentration [a]	Ion	Tolerance concentration [a]	Ion	Tolerance concentration [a]
Al(III)	50	Cr(III)	100	Ni(II)	100
As(III)	1000	Cu(II)	65	Pb(II)	25
Ca(II)	100	Fe(III)	4.2	Sn(II)	1000
Cd(II)	50	Mg(II)	150	V(V)	100
Co(II)	2.5	Mo(VI)	50	Zn(II)	5

[a] Concentration: $\mu g\ ml^{-1}$, within $\pm 5\%$ error.

Table 3
Determination of mercury(II) and silver(I) in waters and a synthetic sample

Sample	Mercury(II) content [a] (ng ml^{-1})			Silver(I) content [a] (ng ml^{-1})		
	Suggested method (R.S.D. %)	Known	AAS method	Suggested method (R.S.D. %)	Known	AAS method
Tap water	29.42 (5.20)		28.11	47.85 (4.89)		45.68
Wastewater	0.263 [b] (4.84)		0.248 [b]	0.410 [b] (4.05)		0.429 [b]
Synthetic sample	38.85 (3.52)	40.0		41.74 (3.20)	40.0	

[a] Mean of six determinations.
[b] Concentrations in wastewater, μg ml^{-1}.

For Hg(II):

$$\sum A_t(100) = 3.488C(\mu\text{g ml}^{-1}) - 0.0005, \quad r = 0.9995 \tag{1}$$

$$\sum A_t(200) = 5.502C(\mu\text{g ml}^{-1}) - 0.0018, \quad r = 0.9998 \tag{2}$$

and for Ag(I):

$$\sum A_t(100) = 1.211C(\mu\text{g ml}^{-1}) + 0.0015, \quad r = 0.9997 \tag{3}$$

$$\sum A_t(200) = 1.722C(\mu\text{g ml}^{-1}) + 0.0021, \quad r = 0.9992 \tag{4}$$

The linear calibration graphs were 0–75 ng ml^{-1} Hg(II) and 0–64 ng ml^{-1} Ag(I), and the working equations were derived, by considering the surplus item due to the deviation from origin of coordinates in Eqs. 1–4, as:

$$\sum A_{tj}(100) = 3.488C_{\text{Hg}} + 1.211C_{\text{Ag}} + 0.0010 \tag{5}$$

$$\sum A_{tj}(200) = 5.502C_{\text{Hg}} + 1.722C_{\text{Ag}} + 0.0003 \tag{6}$$

The experimental results indicated that the interactions between Hg(II) and Ag(I) are negligible within certain concentration ranges.

The influence of foreign ions has been studied, and the results are summarized in Table 2. It can be seen easily that most of the commonly coexisting foreign ions have no obvious effect on the determinations, except for the small interferences of Fe^{3+}, Co^{2+} and Zn^{2+}.

3.6. Applications of the method

25 ml of wastewater were transferred to a 200 ml flask, and 10 ml H_2SO_4 (1 + 1) and 1.5 ml saturated potassium permanganate were added. The solution was heated to boiling, digested for 2 h, and 5% ascorbic acid was then added drop-wise until the solution was completely decoloured. The solution was adjusted to pH 3.2 with NaOH, and diluted to 200 ml.

Tap water solution was determined directly.

A synthetic solution was prepared by dissolving a known amount of $AgNO_3$ and $Hg(NO_3)_2 \cdot 3H_2O$ in an appropriate volume of water, and adjusted to pH 3.2.

Table 3 lists the concentrations of mercury(II) and silver(I) determined with the proposed method and atomic absorption spectrometry.

References

[1] K.M. Rao, T.S. Reddy and S.B. Rao, Analyst (London), 113 (1988) 983.
[2] A. Velasco, M. Silva and M. Valcarcel, Microchem. J., 42 (1988) 110.
[3] Z.H. Chang, W. Zhou and Y.N. Wen, Godeng Xuexiao Huaxue Xuebao, 8 (1987) 407.
[4] H.L. Jiang and D.W. Ruan, Huaxue Xuebao, 49 (1991) 757.
[5] S.M. Wu and L.Q. Tian, Yiqi Yibiao Yu Fenxi Jiance, 1 (1992) 55.
[6] G.Z. Fang and Z.P. Tang, Fenxi Huaxue, 15 (1987) 46.
[7] M.L. Wang and X.P. Fang, Lihua Jianyan, 26 (1990) 29.
[8] J.H. Wang and R.H. He, Anal. Chim. Acta, 276 (1993) 419.

ELSEVIER

Analytica Chimica Acta 294 (1994) 201–206

ANALYTICA CHIMICA ACTA

Calixarene-coated amperometric detectors

Joseph Wang *, Jie Liu

Department of Chemistry and Biochemistry, New Mexico State University, Las Cruces, NM 88003, USA

Received 24th January 1994; revised manuscript received 25th February 1994

Abstract

Calixarene coatings are shown to impart high selectivity onto amperometric detection of neurotransmitters (e.g., dopamine, epinephrine), while excluding common electroactive interferences (e.g., ascorbic and uric acids, acetaminophen) from reaching the surface. The new selectivity dimension, attributed to host–guest interactions, is thus used for on-line monitoring of neurotransmitters at a calixarene-coated wall-jet detector. The recognition-dependent film offers attractive dynamic properties, is stable under vigorous hydrodynamic conditions, and maintains its unique permselective properties over prolonged periods. Selective assays of complex urine samples are illustrated. The transport properties and analytical performance are explored under different conditions. Sensing opportunities accrued from the discriminative properties of calixarene-coated amperometric probes are discussed.

Key words: Amperometry; Calixarene coatings; Detectors; Neurotransmitters

1. Introduction

Amperometric sensors and detectors offer many opportunities for clinical diagnostics, environmental surveillance or industrial quality control. However, despite the remarkable sensitivity, fast response, miniaturization capability and low cost, there are still problems of selectivity and stability (due to overlapping signals of coexisting electroactive species or adsorption of surface-active materials). Such problems can be addressed by covering the transducer or detector surface with an appropriate permselective film that reject undesired constituents, while allowing transport of the target analyte [1–3]. A variety of discriminative coatings, based on different transport properties, have been used over the past ten years, to control the access to the surface of amperometric devices [4–15]. These include size-exclusion cellulose acetate [4–15], polyphenol [6,7], poly(phenylenediamine) [7,8], or poly(vinylchloride) [9] films, charge-exclusion coatings such as perfluorinated (Nafion) [10] or polyester (Eastman Kodak AQ) ionomers [11,12], or multilayers which combine the properties of different films [16–18].

We describe here the permselectivity properties and analytical utility of calixarene-coated amperometric detectors. Calixarenes are macrocyclic *tert.*-butylphenol-formaldehyde condensates, capable (in their cone conformation) of forming

* Corresponding author.

SSDI 0003-2670(94)00129-A

inclusion compounds. Such molecular recognition events have received considerable attention in past years [19,20]. Calixarene derivatives have been used recently in electroanalysis, as ionophores for potentiometric ion-selective electrodes [21,22] and field effect transistors [23,24]. In addition, calixarene-modified carbon paste electrodes were employed for preconcentration/voltammetric measurements of heavy metals [25]. The utility of calixarene-based recognition films (and of other macrocyclic receptor compounds) for serving as membrane carriers in amperometric detection of biological compounds has not been reported.

This study demonstrates that the unique transport properties of calixarene coatings can create a new dimension of selectivity in amperometric monitoring. In particular, the new discriminative properties allow selective flow-injection detection of neurotransmitters (e.g., dopamine, epinephrine) in the presence of otherwise interfering species, such as ascorbic and uric acids (Fig. 1). The selectivity improvements are coupled with attractive dynamic properties and good mechanical stability (under vigorous hydrodynamic conditions). The calixarene used for the electrode modification is C-undecylcalix[4]resorcinarene (Fig. 1), which is now available commercially [26]. This bowl-shaped compound is capable of forming complexes with polar oxygen-functionalized guests. We wish to report on these permselective properties and the resulting analytical opportunities in the following sections.

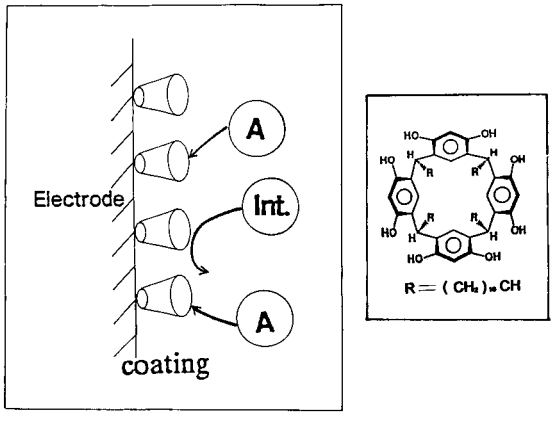

Fig. 1. Schematic illustration of the permselective action of calixarene coatings. Also shown, the chemical structure of the calixarene compound (C-undecylcalix[4]resorcinarene) used in the present study.

2. Experimental

2.1. Apparatus

All experiments were conducted with a voltammetric analyzer (Model CV-27, Bioanalytical Systems (BAS)), in connection with a BAS *X–Y–t* recorder. The "home-made" flow-injection system consisted of a 300-ml carrier reservoir, a Rainin Model 5041 sample injection valve (20 μl loop), interconnecting PTFE tubing (1.0 mm i.d.), and a large volume wall-jet amperometric detector. The detector configuration was described earlier [27]. All potentials were measured against the Ag/AgCl (3 M NaCl) reference electrode (Model RE-1, BAS).

2.2. Reagents

All solutions were prepared with doubly-distilled water. Fluka provided the C-undecylcalix[4]resorcinarene monohydrate, while tetrahydrofuran (THF) was purchased from Fisher Scientific. Ascorbic acid, acetaminophen, uric acid, catechol, epinephrine, and dopamine (Sigma), 4-*tert.*-butylcalix[6]arene, hydrogen peroxide (Aldrich), were used without further purification, and their solutions were prepared daily. The supporting electrolyte-carrier solution was a 0.05 M phosphate buffer (pH 7.4). The urine sample was obtained from a healthy volunteer and diluted with the supporting electrolyte solution.

2.3. Procedure

Before its modification, the platinum disk electrode (1.5 mm diameter, Model-2013, BAS) was hand-polished with a 0.05 μm alumina slurry, rinsed with doubly-distilled water and sonicated in a water bath for 2 min. The coating solution was prepared by dissolving the desired amount (usually 2 mg) of C-undecylcalix[4]resorcinarene

monohydrate in 1 ml of tetrahydrofuran. The electrode was coated by placing (with a micropipet) 5 μl of the above calix[4]arene solution on the electrode (to cover the active disk and its surroundings) and allowing the solvent to evaporate in air for 5 min. Flow-injection measurements were made by applying the desired working potential (+0.60 V) and allowing the transient current to decay. Flow of the carrier solution was maintained by gravity. All experiments were performed at room temperature.

3. Results and discussion

3.1. Transport properties

Fig. 2 shows the dependence of the film permeability for seven electroactive compounds of biological significance. The ratio between the current at the film-coated electrode over that at the bare one, i_m/i_b, is used as a measure of the permeability. Effective discrimination ($i_m/i_b < 0.02$) is observed against ascorbic acid, acetaminophen and uric acid. Significantly higher permeability ($i_m/i_b > 0.10$) is observed for the neurotransmitters epinephrine and dopamine. Overall, the permeability decreases in the following order: dopamine > epinephrine > catechol > hydrogen peroxide ≫ uric acid ≈ acetaminophen ≈ ascorbic acid.

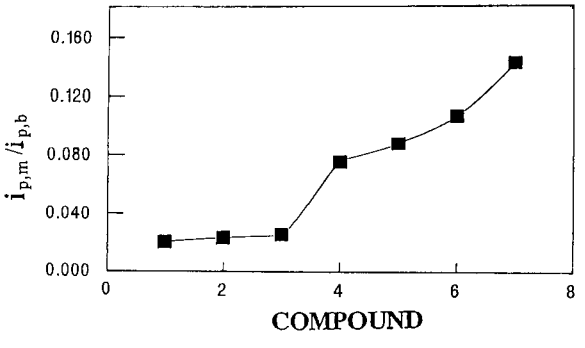

Fig. 2. Permeability profile of the calixarene-coated flow detector using the following solutes: ascorbic acid (1), acetaminophen (2), uric acid (3), hydrogen peroxide (4), catechol (5), epinephrine (6) and dopamine (7). Flow-injection conditions: operating potential, +0.60 V; flow rate, 1.5 ml min^{-1}; carrier, 0.05 M phosphate buffer (pH 7.4); solute concentration, 1×10^{-4} M.

The permeability profile of Fig. 2 is of great analytical significance considering the similar size (MW 150–190) of the neurotransmitters and common electroactive interferences, which precludes the use of common size-selective coatings [5–7] for such differentiation. Similarly, the charged-selective Nafion film offers discrimination against the anionic ascorbic and uric acids, but not against the neutral acetaminophen. Permeability profiles, similar to the one shown in Fig. 2, were observed also for coatings containing different amounts of the calixarene (ranging from 1 to 5 mg per ml THF). Yet, the most favorable results (in terms of overall permselectivity, neurotransmitter/interferences) were obtained with the 2 mg/ml solution. Coatings prepared from another commercial calixarene, 4-*tert.*-butylcalix[6]-arene, also displayed a favorable permselective response towards catecholamines, but did not offer the desired rejection of uric acid. No apparent permeability trends were observed in controlled experiments, involving casting of the THF solvent (without the calixarene host). The clear selectivity pattern of Fig. 2 may be attributed to molecular recognition, involving cavity-shape fitting and hydrogen-bonding interactions, as common for resorcinol-derived calixarenes [26,28,29]. Encapsulation of the neutral ring portion of the catecholamine guests within the host cavity may thus be facilitated by their spatial structural arrangement. In contrast, the charged rings of ascorbic and uric acids may prevent their inclusion. While offering significant analytical advantages (see next section), detailed spectroscopic investigations and crystal structure studies are required to confirm these molecular recognition claims.

Fig. 3 shows the flow rate effect upon the response to dopamine at the calixarene-coated detector. The flow-injection peak decreases gradually upon increasing the flow rate between 0.3 and 1.2 ml/min, and remained stable at higher rates. Apparently, lower flow rates (i.e., longer exposure times) facilitate the binding of the guest analyte by the host layer. Such behavior differs greatly from the flow-rate independence commonly observed at polymer-coated electrodes

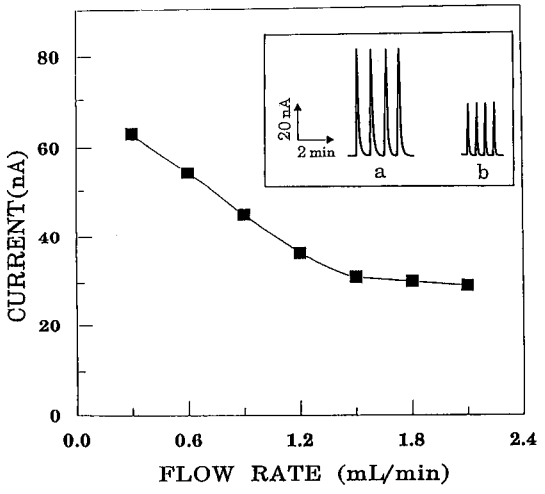

Fig. 3. Effect of flow rate on the flow-injection response to 1×10^{-4} M dopamine. Also shown (inset) are the FIA peaks at flow rates of 0.3 (a) and 2.1 (b) ml min^{-1}. Other conditions, as in Fig. 2.

[5,10] where transport through the film is the major contributor to the total diffusional transport. Also shown in Fig. 3 (inset) are characteristic flow-injection current–time profiles at 0.3 (a) and 2.1 (b) ml/min. Short response times and rapid return to the baseline are observed for both flow rates, indicating rapid depletion from the host layer after the passage of the sample zone (i.e., in the presence of the carrier/blank solution). The peak widths (at 0.6 C_{max}) are 9 (a) and 7 (b) s, allow high injection rates of 72–90 samples/hour. Overall, the calixarene-coated detector exhibits an attractive dynamic behavior, similar to that common at naked electrode flow cells. The latter displayed peak widths of 8–10 s over the same flow rate range (not shown).

3.2. Analytical utility

The calixarene-coated amperometric detector exhibits a well-defined concentration dependence and reproducible data. For example, Fig. 4A displays the flow-injection response to epinephrine solutions of ascending concentration (1×10^{-5}–8×10^{-5} M, a–h). Well-defined peaks, proportional to the neurotransmitter concentration, and accompanied by a low noise level, are observed. The calibration plot, constructed from these injections, was linear (sensitivity, 0.25 nA/μM; correlation coefficient, 0.997; not shown). A detection limit of 3×10^{-6} M (27 ng) epinephrine can be estimated based on the signal-to-noise characteristics ($S/N = 3$) of the 1×10^{-5} M epinephrine peak (a). Highly reproducible results are indicated from the prolonged series of 24 repetitive injections of a 1×10^{-4} M dopamine solution (shown in Fig. 4B). This series yielded a relative standard deviation of 1.6% (mean, 30.4 nA; range, 29.5–31.0 nA). Such precision compares favorably with that common at bare-electrode detectors.

The unique permselective transport properties of calixarene monolayers (as displayed in Fig. 2) provide an effective approach for enhancing the selectivity of amperometric flow detectors. The new dimension of selectivity is illustrated in Fig. 5, for on-line monitoring of an untreated urine sample. The conventional (bare) electrode displays a large contribution of the urine oxidizable components (A(a)), which does not permit the detection of the spiked (1×10^{-4} M) dopamine (A(b)). The calixarene film, in contrast, effectively restricts the access of most electroactive constituents (B(a, c, e, g)), thus allowing selective detection of the spiked dopamine (B(b, d, f, h)).

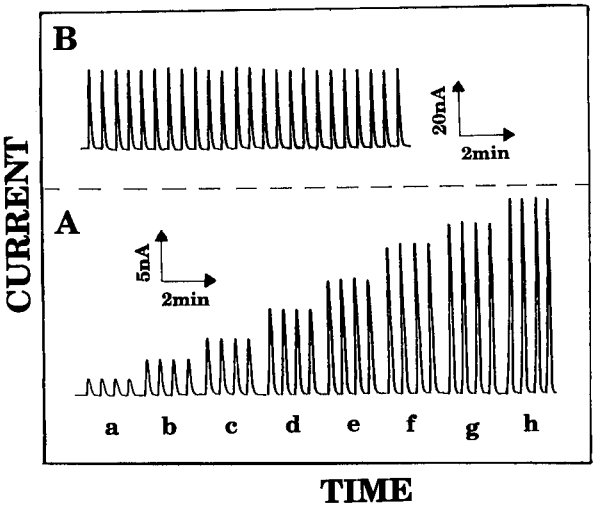

Fig. 4. Flow-injection calibration (A) and precision (B) experiments. Analytes: (A) epinephrine, $1\text{–}8\times10^{-5}$ M (a–h); (B) dopamine, 1×10^{-4} M. Conditions, as in Fig. 2.

Notice also that the exclusion of endogenous electroactive species is retained over a long 6 h period (compare B (a vs. h)). Such behavior reflects the good mechanical stability of the film under the vigorous hydrodynamic conditions (existing in the wall-jet cell), and indicates that surface-active constituents of the urine sample do not "block" the calixarene film. Remarkable stability was indicated from another prolonged experiment involving injections of dopamine and acetaminophen solutions every second day. Effective discrimination against the acetaminophen ($K_{dop/acet} = 12$) was retained over the entire (36 days) experimental period (not shown). Yet, whenever needed, the modification procedure and cell construction permit fast and easy replacement of the coating. The preparation of the calixarine layer is highly reproducible, with ca. 5% variability in the permeability between different castings.

Another example of selective flow-injection detection is illustrated in Fig. 6. The bare electrode (A) does not allow selective detection of dopamine in the presence of ascorbic acid (b), acetaminophen (c) or uric acid (d); a large additive response (associated with the oxidation of these four compounds at the operating potential) is observed. In contrast, and as expected from the permeability profile of Fig. 2, the calixarene-coated electrode (B) excludes the ascorbic acid, acetaminophen and uric acid, and permits a relatively selective response.

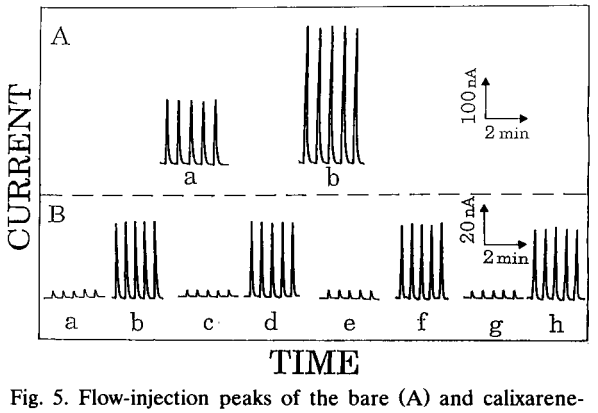

Fig. 5. Flow-injection peaks of the bare (A) and calixarene-coated (B) detectors to a diluted (1:20) urine sample (A (a) and B (a, c, e and g)) and to the diluted urine samples containing 1×10^{-4} M dopamine (A (b) and B (b, d, f and h)). Peaks B (a–h) were recorded in 1-h intervals. Conditions, as in Fig. 2.

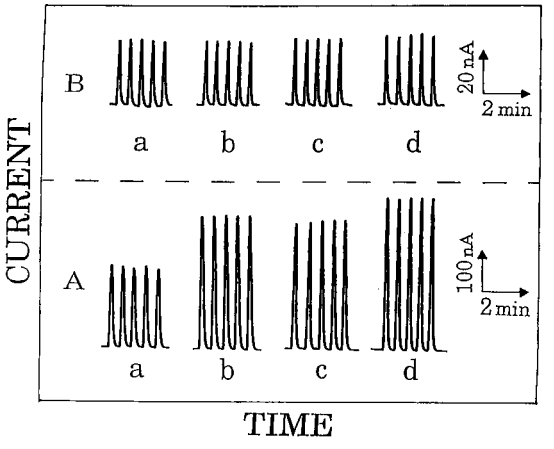

Fig. 6. Flow-injection detection of dopamine at the bare (A) and calixarene-coated (B) detectors: (a) 1×10^{-4} M dopamine; (b) same as (a) but after addition of 1×10^{-4} M acetaminophen; (c) same as (a) but after addition of 1×10^{-4} M ascorbic acid; (d) same as (a) but after addition of 1×10^{-4} M uric acid. Conditions, as in Fig. 2.

4. Conclusions

We have presented data which demonstrate that calixarene-coated electrodes can be used to enhance the selectivity of amperometric monitoring of neurotransmitters. These experiments represent the first example of using recognition-based films as permselective membrane barriers in amperometric detection. The coupling of the new discriminative properties with ultramicroelectrodes should be valuable for neurochemical studies. This study indicates also the utility of flow-injection amperometric measurements for rapid characterization of the affinity of electroactive compounds and calixarene layers, and potentially for exploring host–guest interactions, in general. The diverse host–guest chemistry at other calixarene derivatives (displaying different conformational properties and hydrogen bonding interactions) might be useful for designing coatings selective for other target analytes. Many exciting

applications are anticipated in the near future, considering the numerous potential chemical modifications of calixarene compounds. Similarly, functionalized calixarenes (e.g., with biological entities) may result with novel sensing devices. The relatively facile transport of hydrogen peroxide (see Fig. 2) indicates promise for use in amperometric biosensors. Other amperometric schemes (e.g., liquid chromatographic detectors, biosensors) should benefit from the selectivity improvements accrued from calixarene films. It is hoped that discriminative layers made of other macrocyclic receptor compounds (e.g., cyclodextrins or crown ethers) would find greater utility in amperometric measurements.

References

[1] R.W. Murray, A.G. Ewing and R.A. Durst, Anal. Chem., 59 (1987) 379A.
[2] J. Wang, Electroanalysis, 3 (1991) 255.
[3] R.P. Baldwin and K. Thomsen, Talanta, 38 (1991) 1991.
[4] G. Sittampalam and G.S. Wilson, Anal. Chem., 55 (1983) 1608.
[5] J. Wang and L.D. Hutchins, Anal. Chem., 57 (1985) 1536.
[6] T. Ohsaka, T. Hirokawa, H. Miyamoto and N. Oyama, Anal. Chem., 59 (1987) 1758.
[7] S. Sasso, P. Pierce, R. Walla and A. Yacynych, Anal. Chem., 62 (1990) 1111.
[8] C. Malitesta, F. Palmisano, L. Torsi and P.G. Zambonin, Anal. Chem., 62 (1990) 2735.
[9] I. Christie, P. Treloar and P. Vadgama, Anal. Chim. Acta, 269 (1992) 65.
[10] J. Wang, P. Tuzhi and T. Golden, Anal. Chim. Acta, 194 (1984) 129.
[11] J. Wang and T. Golden, Anal. Chem., 61 (1989) 1397.
[12] G. Bremle, B. Persson and L. Gorton, Electroanalysis, 3 (1991) 77.
[13] J. Wang and Z. Lu, Anal. Chem., 62 (1990) 826.
[14] F. Malem and D. Mandler, Anal. Chem., 65 (1993) 37.
[15] J. Wang, H. Wu and L. Angnes, Anal. Chem., 65 (1993) 1893.
[16] J. Wang and P. Tuzhi, Anal. Chem., 58 (1986) 3257.
[17] I. Christie, M. Baker, F. Keedy and P. Vadgama, Anal. Chim. Acta, 272 (1990) 145.
[18] F. Mizutani, S. Yabuki and T. Katsura, Anal. Chim. Acta, 274 (1993) 201.
[19] J. Vicens and V. Bohmer, Calixarenes: A Versatile Class of Macrocyclic Compounds, Kluwer, Dordrecht, 1990.
[20] C.D. Gutsche, Calixarenes, Royal Society of Chemistry, Cambridge, 1989.
[21] K. Kimura, T. Miura, M. Matsuo and T. Shono, Anal. Chem., 62 (1990) 1510.
[22] A. Cadogan, D. Diamond, M. Smyth, M. Deasy, M. McKervey and S. Harris, Analyst, 114 (1989) 1551.
[23] P. Cobben, R. Egberink, J. Bomer, P. Bergveld, W. Verboom and D. Reinhoudt, J. Am. Chem. Soc., 114 (1992) 10573.
[24] Y. Tsujimura, M. Yokoyoma and K. Kimura, Electroanalysis, 5 (1993) 803.
[25] D. Arrigan, G. Svehla, S. Harris and M. McKervey, Anal. Proc., 29 (1992) 27.
[26] Reagent of the Year, Fluka Chemie AG, 1993.
[27] J. Wang and B. Freiha, Anal. Chem., 57 (1985) 1776.
[28] K. Kurihara, K. Ohto, Y. Tanaka, Y. Aoyama and T. Kunitake, J. Am. Chem. Soc., 113 (1991) 444.
[29] V. Böhmer and P. O'Sullivan, Trends Polym. Sci., 1 (1993) 267.

ELSEVIER

Analytica Chimica Acta 294 (1994) 207–213

ANALYTICA CHIMICA ACTA

Silver-selective membrane electrodes using acyclic dithia benzene derivative neutral carriers. Comparison with related macrocyclic compounds

Jaume Casabó [a,*], Teresa Flor [a], María I. Romero [a], Francesc Teixidor [b], Consuelo Pérez-Jiménez [b]

[a] *Departament de Química, Universitat Autònoma de Barcelona, 08193 Bellaterra, Barcelona, Spain*
[b] *Institut de Ciència dels Materials (C.S.I.C.), 08193 Bellaterra, Barcelona, Spain*

Received 19th November 1993; revised manuscript received 4th March 1994

Abstract

Four new acyclic dithia benzene derivatives have been synthesized: 1,3-bis[(ethylthio)methyl]benzene; 1,3-bis[(pentylthio)methyl]benzene; 1,3-bis[(octylthio)methyl]benzene, and 1,3-bis[(dodecylthio)methyl]benzene. All compounds have been tested as silver(I) ion sensors in membrane-based ion-selective electrodes, exhibiting good sensitivity, detection limits, reproducibility and selectivity. The chemical recognition of silver(I) by these receptors is compared to the behaviour presented by closely related macrocyclic and acyclic polythia compounds.

Key words: Sensors; Acyclic dithia benzene derivatives; Silver-selective membrane electrodes; Macrocyclic compounds

1. Introduction

The chemical recognition of metal ions is a very difficult task due to their ability to show several coordination numbers and their affinity towards different coordination centres. All these features make them suitable to coordinate with a wide range of ligands, even to force ligand rearrangements in order to fit their coordination preferences. As a result it is very difficult to design a specific receptor for one particular metal ion.

The alkali and alkali earth elements, except lithium, beryllium and magnesium, are remarkable exceptions. The coordination of these elements is predominantly ionic. They generally display high coordination numbers and exhibit affinity towards hard coordination centres like oxygen and nitrogen atoms. These characteristics explain the remarkable selectivity and chemical recognition shown by some macrocyclic polyethers towards these metal ions [1–7].

The d^{10} transition metal ions, Ag^+ and Hg^{2+}, display singular coordination characteristics. Both have a preference for a coordination number of two. Furthermore they display great affinity for soft coordination centres like sulphur, as well as

* Corresponding author.

SSDI 0003-2670(94)00135-9

other elements of the second and third transition metal series.

Recently [8,9] we have reported a family of dithia macrocycles designed to take in account the features of these d^{10} cations (Fig. 1), forcing them to hold a "linear" coordination by the two sulphur atoms. We have found that these receptors exhibit high selectivity for Ag^+, as well as that for Hg^{2+}, when implemented in membranes of solid state electrodes. We have established that the selectivity for silver(I) is not due to the size of the macrocyclic cavity, but to the geometrical arrangement of the soft sulphur coordination centres, regardless of the heteroatom in the aliphatic chain.

Few such electrodes are reported in the literature, all of them based on polythiacrown ether derivatives. Ion-selective membrane electrodes based on 1,4-dithia-12-crown-4, 1,7-dithia-12-crown-4, 1,4-dithia-15-crown-5, and monobenzo-15-crown-5 macrocycles were tested as sensors for the Ag^+ electrode [10]. They exhibit good sensitivity but no Nernstian response to the activity changes of the Ag^+ ion. Other macrocyclic molecules, basically with the same structure as the crown compounds but with lipophilic chains attached to the macrocyclic ring, have been reported and tried as sensors in Ag^+-selective polymeric membrane electrodes [11,12] with similar results, but these display Nernstian response. The

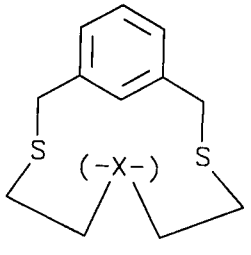

X = C (a)

X = O (b)

X = S (c)

Fig. 1. Schematic drawing of macrocyclic dithia benzene derivatives.

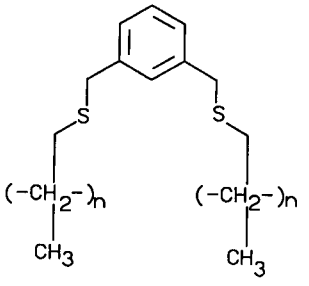

Fig. 2. Schematic drawing of the acyclic dithia benzene derivatives described in this paper.

electrode characteristics of the ion-selective membrane electrodes based on the macrocycles [8,9] synthesized by us have a better response than those reported before and superior to that of conventional Ag_2S-based solid state electrodes.

To gain further insight in the metal ion chemical recognition phenomena problems of this sort of compounds we have developed a closely related family of acyclic dithia receptors (Fig. 2). The objective is to elucidate if the macrocyclic nature of these dithia compounds is necessary in the chemical recognition of Ag^+. Furthermore, we have selected several molecules with different chain lengths to study the effect of chain length on the behaviour of these receptors. Several acyclic ligands used as sensors in ion-selective electrodes have been reported in the literature [13]. Acyclic receptors could form the base of economical and easily made commercial electrodes.

2. Experimental

2.1. General

Microanalyses (C, H, N) were performed in our analytical laboratory on a Perkin-Elmer 240-B system. ^1H NMR spectra were run on a Bruker WP80 54 apparatus in $CDCl_3$ solution. IR spectra were recorded on a Perkin-Elmer 1710 FT spectrometer as KBr pellets. Mass spectrometry was performed on a Hewlett-Packard HP2985 GC/MS instrument. Unless specifically men-

tioned, the syntheses were performed under a nitrogen atmosphere, using dehydrated and deoxygenated solvents. Solvents were placed under vacuum to eliminate the dissolved oxygen.

2.2. Synthesis of 1,3-bis[(ethylthio)methyl]benzene (LIE)

To a solution of sodium (5.52 g, 0.24 mol) in methanol (80 ml), ethanethiol (15.37 g, 0.24 mol) was added and the mixture was allowed to stand for 1 h. To the aforementioned clear solution, dichloro-*m*-xylene (21.22 g, 0.12 mol) dissolved in dried methanol (100 ml) was added and refluxed for 3 h under dry nitrogen atmosphere.

After refluxing, the solvent was evaporated and the solid obtained was treated with water (200 ml). The mixture was extracted with diethyl ether (twice, 100 ml each), washed with saturated Na_2CO_3 solution (twice, 50 ml each) and water (twice, 50 ml each), finally the ethereal extract was dried over $MgSO_4$ (1 h). An oily like material was obtained by evaporation of the ether which was dissolved in toluene and chromatographed over neutral Al_2O_3. The fraction eluted with toluene was evaporated until a dense colourless liquid was obtained. Yield, 8.15 g; 40%. Found: C, 63.7; H, 8.0; S, 28.3. Calculated for $C_{12}H_{18}S_2$: C, 63.66; H, 8.01; S, 28.32. ^{1}H NMR, δ_H (400 MHz, $CDCl_3$): 1.2 (6, t, $-CH_2-CH_3$), 2.4 (4, c, CH_3-CH_2-S), 3.6 (4, s, $S-CH_2-Ph$), 7.1 (7, m, Ph), 7.2 (1, s, Ph).

2.3. Synthesis of 1,3-bis[(penthylthio)methyl]benzene (LIP)

To a solution of KOH (5.61 g, 0.1 mol) in 1-butanol (150 ml), 1-penthanethiol (10.63 g, 0.1 mol, 98%) was added. To the aforementioned clear solution, dichloro-*m*-xylene (8.84 g, 0.05 mol) dissolved in dried 1-butanol (150 ml) was added and refluxed for 3 h under dry nitrogen atmosphere.

The KCl precipitated was filtered and the clear solution was evaporated. A yellowish oily like material was obtained which was extracted with benzene (150 ml). The benzene solution was washed with saturated solution of Na_2CO_3 (twice, 75 ml each) and water (twice, 75 ml each). Finally the benzene extract was dried over Mg_2SO_4 (1 h). An oily like material was obtained by evaporation of the benzene which was dissolved one more time in benzene (10 ml) and chromatographed over neutral Al_2O_3. The fraction eluted with benzene was evaporated until a colourless liquid was obtained. Yield, 5.90 g; 38%. Found: C, 69.7; H, 9.8; S, 20.7. Calculated for $C_{18}H_{30}S_2$: C, 69.61; H, 9.74; S, 20.65. ^{1}H NMR, δ_H (400 MHz, $CDCl_3$): 0.9 (6, t, $-CH_2-CH_3$), 1.3 (8, m, $S-CH_2-Ph$), 1.5 (4, m, $CH_3-CH_2-CH_2-$), 2.4 (4, t, $-CH_2-CH_2-S-$), 3.7 (4, s, $S-CH_2-Ph$), 7.2 (4, m, Ph).

2.4. Synthesis of 1,3-bis[(octylthio)methyl]benzene (LIO)

This molecule was synthesized using the same procedure employed in the LIP compound. The only difference was the solvent utilized in the extraction and chromatographic procedures: toluene was used instead of benzene, in this case. Yield, 32%. Found: C, 73.0; H, 11.0; S, 16.0%. Calculated for $C_{24}H_{42}S_2$: C, 73.07, H, 10.65; S, 16.27%. ^{1}H NMR, δ_H (400 MHz, $CDCl_3$): 0.9 (6, t, $-CH_2-CH_3$), 1.3 (20, m, $CH_3-(CH_2)_n-R$, $n = 5$), 1.5 (4, m, $-S-CH_2-CH_2-R$), 2.4 (4, t, $-S-CH_2-R$), 3.7 (4, s, $-S-CH_2-Ph$), 7.2–7.3 (4, m, Ph).

2.5. Synthesis of 1,3-bis[(dodecylthio)methyl]benzene (LIDO)

This compound was synthesized as described for LIO. Yield, 31%. Found: C, 75.4; H, 11.9, S, 12.6%. Calculated for $C_{32}H_{58}S_2$: C, 75.87; H, 11.46; S, 12.67%. ^{1}H NMR, δ_H (400 MHz, $CDCl_3$): 0.8 (6, t, $-CH_2-CH_3$), 1.2 (36, m, $CH_3-(CH_2)_n-R$, $n = 9$), 1.5 (4, q, $-S-CH_2-CH_2-R$), 2.4 (4, t, $-S-CH_2-R$), 3.6 (4, s, $-S-CH_2-Ph$), 7.1–7.2 (4, m, Ph).

2.6. Construction of electrodes

The sensor membranes were prepared and assembled as previously described [14–16]. The sensor material (macrocycles, 7%) with dioctylphtha-

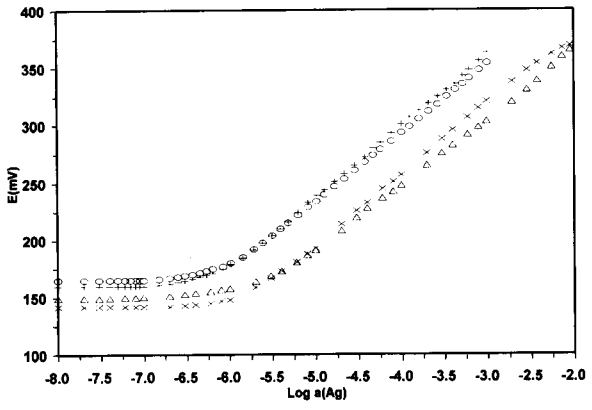

Fig. 3. Ag^+ response for the membrane-based ion-selective electrodes based on: +, LIE; *, LIP; ×, LIO; ▲, LIDO.

late (31%) as plasticizer and poly(vinyl chloride) (PVC) (62%) were dissolved in tetrahydrofuran. The sensor solution was added drop-wise on a conductive circular flat cavity (0.2 mm deep) drilled in the end of an electrode body tube sealed with a layer of a conducting polymer material. After drying, the thickness of the resulting convex membrane was 0.3 mm. The conductive material (graphite-loaded epoxy resin) used as solid internal contact of the membrane electrode has been described previously [15,16]. The electrode was usually conditioned before use by soaking for 24 h in a 10^{-3}M $Ag(NO_3)$ solution.

2.7. Measurements of e.m.f.

The response characteristics, the response time of the constructed membrane electrodes and the selectivity coefficients $k^{pot}_{A,B}$ (fixed interference method) [17] were determined by the reported standard methods. For measuring the membrane potentials the following electrochemical cell was used: solid internal contact/sensor membrane/working solution/reference electrode. The e.m.f. was measured relative to a Ag–AgCl double junction reference electrode (Orion 90-02-00) with the outer chamber filled with 0.1 M potassium nitrate solution. A Crison (Barcelona) digital potentiometer (±0.1 mV) was used. All measurements were carried out at 25 ± 0.1°C.

Table 1
Response characteristics and selectivity coefficients

	Response characteristics for			
	LIE	LIP	LIO	LIDO
Detection limit (mol/dm^3)	5.60×10^{-7}	7.10×10^{-7}	1.26×10^{-6}	1.58×10^{-6}
Slope (mV/decade)	59.1 ± 0.7	59.5 ± 0.1	60.5 ± 0.5	57.9 ± 0.5
Response time (s)	< 5	< 4	< 5	< 10
Effective pH range	1.7–9.5	1.9–9.2	2.0–10	1.8–9.5
Lifetime (months)	> 9	> 7	> 7	> 4
	Selectivity coefficients $k^{pot}_{Ag/M}$			
Ni	2.50×10^{-6}	2.20×10^{-6}	4.30×10^{-6}	3.90×10^{-6}
Mg	2.80×10^{-6}	3.48×10^{-6}	5.50×10^{-6}	6.90×10^{-6}
Sr	4.10×10^{-6}	4.08×10^{-6}	– [a]	– [a]
Cd	7.00×10^{-6}	2.78×10^{-6}	3.50×10^{-6}	1.20×10^{-5}
Zn	7.70×10^{-6}	3.87×10^{-6}	4.30×10^{-6}	1.70×10^{-5}
Ca	8.05×10^{-6}	4.53×10^{-6}	4.50×10^{-6}	9.10×10^{-6}
Co	8.70×10^{-6}	5.51×10^{-6}	9.80×10^{-6}	1.40×10^{-5}
Pb	8.80×10^{-6}	3.52×10^{-6}	5.80×10^{-5}	9.90×10^{-6}
Tl	1.10×10^{-5}	1.43×10^{-5}	2.30×10^{-5}	5.70×10^{-5}
K	1.70×10^{-5}	1.04×10^{-5}	1.30×10^{-5}	4.80×10^{-5}
Cu	1.70×10^{-5}	8.82×10^{-6}	1.10×10^{-5}	8.80×10^{-6}
Na	1.90×10^{-5}	1.47×10^{-5}	1.20×10^{-5}	2.60×10^{-5}
Hg	9.70×10^{-4}	1.04×10^{-3}	1.80×10^{-3}	1.60×10^{-3}

[a] No values available for Sr(II) and these receptors.

3. Results

The molecules synthesized were obtained by a general reaction of 1 mol of dichloro-*m*-xylene with 2 mol of the corresponding thiolate. The reaction takes place with high yields, without high dilution conditions. All products are colourless, oily-like materials.

The reproducibility and stability of the manufactured electrodes were evaluated by repeated calibrations with $AgNO_3$. Typical calibration graphs and response characteristics of the four prepared electrodes are reported in Fig. 3 and Table 1, respectively. All four membrane based electrodes display a Nernstian response to silver ions as $AgNO_3$ solutions, over an activity range of 1×10^{-7} to 1×10^{-2} mol/dm^3.

In all cases, the electrode reproducibility has been excellent, better than that displayed by conventional electrodes having internal reference solutions. The existence of a unique solution/membrane interface in the all-solid-state electrodes, diminishes the risk of leaching of the sensing system confined within the membrane.

The electrodes life-time was studied by periodically re-calibrating in standard solutions and calculating the response slope over the range 1×10^{-7} to 1×10^{-2} mol/dm^3 $AgNO_3$. During the testing period, the electrodes were used for a minimum of 4 h per week and stored in a 1×10^{-3} mol/dm^3 $AgNO_3$ solution when not in use. Following interfering ion measurements new Ag calibration tests had been recorded and no "poisoning", by any of the interfering ions studied, was evident.

In each case, the electrode response was pH independent between 2 and 9. This was adjusted for $AgNO_3$ (10^{-4} and 10^{-3} mol/dm^3) test solutions, HNO_3 and KOH, as appropriate.

Excellent response times ($t_{95\%}$) are also found, being no more than 10 s. Slight, but not significant, differences between them are observed. The mixed solution method has been used to study the interference of foreign ions. The selectivity coefficients, $k^{pot}_{A,B}$, display very good selectivity with respect to many common ions. Only Hg^{2+} is a significant interferent ion. Even so, the corresponding selectivity coefficient for Ag^+ with respect to Hg^+ is still in the range 1.0×10^{-3}–9.7×10^{-4}.

The response towards Hg^{2+} is worth to be considered because its peculiar aqueous chemistry. Baes and Mesmer [18] reported the existence of several hydrolized species depending on the Hg^{2+} concentration and pH, mostly: $[HgOH]^+$, $Hg(OH)_2$, $[Hg(OH)_3]^-$, $[Hg_2OH]^{3+}$ and $[Hg_3(OH)_3]^{3+}$. The hydrated Hg^{2+} ion exists only at pH values < 2. Due to the nature of these species it a complex behaviour of these electrodes toward Hg(II) was expected. The response at a non-controlled pH is not Nernstian, showing several linear steps depending on the Hg^{2+} activity, evidencing the existence of different hydrolytic species in solution. However, the response is smaller than in the Ag^+ case. In fact, Hg^{2+} can be considered as an interferent ion for Ag^+ (Table 1). Up to now, no attempts have been made to measure the Hg^{2+} response at pH < 2, where Hg(II) exists in aqueous solution. The remarkable behaviour of Hg^{2+} will be discussed below. Due to these problems, these membrane based electrodes are not easily conditioned for quantitative determination of mercury in solution.

4. Discussion

According to Table 1 the metal cations tested as interferences with respect to Ag(I) could be roughly divided in two categories. Divalent ions such as Ni, Mg, Sr, Cd, Zn, Ca, Co and Pb exhibit slightly less interference than the monovalent cations Tl, K and Na. Cu is in the borderline. Hg(II) is the most serious interferent with respect to silver(I)

There is no general improvement in the performance of the electrodes by increasing the chain length of the sensor molecules, as it would be expected from their stronger lipophilicity and better compatibility with the membrane components (Table 1). The best results are obtained with the LIP receptor with a medium chain length. This sensor shows the best Ag^+ discrimination with respect to Ni, Cd, Zn, Ca, Co, Pb, K and Cu. A longer chain, probably reduces the mobility of the complex within the membrane perturbing the

kinetic processes, as is evidenced by the relatively longer response time of the LIDO based electrode.

According to the values presented in Table 1 and after comparison with the results reported in the literature [9] (displayed in Fig. 1), it can be concluded that there are slight, but not significant, differences between these dithia receptors, regardless of the macrocyclic or acyclic nature, or the presence of heteroatoms in these compounds. All these silver ion-selective membrane electrodes exhibit good electrode characteristics and selectivity coefficients.

We have demonstrated that the selectivity towards Ag^+ exhibited by the dithia macrocycles reported in Ref. [9] (Fig. 1) is independent of the macrocyclic cavity size, because there is enough room to allocate any of the metal ions tested. In addition, the flexibility of the twisted aliphatic chain could conform to the required ion size. Only the geometrical arrangement of the thioether atoms in the receptor, the Ag^+ affinity for soft coordination centres and its tendency for two linear coordination, provide a logical explanation. These considerations are also valid for the open chain compounds described in this paper.

Hg^{2+} could behave similarly to Ag(I), but it is only an interferent. The explanation could be attributed to the metallation of the singular 2-hydrogen in the benzene ring, as it is detected by ^1H NMR [19]. This C–Hg bond probably affects the necessary kinetic lability of the resulting mercury complex within the membrane and perturbs the electrode response. If Hg(II) is removed, the dithia receptors become highly selective for silver.

There is a very closely related macrocyclic and acyclic family of NS_2 ligands, which has extensively been studied by us (Fig. 4). We have reported several metallic complexes of these ligands, some of them completely characterized by x-ray diffraction methods [20–24]. Distorted trigonal bipyramid, square pyramid or even octahedral geometries around the metal ion were found. These NS_2 ligands afford isolable solid complexes with a variety of transition metal ions in a pentacoordinate or hexacoordinate fashion. Furthermore, the membrane-based ion-selective electrode based on 15-aza-6-oxa-3,9-dithiabicyclo-[9,3,1]pentadeca-1(15),11,13-triene (3.j) macrocycle exhibits Nernstian response toward Cu(II), Ni(II) and Co(II), although Ni(II) and Co(II) can be considered as interferents for Cu^{2+} with $k_{A,B}^{kpot} = 0.1$ [24]. No special selectivity has been found in this family of NS_2 ligands.

As a conclusion, a very different behaviour is observed with the sensors described here or elsewhere [8,9], with respect to the closely related NS_2 family of ligands. They present high selectivity towards Ag^+ because their structural features

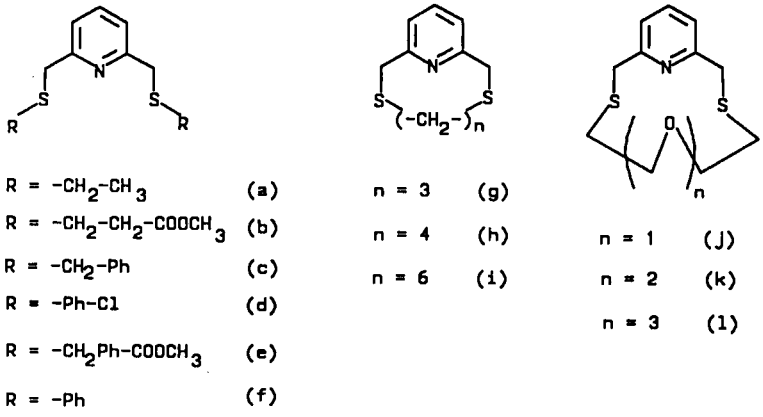

Fig. 4. Schematic diagram of NS_2 dithia pyridine derivatives.

fit the coordination tendencies of Ag(I) better than for any of the remainder cations tested.

Acknowledgments

This work was partially supported by Comisión Interministerial de Ciencia y Tecnología (C.I.C.Y.T) Spanish Government, through grant No. MAT91-0952 and by Fundación Ramón Areces Spain.

References

[1] C.J. Pedersen, J. Am. Chem. Soc., 89 (1967) 2495.
[2] K. Kimura, T. Haeda, H. Tamura and T. Shono, J. Electroanal. Chem., 95 (1979) 91.
[3] K.W. Fung and K.H. Wong, J. Electroanal. Chem., 111 (1980) 359.
[4] H. Tamura, K. Kimura and T. Shono, Anal. Chem., 54 (1982) 1224.
[5] A. Yamauchi and J.N. Ishibashi, Anal. Chim. Acta, 136 (1982) 399.
[6] T. Shono, M. Okahara, I. Ikeda, K. Kimura and H. Tamura, J. Electroanal. Chem., 132 (1982) 99.
[7] K. Kimura, H. Tamura and T. Shono, J. Chem. Soc. Chem. Commun., (1984) 492.
[8] J. Casabó, C. Pérez-Jiménez, L. Escriche, S. Alegret, E. Martínez-Fábregas and F. Teixidor, Chem. Lett., (1990) 1107.
[9] J. Casabó, L. Mestres, L. Escriche, F. Teixidor and C. Pérez-Jiménez, J. Chem. Soc. Dalton Trans., (1991) 1969.
[10] M.-T. Lai and J.-S. Shih, Analyst, 111 (1986) 891.
[11] M. Oue, K. Akama, K. Kimura, T. Tanaka and J. Shono, J. Chem. Soc. Perkin Trans., (1989) 1675.
[12] M. Oue, K. Akama, K. Kimura, M. Tanaka and T. Shono, Anal. Sci., 5 (1989) 165.
[13] W.E. Morf, D. Ammann, R. Bissig, E. Pretsch and W. Simon, in R.M. Izatt and J.J. Christensen, Progress in Macrocyclic Chemistry, Vol. 1, Wiley, New York, 1979.
[14] S. Alegret, J. Alonso, J. Bartrolí, J.M. Paulís, J.L.F.C. Lima and A.A.S.C. Machado, Anal. Chim. Acta, 164 (1984) 147.
[15] S. Alegret, J. Alonso, J. Bartrolí, J.L.F.C. Lima and A.A.S.C. Machado, in J.L. Aucouturier et al. (Eds.), Proceedings of the 2nd International Meeting of Chemical Sensors, Bordeaux Chemical Sensors, Talance, 1986, p. 751.
[16] S. Alegret and E. Martínez-Fábregas, Biosensors, 4 (1989) 287.
[17] Compendium of Analytical Nomenclature, Pergamon, Oxford, 1978, pp. 168–173.
[18] C.F. Baes and R.E. Mesmer, The Hydrolisis of Cations, Wiley, New York, 1976.
[19] J. Casabó, F. Teixidor and C. Pérez-Jiménez, unpublished results.
[20] F. Teixidor, L. Escriche, J. Casabó, E. Molins and C. Miravitlles, Inorg. Chem., 25 (1986) 4060.
[21] L. Escriche, M. Sanz, J. Casabó, F. Teixidor, E. Molins and C. Miravitlles, J. Chem. Soc., Dalton Trans., (1989) 1739.
[22] F. Teixidor, G. Sánchez-Castelló, N. Lucena, L. Escriche, R. Kivekäs, M. Sundberg and J. Casabó, Inorg. Chem., 30 (1991) 4931.
[23] F. Teixidor, L. Escriche, I. Rodríguez, J. Casabó, J. Rius, E. Molins, B. Martínez and C. Miravitlles, J. Chem. Soc., Dalton Trans., (1989) 1381.
[24] J. Casabó, L. Escriche, S. Alegret, C. Jaime, C. Pérez-Jiménez, L. Mestres, J. Rius, E. Molins, C. Miravitlles and F. Teixidor, Inorg. Chem., 30 (1991) 1893.

ELSEVIER

Analytica Chimica Acta 294 (1994) 215–220

ANALYTICA CHIMICA ACTA

Protonation constants of some pyridine derivatives in ethanol–water mixtures

Esma Kılıç [a,*], Fitnat Köseoğlu [b], Özlem Başgut [a]

[a] *Department of Chemistry, Faculty of Science, University of Ankara, Ankara, Turkey*
[b] *Department of Chemistry, Faculty of Gazi Education, University of Gazi, Ankara, Turkey*

Received 10th August 1993; revised manuscript received 3rd March 1994

Abstract

Protonation constants of a number of mono- and disubstituted pyridines were determined potentiometrically in 0, 10, 20, 30, 40, 50, 60, 70, 80% (v/v) ethanol–water mixtures at 25°C with an ionic strength of 0.1 M. Data were calculated by a computer programme. The logarithm of the protonation constants of pyridines linearly decreased with increase of ethanol contents but the values determined in water and 80% ethanol did not follow this linear trend. Furthermore, the effects of the substituents on the basicity of pyridine, the additivities of these effects and the applicability of the Hammett equation to the behaviour of substituents are discussed.

Key words: Potentiometry; Titrimetry; Protonation constants; Pyridine derivatives

1. Introduction

Recently, there has been increasing interest in properties of weak acids and bases in mixed organic solvent systems and water–organic solvent mixtures [1–6]. The basicities of pyridine and its derivatives have been studied in water by many workers, however, there is no systematic study to date on the determination of the protonation constants and the behaviour of pyridine ring substituents in ethanol–water mixtures [6–11]. The present work, therefore, deals with the determination of the stoichiometric protonation constants of pyridine derivatives in various ethanol–water mixtures. These protonation constants can be employed for the design of analytical procedures. We have determined potentiometrically the protonation constants of seventeen pyridines substituted in the 2-, 3- and 4-positions by methyl, ethyl and amino groups in ethanol–water mixtures of composition 0–80% (v/v) of ethanol. The constants were calculated using a recently developed computer method [12,13].

It is well known that structural and solvent effects are the two major factors that influence the basicity of a compound. Moreover, it is sometimes extremely difficult to assess how much each effect contributes to the basicity. The substituent and solvent effects on the protonation constants of pyridines have therefore been investigated and the additivity effects of the substituents are discussed.

* Corresponding author.

SSDI 0003-2670(94)00137-B

2. Experimental

2.1. Chemicals and standard solutions

Pyridine (99.0%), 2-methylpyridine (98.5%), 3-methylpyridine (97.0%), 4-methylpyridine (96.0%), 2-ethylpyridine (98.0%), 3-ethylpyridine (97.0%), 4-ethylpyridine (99.0%), 2-aminopyridine (98.0%), 3-aminopyridine (98.0%), 4-aminopyridine (98.0%), 2-amino-3-methylpyridine (98.0%), 2-amino-4-methylpyridine (98.0%), 2-amino-5-methylpyridine (97.0%), 2-amino-6-methylpyridine (98.0%), 2,3-diaminopyridine (98.0%), 3,4-diaminopyridine (98.0%) and 2-amino-5-chloropyridine (98.0%) were purchased from Merck and the purity of the substances was controlled by potentiometric titration. Ethanol utilized was purified as described in Ref. [14]. Doubly distilled conductivity water was used as aqueous medium as well as for preparation of ethanol–water mixtures. All other chemicals used in this investigation were of reagent grade purity.

0.10 M Perchloric acid solution was prepared in water and standardized against sodium carbonate. 0.10 M Sodium hydroxide solutions were prepared as 0, 10, 20, 30, 40, 50, 60, 70 and 80% (v/v) aqueous ethanol solutions and stored in a glass bottle protected against the atmosphere. The base solutions were standardized via a linear least-squares fit of Gran plots for end-point determination obtained from perchloric acid [15,16].

2.2. Procedure

All potentiometric measurements were performed in a 80-ml jacketed titration cell thermostated at 25.0 ± 0.1°C and under nitrogen atmosphere. An Orion 720A Model pH-ionmeter, fitted with a combined pH electrode (Ingold) containing a filling solution of 0.01 M NaCl + 0.09 M $NaClO_4$ was used for measuring the cell e.m.f. values. The potentiometric cell was calibrated before each experiment so that the hydrogen ion concentration rather than the activity was measured [12,17]. For all the solvent mixtures examined, reproducible values of autoprotolysis constants, K_{ap}, were calculated from several series of [H] and [OH] measurements at 0.1 M $NaClO_4$ [18–20].

The following solutions prepared in water and each of the solvent mixtures studied (total volume = 50.0 ml) were titrated potentiometrically with CO_2-free standard 0.1 M sodium hydroxide dissolved in the corresponding solvents: (i) 2.5×10^{-3} M $HClO_4$ (for cell calibration); (ii) 2.5×10^{-3}–7.5×10^{-3} M $HClO_4$ + 1.5×10^{-3} M pyridine derivatives. During each titration the ionic strength was maintained at 0.1 M $NaClO_4$ and a potential reading was taken after a suitable time (normally 2–3 min) for equilibration.

The protonation constants of the pyridine derivatives were calculated by analysing the titration data using the computer programme developed by Motekaitis and Martell [12,13].

3. Results and discussion

The stoichiometric protonation constants (log β) for pyridine and mono- and di-substituted pyridines in ethanol–water mixtures at 25°C are given in Tables 1 and 2. The values of log β obtained in water are in good agreement with data available in the literature [7–11].

It is observed that a linear relationship exists between the aforementioned protonation constants and the percentage of ethanol. The linear equations and the related correlation coefficients for all pyridine derivatives are given in Table 3. Many studies have shown that the equilibrium constant is linearly related to the fraction of organic solvent [6,21–25]. Our results obtained for pyridines are also in good agreement with those. However, for all the compounds examined, the constants determined in water and in 80% ethanol did not follow the linear trend which was observed in the other ethanol–water mixtures. The variation of the protonation constants for pyridine, 2-methylpyridine, 3-methylpyridine and 4-methylpyridine with the percentage of ethanol is shown in Fig. 1 as an example. The dissociation constants of charged acids in alcohol–water mixtures vary with solvent composition in a manner which is not completely understood. Bates and co-workers [26–28] and Chattopadhyay and Lahiri [29] have examined the effect of a change in solvent composition on the dissociation of BH^+

Table 1
Stoichiometric protonation constants of some monosubstituted pyridines at 25°C for different ethanol–water mixtures (μ = 0.1 M $NaClO_4$) [a]

Pyridines	Water		10% Ethanol–90% water		20% Ethanol–80% water		30% Ethanol–70% water		40% Ethanol–60% water		50% Ethanol–50% water		60% Ethanol–40% water		70% Ethanol-30% water		80% Ethanol-20% water	
	log β	Δlog β [b]	log β	Δlog β [b]	log β	Δlog β [b]	log β	Δlog β [b]	log β	Δlog β [b]	log β	Δlog β [b]	log β	Δlog β [b]	log β	Δlog β [b]	log β	Δlog β [b]
H	5.25	0	5.28	0	5.05	0	4.90	0	4.58	0	4.42	0	4.19	0	3.85	0	3.79	0
2-CH_3	6.10	0.85	5.95	0.67	5.80	0.75	5.50	0.60	5.20	0.62	5.00	0.58	4.73	0.54	4.48	0.63	4.50	0.71
3-CH_3	5.79	0.54	5.73	0.45	5.50	0.45	5.30	0.40	5.00	0.42	4.70	0.28	4.50	0.31	4.10	0.25	4.00	0.21
4-CH_3	6.15	0.90	6.05	0.77	5.85	0.80	5.65	0.75	5.30	0.72	5.10	0.68	4.80	0.61	4.55	0.70	4.43	0.64
2-C_2H_5	6.05	0.80	5.85	0.57	5.65	0.60	5.45	0.55	5.15	0.57	4.95	0.53	4.70	0.51	4.35	0.50	4.26	0.47
3-C_2H_5	5.70	0.45	5.65	0.37	5.45	0.40	5.23	0.33	4.95	0.42	4.63	0.23	4.35	0.16	4.10	0.25	3.95	0.16
4-C_2H_5	6.10	0.85	6.00	0.72	5.78	0.73	5.55	0.65	5.27	0.69	5.05	0.63	4.75	0.56	4.50	0.65	4.42	0.63
2-NH_2	6.70	1.45	6.80	1.52	6.72	1.67	6.60	1.70	6.45	1.87	6.25	1.83	6.05	1.86	5.83	1.98	5.78	1.99
3-NH_2	6.20	0.95	6.10	0.82	6.00	0.95	5.79	0.89	5.71	1.12	5.55	1.13	5.35	1.16	5.15	1.30	5.10	1.31
4-NH_2	9.10	3.85	9.07	3.79	9.00	3.95	8.90	4.00	8.75	4.17	8.63	4.21	8.45	4.26	8.24	4.39	8.17	4.38

[a] All errors are 0.03 or lower.
[b] Δlog β = log β − log β (pyridine).

Table 2
Stoichiometric protonation constants of some disubstituted pyridines at 25°C for different ethanol–water mixtures (μ = 0.1 M $NaClO_4$) [a]

Pyridines	Water		10% Ethanol–90% water		20% Ethanol–80% water		30% Ethanol–70% water		40% Ethanol–60% water		50% Ethanol–50% water		60% Ethanol–40% water		70% Ethanol–30% water		80% Ethanol–20% water	
	log β		log β		log β		log β		log β		log β		log β		log β		log β	
	obs.	calc.	obs.	calc.	obs.	calc.	obs.	calc.	obs.	calc.	obs.	calc.	obs.	calc.	obs.	calc.	obs.	calc.
2-NH_2–3-CH_3	7.03	7.24	7.15	7.25	6.95	7.17	6.80	7.00	6.66	6.87	6.48	6.53	6.35	6.36	6.13	6.08	6.05	5.99
2-NH_2–4-CH_3	7.30	7.60	7.32	7.57	7.25	7.52	7.10	7.35	7.00	7.17	6.78	6.83	6.60	6.66	6.49	6.53	6.46	6.42
2-NH_2–5-CH_3	6.98	7.24	7.04	7.25	6.95	7.17	6.76	7.00	6.60	6.87	6.35	6.53	6.23	6.35	6.15	6.08	6.18	5.99
2-NH_2–6-CH_3	7.25	7.55	7.18	7.47	7.10	7.47	7.00	7.20	6.80	7.07	6.63	6.93	6.42	6.59	6.33	6.46	6.27	6.49
2,3-di NH_2	7.00	7.65	6.85	7.62	6.80	7.67	6.70	7.49	6.63	7.57	6.55	7.38	6.40	7.21	6.30	7.13	6.25	7.09
3,4-di NH_2	9.10	10.05	9.00	9.89	8.85	9.95	8.80	9.79	8.70	9.87	8.65	9.76	8.55	9.61	8.36	9.54	8.22	9.48
2-NH_2–5-Cl	4.83	-	4.87	-	4.65	-	4.45	-	4.25	-	4.07	-	3.90	-	3.70	-	3.70	-

[a] All errors are 0.03 or lower.

and the related Gibbs energies of transfer in mixed solvents. In these publications it is suggested that electrostatic charging effects resulting from the change of dielectric constant with solvent composition are of minor importance in explaining solvent effects and that solute–solvent interactions have greater significance in the interpretation of solvent effects. Thus, we can explain our results obtained for pyridines by specific solvation effects. log β values are related to an equilibrium of the type $B + H^+ \leftrightarrow BH^+$ (where B stands for pyridines). As can be seen from Fig. 1, these values decrease linearly as the concentration of ethanol increases from 10 to 70%. Since ethanol would solvate B better than BH^+, the log β values, which are related to the formation of BH^+, would decrease on addition of ethanol. The derivations of linearity in water and 80% ethanol may result from the preferential solvation of solute by one of the components of the solvent mixture that could change the effective dielectric constant value in the cibotactic region [30]. Furthermore, another factor why an increase in the

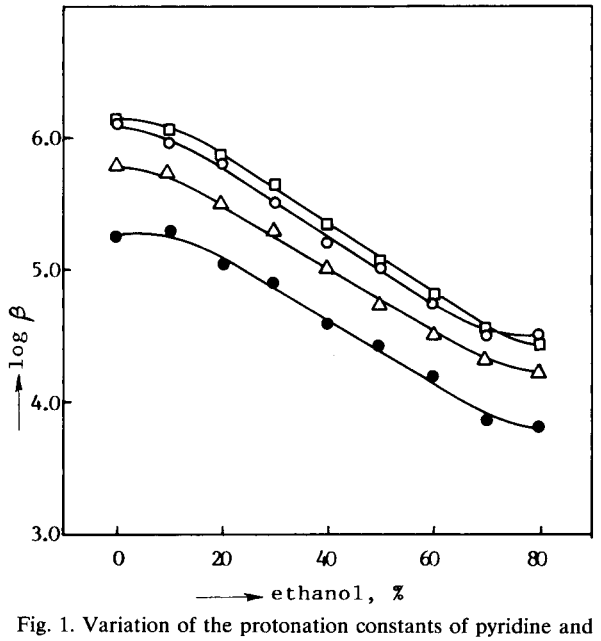

Fig. 1. Variation of the protonation constants of pyridine and methylpyridines against the percentage of ethanol: (●) pyridine, (○) 2-methylpyridine, (△) 3-methylpyridine, (□) 4-methylpyridine.

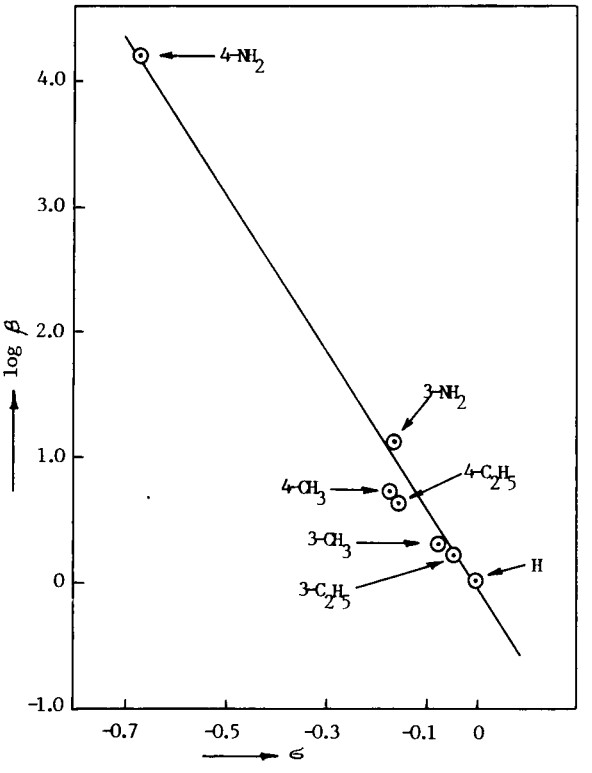

Fig. 2. Plot of the $\Delta \log \beta$ of substituted pyridines against the Hammett substituent constants (σ) in ethanol–water (50:50).

log β values of all pyridine derivatives is produced in ethanol rich regions can be satisfactorily explained by differences in solvent stabilization of the ionic species (H^+ and BH^+), brought about by changing the percentage of ethanol [27,28].

Table 1 shows that methyl- and ethylpyridines are stronger bases than pyridine and that the basicity order found experimentally for the alkylpyridines is 3-alkylpyridine < 2-alkylpyridine < 4-alkylpyridine in all media investigated. These results can be explained on the basis of electronic and steric effects of the alkyl groups [30]. A comparison of the basicities of methyl- and ethylpyridine derivatives shows that each ethylpyridine is a slightly weaker base than its methyl analogue regardless of the medium. In a previous study, we have also observed that salicylideneethylanilines are weaker bases than salicylidenemethylanilines in dioxan–water and ethanol–water mixtures [1,31]. An inspection of the log β values for aminopyridines reveals that the order

Table 3
Linear relationship between the protonation constants of pyridine derivatives and the percentage of ethanol (from 10 to 70% ethanol)

Pyridine	Equation	Correlation coefficients, r
Pyridine	$\log \beta = -2.369(\%) + 5.564$	−0.994
2-CH_3	$\log \beta = -2.603(\%) + 6.290$	−0.998
3-CH_3	$\log \beta = -2.771(\%) + 6.097$	−0.996
4-CH_3	$\log \beta = -2.643(\%) + 6.398$	−0.998
2-C_2H_5	$\log \beta = -2.557(\%) + 6.192$	−0.997
3-C_2H_5	$\log \beta = -2.774(\%) + 6.033$	−0.999
4-C_2H_5	$\log \beta = -2.577(\%) + 6.310$	−0.999
2-NH_2	$\log \beta = -1.800(\%) + 7.127$	−0.995
3-NH_2	$\log \beta = -1.637(\%) + 6.328$	−0.993
4-NH_2	$\log \beta = -1.506(\%) + 9.339$	−0.993
2-NH_2-3-CH_3	$\log \beta = -1.609(\%) + 7.286$	−0.998
2-NH_2-4-CH_3	$\log \beta = -1.577(\%) + 7.580$	−0.995
2-NH_2-5-CH_3	$\log \beta = -1.669(\%) + 7.258$	−0.989
2-NH_2-6-CH_3	$\log \beta = -1.646(\%) + 7.454$	−0.995
2,3-di NH_2	$\log \beta = -0.994(\%) + 7.011$	−0.993
3,4-di NH_2	$\log \beta = -0.929(\%) + 9.070$	−0.974
2-NH_2-5-Cl	$\log \beta = -1.880(\%) + 5.016$	−1.000

is pyridine < 3-aminopyridine < 2-aminopyridine < 4-aminopyridine in all media. The reason why the amino-derivatives are more basic than the pyridine derivatives can be explained on the grounds that the amino group is capable of releasing electrons by a resonance mechanism. The fact that 2- and particularly 4-aminopyridines exhibit high basic strengths is due to the predominant resonance effect in the case of *ortho*- and *para*-position substituents [32,33].

When the basicities of 2-aminomethylpyridines and diaminopyridines are examined, the following orders are found in all solvent mixtures: pyridine < 2-amino-5-methylpyridine < 2-amino-3-methylpyridine < 2-amino-6-methylpyridine < 2-amino-4-methylpyridine and pyridine < 2,3-diaminopyridine < 3,4-diaminopyridine, respectively. It can be seen that disubstituted pyridines, except 2-amino-5-chloropyridine, are stronger bases than pyridine and *meta*-methyl derivatives are weaker bases than *ortho*- and *para*-methyl derivatives as in the case of mono-substituted pyridines. The fact that 2-amino-5-chloropyridine is the least basic one among all the pyridines studied is due to the electron-withdrawing effect of the chloro group.

It is well known that the effect of two or more substituents is approximately the algebraic sum of the effects of the individual groups [1,34,35]. However, there is no systematic discussion on the additivities of substituent effects on the basicity of pyridine in ethanol–water mixtures. In order to test the cumulative effect of substituents, the differences ($\Delta \log \beta$) between the logarithmic values of the protonation constants of pyridine and those of methyl- and aminopyridines are presented (Table 1) and predictions have been made for the log β values of some disubstituted pyridine derivatives. The calculated and the observed log β values are given in Table 2. The observed and the calculated results show that the principle of additivity predicts a cumulative effect of substituents in the case of 2-amino-3-methyl-, 2-amino-4-methyl-, 2-amino-5-methyl- and 2-amino-6-methylpyridines. The principle of additivity in the case of 2,3-diamino- and 3,4-diaminopyridines, however, is apparently not valid since the differences between the observed and the calculated values are found to be 0.65–1.26. This may be the result of the formation of a hydrogen bond between the two amino groups.

The Hammett equation and its extended forms have been widely used for the study of various reactions such as dissociation of acids and bases [30,36]. The applicability of the Hammet equation to the prediction of the effect of substituents on the basicity of substituted pyridines in water was

Table 4
Reaction constants for the reactivity of pyridine derivatives at 25°C (reaction: $B + H^+ \leftrightarrow BH^+$)

Ethanol (%)	ρ	s [a]	r [b]	n [c]
0	−5.638	0.103	−0.997	6
10	−5.706	0.107	−0.995	6
20	−5.935	0.138	−0.995	6
30	−6.131	0.148	−0.995	6
40	−6.311	0.205	−0.990	6
50	−6.597	0.194	−0.992	6
60	−6.735	0.228	−0.989	6
70	−6.875	0.243	−0.988	6
80	−6.949	0.259	−0.987	6

B = Pyridines.
[a] Standard deviation of the regression line.
[b] Correlation coefficient.
[c] Number of compounds entering the determination of ρ.

discussed in the literature [7,37]. In the present paper, we intended to study the question whether the Hammett equation can be used to predict the effect of substituents on the basicity of pyridines in ethanol–water mixtures. For this purpose, the variation of $\Delta \log \beta$ values with the Hammett substituent constants (σ) was investigated for each ethanol–water mixture studied and the plot obtained for 50% ethanol–water is given Fig. 2 as an example. It is found that the linear relationships exist between the $\log \beta$ and σ values for all media. The relevant reaction constants (ρ) and the usual measures of the precision with which the data are represented by the Hammett equation are given in Table 4. From these observations, it can be concluded that the Hammett equation very adequately represents the basicities of substituted pyridines in ethanol–water mixtures like it does for water.

References

[1] T. Gündüz, E. Kılıç, F. Köseoğlu and E. Canel, Anal. Chim. Acta, 282 (1993) 489.
[2] G. Wada, E. Tamura, M. Okina and M. Nakamura, Bull. Chem. Soc. Jpn., 55 (1982) 3064.
[3] Z. Pawlak, J. Chem. Thermodynamics, 19 (1987) 443.
[4] C.F. Wells, J. Chem. Soc., Faraday Trans. I, 80 (1984) 2445.
[5] K.S. Siow and K.P. Ang, J. Solution Chem., 18 (1989) 937.
[6] M.S.K. Niazi and J. Mollin, Bull. Chem. Soc. Jpn., 60 (1987) 2605.
[7] H.H. Jaffe and G.O. Doak, J. Am. Chem. Soc., 77 (1955) 4441.
[8] H.D. Mc Daniell and H.C. Brown, J. Org. Chem., 23 (1958) 120.
[9] R.H. Linnell, J. Org. Chem., 25 (1960) 290.
[10] M. Paabo, R.A. Robinson and R.G. Bates, Anal. Chem., 38 (1966) 1573.
[11] T.R. Harkins and H. Freiser, J. Am. Chem. Soc., 77 (1955) 1374.
[12] A.E. Martell and R.J. Moteaitis, The Determination and Use of Stability Constants, VCH, Weinheim, 1988.
[13] R.J. Motekaitis and A.E. Martell, Can. J. Chem., 60 (1982) 168.
[14] D.D. Perrin and W.L.F. Armarega, Purification of Laboratory Chemicals, Pergamon, Oxford, 1st edn., 1966.
[15] G. Gran, Acta Chem. Scand., 4 (1950) 559.
[16] G. Gran, Analyst, 77 (1952) 661
[17] M. Meloun, J. Havel and H. Högfeldt, Computation of Solution Equilibria, Wiley, New York, 1988.
[18] E.P. Serjeant, Potentiometry and Potentiometric Titrations, Wiley, New York, 1984.
[19] E.M. Woolley, D.G. Hurkot and L.G. Hepler, J. Phys. Chem., 74 (1970) 3908.
[20] S. Rondinini, P. Longhi, P.R. Mussini and T. Mussini, Pure Appl. Chem., 59 (1987) 1693.
[21] C.C. Panichajakul and E.M. Woolley, Anal. Chem., 47 (1975) 1880.
[22] L.G. Van Uitert, C.G. Haas, W.C. Fernalius and B.E. Douglas, J. Am. Chem. Soc., 75 (1953) 455.
[23] H. Irving and H. Rossotti, Acta. Chem. Scand., 10 (1956) 72.
[24] H. Irving and H. Rossotti, Analyst, 80 (1955) 245.
[25] P.S. Gentile, M. Cefola and A.V. Celiano, J. Phys. Chem., 67 (1963) 1447.
[26] M. Paabo, R.G. Bates and R.A. Robinson, J. Phys. Chem., 70 (1965) 247.
[27] R.G. Bates, J. Electroanal. Chem., 29 (1971) 1.
[28] R.G. Bates, Determination of pH, Theory and Practice, Wiley, New York, 2nd edn., 1973.
[29] A.K. Chattopadhyay and S.C. Lahiri, Electrochim. Acta, 27 (1982) 269.
[30] N.S. Isaacs, Physical Organic Chemistry, Longman, New York, 1986.
[31] F. Köseoğlu, E. Kılıç, E. Canel, N. Yılmaz, Anal. Chim. Acta, in press.
[32] F.R.S. Sidgwick, The Organic Chemistry of Nitrogen, Clarendon, Oxford, 1966.
[33] G.B. Barlin, J. Chem. Soc., (1964) 2150.
[34] K. Clarke and K. Rothwell, J. Chem. Soc., (1960) 1885.
[35] R.J.L. Andon, J.D. Cox and E.F.G. Herington, Trans. Faraday Soc., 50 (1954) 918.
[36] A.J. Hoefnagel and B.M. Webster, J. Chem. Soc., Perkin Trans. II, (1989) 977.
[37] A. Bryson, J. Am. Chem. Soc., 82 (1960) 4871.

ELSEVIER

Analytica Chimica Acta 294 (1994) 221–226

ANALYTICA CHIMICA ACTA

A rapid method for the determination of ^{137}Cs in environmental water samples

Chuarn-Yuh Huang, Jun-Der Lee, Chia-Lian Tseng, Jem-Mau Lo *

Institute of Nuclear Science, National Tsing Hua University, Hsinchu, 30043, Taiwan

Received 20th October 1993; revised manuscript received 12th March 1994

Abstract

This work deals with a simple, rapid, and efficacious design for the measurement of ^{137}Cs in seawater. An adsorption filter is fabricated by coating copper(II) hexacyanoferrate(II) (CuCF) onto a densely twilled nylon cloth. The CuCF–nylon cloth filter is cut into round pieces and screwed into a polyethylene (PE) column. The ^{137}Cs-containing seawater sample is allowed to pass through the CuCF–nylon cloth filter into the column and ^{137}Cs in seawater can thus be efficiently adsorbed. The analysis for less than μCi level of ^{137}Cs in 4 l seawater is illustrated to have a recovery better than 97%. The detection limit for ^{137}Cs in seawater can be greatly improved by the enrichment of ^{137}Cs on the adsorption filter.

Key words: Ion exchange; Adsorption; Cesium-137; Radiometry; Seawater; Waters

1. Introduction

^{137}Cs is produced in large amounts as a fission product from nuclear fuel and is one of the radioactive pollutants with the largest impact on the environment. It originates from the fallout of nuclear weapon detonation and/or a nuclear power plant accident such as the Chernobyl disaster. It can be dispersed by diffusion in air and by wind convection and disseminated all over the world. It is also realized that river water or seawater next to a nuclear power plant may be readily polluted by ^{137}Cs being released from the cooling system of the plant. Being an alkali metal Cs^+ is the most stable form, which is easily dissolved and migrated in the aquatic system.

It is difficult to accurately determine ^{137}Cs in environmental water samples at very low concentrations by a direct detection method. A preconcentration procedure is usually needed to serve the need for increased concentration of ^{137}Cs for the final accurate γ detection. The ion-exchange adsorption method with zeolite as the exchanger [1] and the adsorption method with the hexacyanoferrates of transition metals as the adsorbent [1–8] have been mostly frequently investigated for this purpose. However, zeolites (e.g. mordenite, chabazite, etc.) are not suitable as the preconcentration agent in the application of analysis of water samples containing a relatively large amount of sodium ion, e.g., seawater. Sodium

* Corresponding author.

SSDI 0003-2670(94)00124-5

ions will be adsorbed by the zeolite as well and cause serious interference with the ^{137}Cs adsorption. On the other hand, the hexacyanoferrate(II) complexes of transition metals have a high selectivity for Cs^+ and have become a very useful agent for the separation of ^{137}Cs from the environmental water samples. Coprecipitation methods and column adsorption methods using hexacyanoferrates have been developed. Copper(II) hexacyanoferrate(II) is often selected as the agent in practical analysis because it can be readily prepared in a granular or powdery form while most of the other hexacyanoferrates are usually obtained in a colloidal or gelatinous form and are better soluble in water [5]. Watari et al. [2,3] have proposed an column adsorption method using the granular copper(II) hexacyanoferrate(II) supported on an ion-exchange resin for the analysis of trace amounts of ^{137}Cs in seawater. Kawamura and Motojima [4] used copper(II) hexacyanoferrate(II) impregnated zeolite for ^{137}Cs removal from radioactive liquid waste. In the present study, a simple, rapid, and efficacious adsorption method using copper(II) hexacyanoferrate(II) is developed for the measurement of ^{137}Cs in environmental water samples.

2. Experimental

2.1. Preliminary study

All chemicals used in the following were of reagent grade. 0.05 M of various hexacyanoferrate(II) complexes of transition metals were prepared using equal volumes of 0.1 M $K_4Fe(CN)_6$ and 0.2 M of the metal ions in the chloride form including Ni^{2+}, Cu^{2+}, Zn^{2+}, Co^{2+} and Mn^{2+}. Deionized water was used to prepare the solutions. 20 ml of seawater (collected at the coast of Taiwan Strait near Hsinchu, Taiwan) spiked with 0.5 μCi carrier-free ^{137}Cs was used as the testing samples. The ^{137}Cs-containing seawater sample was adjusted to a pH ranging from 1–12.6 and then 0.1 ml of 0.05 M of various hexacyanoferrates were added. After shaking for 5 min to accomplish the ^{137}Cs adsorption, the precipitate was separated by centrifugation. The adsorption efficiency was measured by counting the aliquots of the solutions before and after adsorption and also checked by counting the radioactivities of ^{137}Cs what was originally added and of what remained after the settlement. Thus the effect of pH on the ^{137}Cs adsorption by the hexacyanoferrate(II) complexes of various transition metals could be observed. The effect of the amount of hexacyanoferrates on the ^{137}Cs adsorption was investigated in a similar way by adding different volumes of 0.05 M of the agents to the same seawater samples. All the hexacyanoferrates used in the work were prepared freshly.

2.2. Preparation of adsorption filter

A densely twilled nylon cloth with a thickness of 1 mm was cut into a round piece with a diameter of about 65 mm. The round nylon cloth was glued with PARA-SIL silicone along the surrounding edge about 8 mm wide and placed onto the polyethylene (PE) adsorption column. The nylon cloth filter holder was then tightly screwed onto the column to avoid any leakage. The schematic diagram of the nylon cloth fabricated in the PE adsorption column is shown in Fig. 1. 2 ml of 0.1 M $K_4Fe(CN)_6$ and 2 ml of 0.2 M $CuCl_2$ were added to a flask filled with 20 ml water. After stirring a few seconds, the solution was poured into the column and the copper(II) hexacyanoferrate(II) (abbreviated as CuCF below) formed was allowed to deposit homogeneously on

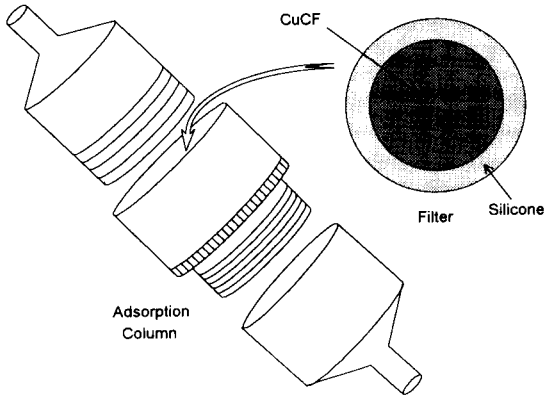

Fig. 1. Adsorption column and adsorption filter.

the nylon cloth by a slight suction. In this way, an adsorption filter of nylon cloth coated with homogeneous CuCF was produced. The adsorption filter was taken from the column and placed onto another adsorption column to be arranged in the set-up for practical ^{137}Cs analysis (see Fig. 2)

2.3. Preconcentration of ^{137}Cs in seawater by adsorption filter for γ spectrometry

Fig. 2 shows the set-up for preconcentration of ^{137}Cs in water samples by the CuCF adsorption filter. 1 l of seawater to which was added 1 ml 0.5 μCi ^{137}Cs was used as the testing sample. Three of the CuCF adsorption filters produced previously were placed on top of each other in the PE adsorption column, and screwed tightly to avoid any leakage. The ^{137}Cs-containing water sample was drawn through the CuCF adsorption filter by a water pump. The flow-rate was about 240 ml min^{-1}. Another run was made using 4 l of seawater spiked with 42 pCi ^{137}Cs as the testing sample. The flow-rate was about 320 ml min^{-1}. Usually the adsorption procedure could be finished within 3 min for 1 l and 13 min for 4 l of the water samples. Thereafter the ^{137}Cs-enriched adsorption filter was taken away for γ counting by an high-purity Ge detector connected with a multi-channel analyzer (MCA) system. Usually the round adsorption filter was mounted on the surface of the detector which means counting with a 2π geometric factor.

3. Results and discussion

In the earlier stage of this study, adsorption behaviour of the various metal hexacyanoferrates for ^{137}Cs in seawater had been extensively and systematically investigated. The effect of pH on the adsorption of ^{137}Cs from seawater by the various hexacyanoferrates is shown in Fig. 3. An adsorption efficiency can be reached of more than 99% for nickel(II) hexacyanoferrate(II) (NiCF) in the pH range 1–12, for copper(II) hexacyanoferrate(II) (CuCF) in the pH range 1–10, for cobalt(II) hexacyanoferrate(II) (CoCF) in the pH range 1–9, and for manganese(II) hexacyanoferrate(II) (MnCF) in the pH range 3–8, respectively. However, the adsorption efficiency is only 60–75% for zinc(II) hexacyanoferrate(II) (ZnCF) in the pH range 1–6. All the curves of adsorption efficiency versus pH show plateaus with a steep slope at the higher pH ends. For natural seawater without pH adjustment the adsorption efficiency can reach a value of > 99%

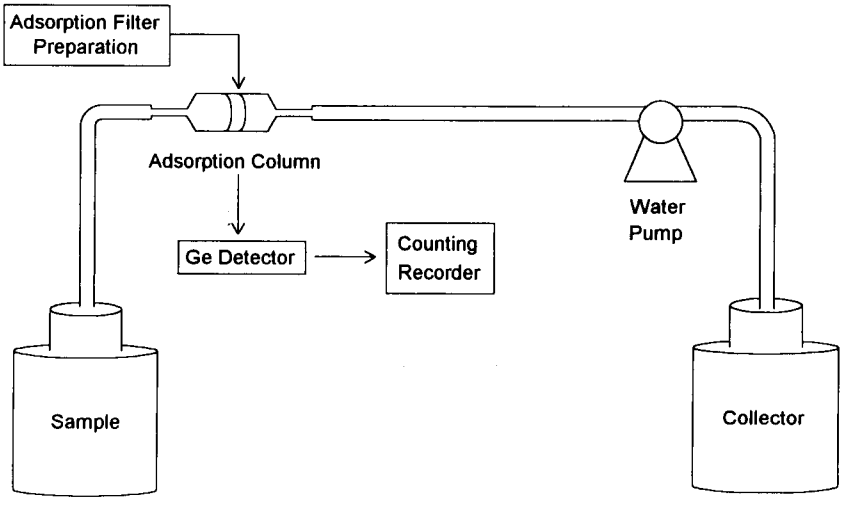

Fig. 2. Set-up for preconcentration of ^{137}Cs in water samples by the adsorption filter proposed.

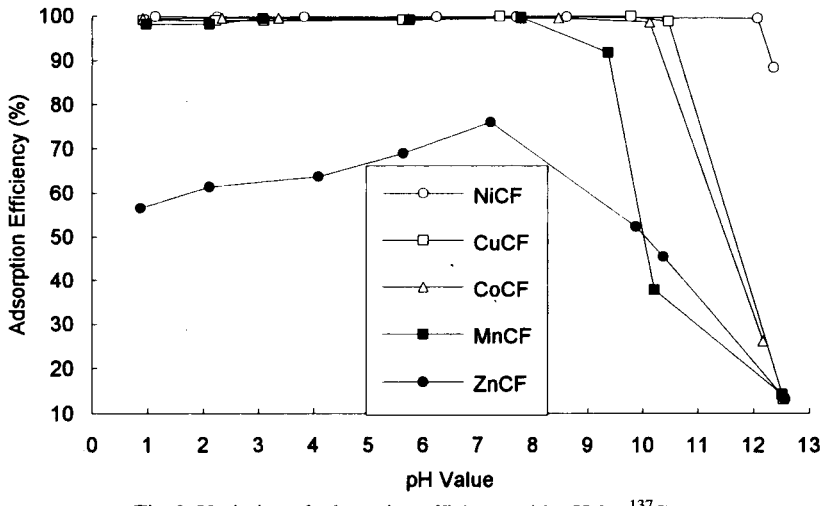

Fig. 3. Variation of adsorption efficiency with pH for ^{137}Cs.

for all the metal hexacyanoferrates except for ZnCF which has a much lower efficiency of 76% (see Fig. 4). The amount of NiCF, CuCF or CoCF that has to be added was at least 1×10^{-3} mmol to attain a complete adsorption for 20 ml of natural seawater containing 0.5 μCi ^{137}Cs (see Fig. 5). The K_d value, calculated from the activity of ^{137}Cs adsorbed on the metal hexacyanoferrate divided by the activity remained in the solution of natural seawater at equilibrium, was found to be 2.16×10^5 for NiCF, 5.28×10^5 for CuCF and 2.64×10^5 for CoCF. The adsorption of ^{137}Cs by the three metal hexacyanoferrates is very fast, reaching > 98% efficiency within 2 min (see Fig. 6).

Based on the optimal conditions obtained from the preliminary work mentioned above, a suitable adsorption filter was developed by coating a metal

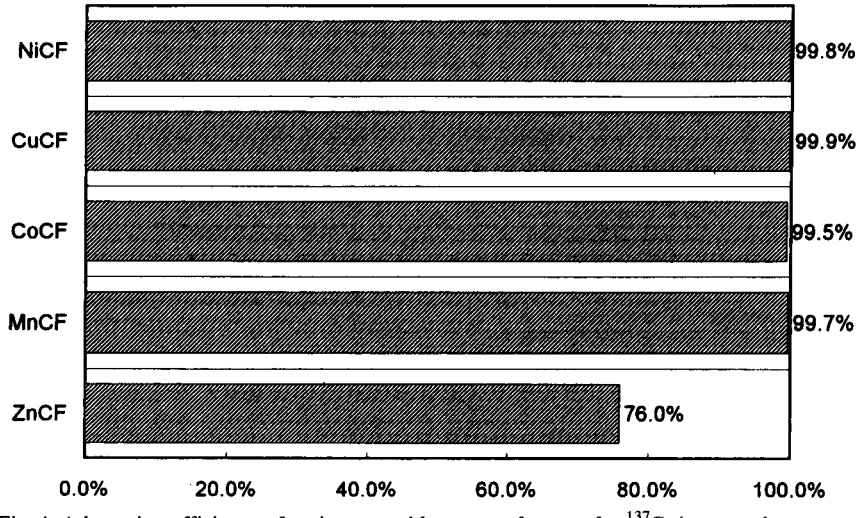

Fig. 4. Adsorption efficiency of various metal hexacyanoferrates for ^{137}Cs in natural seawater.

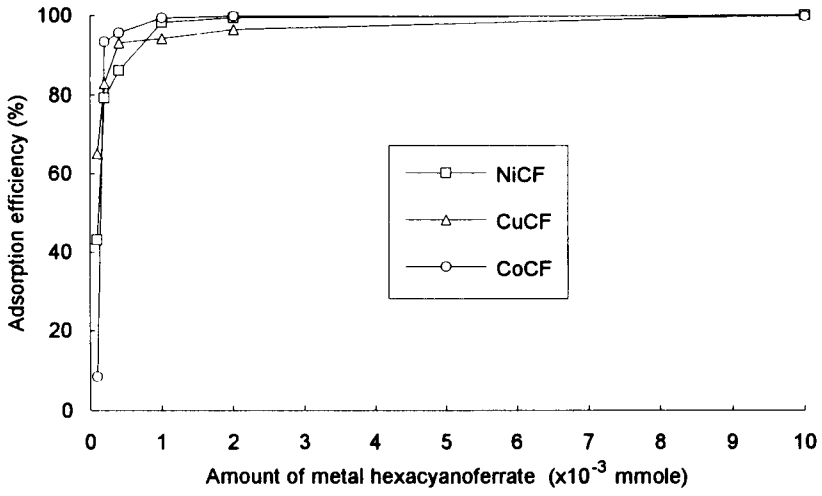

Fig. 5. Effect of amount of various metal hexacyanoferrates on the adsorption of ^{137}Cs from seawater.

hexacyanoferrate on nylon cloth for the preconcentration of ^{137}Cs from water samples. CuCF, NiCF and CoCF, owing to high adsorption efficiency to ^{137}Cs, were tested. The parameters such as the initial concentrations of the hexacyanoferrate ion and the metal ion, the volume of the water sample, the suction rate and temperature may all influence the features and feasibility of the adsorption filters prepared. The particle size of the adsorbent on the nylon cloth may be controlled by the reaction of the metal ion with the hexacyanoferrate ion under the varying conditions such as the concentration, shaking time and temperature. However, this is only applicable to the preparation of the adsorption filter of CuCF on nylon cloth and fails for the other two metal hexacyanoferrates. The CoCF formed was found to be a gelatinous precipitate and not suitable for making a homogeneous coating on the nylon cloth. The NiCF formed was found to be colloidal with

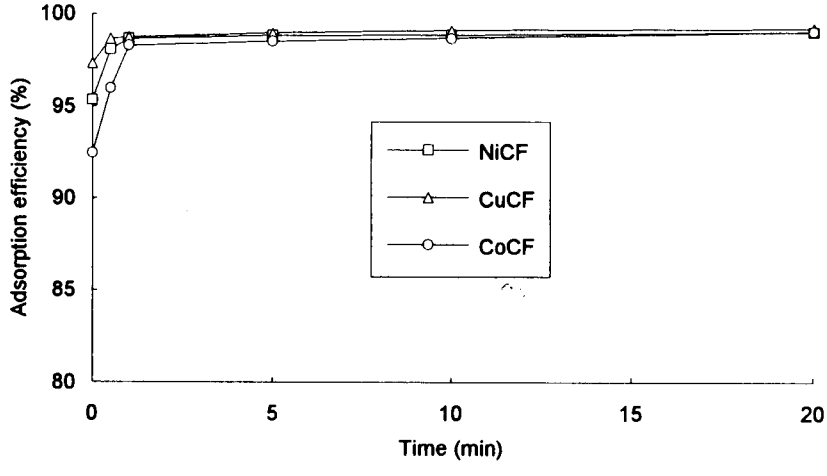

Fig. 6. Dependence of shaking time on adsorption efficiency of ^{137}Cs by the metal hexacyanoferrates.

small particle sizes, and a great part of the colloid could not be retained on the nylon cloth. Therefore CoCF and NiCF were excluded in the preparation of a suitable adsorption filter for concentrating ^{137}Cs from water samples. The remaining work in the study was focused on the use of the CuCF–nylon cloth filter in the practical determination of ^{137}Cs in water samples. The CuCF–nylon cloth adsorption filter obtained according to the procedure described above was found to be efficacious and practical for the ^{137}Cs adsorption from a large sample volume of water. The particle size of CuCF on nylon cloth of the ready-made filter is between 10 and 20 μm in diameter as determined by means of a scanning electron microscope. The distribution of the particles of CuCF on nylon cloth was observed to be homogeneous. The CuCF–nylon cloth was screwed into the PE column in the set-up (see Fig. 2) and the efficiency of adsorption of ^{137}Cs by the CuCF–nylon cloth from 1 l of seawater passing through within a certain period of time was observed. The result is shown in Table 1. When one piece of the CuCF–nylon cloth was applied with a flow-rate of 460 ml min^{-1}, the adsorption efficiency was ca. 65%. Addition of another piece of the CuCF–nylon cloth on top of the first one could improve the adsorption efficiency up to ca. 83% with a flow-rate of 370 ml min^{-1}. When three pieces of the CuCF–nylon cloth were placed onto the PE adsorption column, an adsorption efficiency as high as $\geqslant 98\%$ could be reached with a flow-rate of 240 ml min^{-1}. The lower flow-rate in the cases of using two and three pieces of the filter is expected to have no or only a very limited influence on the pronounced increase in the adsorption efficiency, because the adsorption rate is as fast as found in the preliminary basic study as previously mentioned. The adsorption of 42 pCi ^{137}Cs in 4 l of seawater by means of three pieces of CuCF–nylon cloth packed in the PE column was found to have also a very high efficiency of $\geqslant 95\%$. The reproducibility of five runs of the 4 l-sample test is very good as indicated in Table 2. The success in the analysis of ^{137}Cs in seawater by the proposed method is clear from all of the results mentioned above. Seawater is no doubt the most challenging sample in the ^{137}Cs detection study due to its high content of sodium ion. It can be inferred from the present work that the proposed technique can be easily and practically applied to all the other environmental water samples besides seawater.

Table 1
Adsorption efficiency of 0.5 μCi ^{137}Cs by CuCF–nylon cloth from 1 l of seawater

Number of layers of CuCF–nylon cloth [a]	Average flow-rate (ml min^{-1})	Average adsorption efficiency (%)
1	460	63.5 ± 9.3 [b]
2	370	82.9 ± 2.7 [c]
3	240	97.5 ± 2.5 [c]

[a] The amount coated on a piece of CuCF–nylon cloth being 0.2 mmol.
[b] Mean with standard deviation from 6 repeated runs.
[c] Mean with standard deviation from 3 repeated runs.

Table 2
Adsorption efficiency for 42 pCi ^{137}Cs in 4 l seawater by three layers of CuCF–nylon cloth

Run no.	Absorption efficiency (%)
1	96.41
2	110.8
3	106.7
4	90.0
5	97.4

The average flow-rate is about 320 ml min^{-1}. The amount of CuCF coated on a piece of nylon cloth is 0.5 mmol.

References

[1] V. Pekarek and V. Vesely, Talanta, 19 (1972) 1245.
[2] K. Watari, Kiyoko Imai and Masami Izawa, J. Nucl. Sci. Technol., 4 (1967) 190.
[3] K. Watari, Kiyoko Imai and Masami Izawa, J. Nucl. Sci. Technol., 5 (1968) 309.
[4] K. Kawamura and K. Motojima, Nucl. Technol., 58 (1982) 242.
[5] M.T. Ganzerli Valentini, S. Meloni and V. Maxia, J. Inorg. Nucl. Chem., 34 (1972) 1427.
[6] S. Vlasselaer, W. D'Olieslager and M. D'Hont, Inorg. Nucl. Chem., 38 (1976) 327.
[7] W.F. Hendrickson and G.K. Riel, Health Phys., 28 (1975) 17.
[8] Z. Hölgye, Fresenius J. Anal. Chem., 340 (1991) 59.

PUBLICATION SCHEDULE FOR 1994

	J	F	M	A	M	J	J	A	S	O	N	D
Anal. Chim. Acta	284/3 285/1–2 285/3	286/1 286/2 286/3	287/1–2 287/3 288/1–2	288/3 289/1 289/2	289/3 290/1–2 290/3	291/1–2 291/3 292/1–2	292/3 293/1–2 293/3	294/1 294/2 294/3	295/1–2 295/3 296/1	296/2 296/3 297/1–2	297/3 298/1 298/2–3	299/1 299/2–3 300/1
Vib. Spec.	6/2		6/3		7/1		7/2		7/3		8/1	

INFORMATION FOR AUTHORS

Detailed "Instructions to Authors" for *Analytica Chimica Acta* was published in Volume 289, No. 3, pp. 381–384. Free reprints of the "Instructions to Authors" of *Analytica Chimica Acta* and *Vibrational Spectroscopy* are available from the Editors or from: Elsevier Science B.V., P.O. Box 330, 1000 AH Amsterdam, The Netherlands. Telefax: (+31-20) 5862459.

Manuscripts. The language of the journal is English. English linguistic improvement is provided as part of the normal editorial processing. Authors should submit three copies of the manuscript in clear double-spaced typing on one side of the paper only. *Vibrational Spectroscopy* also accepts papers in English only.

Rapid publication letters. *Letters* are short papers that describe innovative research. Criteria for letters are novelty, quality, significance, urgency and brevity. Submission data: max. of 2 printed pages (incl. Figs., Tables, Abstr., Refs.); short abstract (e.g., 3 lines); *no* proofs will be sent to the authors; submission on floppy disc; *no* revision will be possible.

Abstract. All papers and reviews begin with an Abstract (50–250 words) which should comprise a factual account of the contents of the paper, with emphasis on new information.

Figures. Figures should be prepared in black waterproof drawing ink on drawing or tracing paper of the same size as that on which the manuscript is typed. One original (or sharp glossy print) and two photostat (or other) copies are required. Attention should be given to line thickness, lettering (which should be kept to a minimum) and spacing on axes of graphs, to ensure suitability for reduction in size on printing. Axes of a graph should be clearly labelled, along the axes, outside the graph itself. All figures should be numbered with Arabic numerals, and require descriptive legends which should be typed on a separate sheet of paper. Simple straight-line graphs are not acceptable, because they can readily be described in the text by means of an equation or a sentence. Claims of linearity should be supported by regression data that include slope, intercept, standard deviations of the slope and intercept, standard error and the number of data points; correlation coefficients are optional.

Photographs should be glossy prints and be as rich in contrast as possible; colour photographs cannot be accepted. Line diagrams are generally preferred to photographs of equipment. Computer outputs for reproduction as figures must be good quality on blank paper, and should preferably be submitted as glossy prints.

Nomenclature, abbreviations and symbols. In general, the recommendations of IUPAC should be followed, and attention should be given to the recommendations of the Analytical Chemistry Division in the journal *Pure and Applied Chemistry* (see also *IUPAC Compendium of Analytical Nomenclature, Definitive Rules*, 1987).

References. The references should be collected at the end of the paper, numbered in the order of their appearance in the text (*not* alphabetically) and typed on a separate sheet.

Reprints. Fifty reprints will be supplied free of charge. Additional reprints (minimum 100) can be ordered. An order form containing price quotations will be sent to the authors together with the proofs of their article.

Papers dealing with vibrational spectroscopy should be sent to: Dr J.G. Grasselli, 150 Greentree Road, Chagrin Falls, OH 44022, U.S.A. Telefax: (+1-216) 2473360 (Americas, Canada, Australia and New Zealand) or Dr J.H. van der Maas, Department of Analytical Molecular Spectrometry, Faculty of Chemistry, University of Utrecht, P.O. Box 80083, 3508 TB Utrecht, The Netherlands. Telefax: (+31-30) 518219 (all other countries).

0003-2670/94/$07.00

Intelligent Software for Chemical Analysis

Edited by **L.M.C. Buydens** and **P.J. Schoenmakers**

Data Handling in Science and Technology Volume 13

Various emerging techniques for automating intelligent functions in the laboratory are described in this book. Explanations on how systems work are given and possible application areas are suggested. The main part of the book is devoted to providing data which will enable the reader to develop and test his own systems. The emphasis is on expert systems; however, promising developments such as self-adaptive systems, neural networks and genetic algorithms are also described.

Contents:

1. Introduction. Automation and intelligent software. Expert systems. Neural networks and genetic algorithms. Reader's guide. Concepts. Conclusions. **2. Knowledge-based Systems in Chemical Analysis** (P. Schoenmakers). Computers in analytical chemistry. Sample preparation. Method selection. Method development. Instrument control and error diagnosis. Data handling and calibration. Data interpretation. Validation. Laboratory management. Concluding remarks. Concepts. Conclusions. Bibliography. **3. Developing Expert Systems** (H. van Leeuwen). Introduction. Prerequisites. Knowledge acquisition. Knowledge engineering. Inferencing. Explanation facilities. The integration of separate systems. Expert-system testing validation and evaluation. Concepts. Conclusions. Bibliography. **4. Expert-System-Development Tools** (L. Buydens, H. van Leeuwen, R. Wehrens). Tools for implementing expert systems. Tool selection. Knowledge-acquisition tools. Concepts. Conclusions. Bibliography. **5. Validation and Evaluation of Expert Systems for HPLC Method Development - Case Studies** (F. Maris, R. Hindriks). Introduction. Case study I: Expert systems for method selection and selectivity optimization. Case study II: System-optimization expert system. Case study III: Expert system for repeatability testing, applied for trouble-shooting in HPLC. Case study IV: Ruggedness-testing expert system. General comments on the evaluations. Concepts. Conclusions. Bibliography. **6. Self-adaptive Expert Systems** (R. Wehrens). Introduction - maintaining expert systems. Self-adaptive expert systems: Methods and approaches. The refinement approach of SEEK. Examples from analytical chemistry. Concluding remarks. Concepts. Conclusions. Bibliography. **7. Inductive Expert Systems** (R. Wehrens, L. Buydens). Introduction. Inductive classification by ID3. Applications of ID3 in analytical chemistry. Concluding remarks. Concepts. Conclusions. Bibliography. **8. Genetic Algorithms and Neural Networks** (G. Kateman). Introduction. Genetic algorithms. Artificial neural networks. Concepts. Conclusions. Bibliography. **9. Perspectives.** Limitations of Intelligent Software. Dealing with intelligent software. Potential of intelligent software. **Index.**

ELSEVIER SCIENCE B.V.

© 1993 366 pages Hardbound
Price: Dfl. 350.00 (US $ 200.00)
ISBN 0-444-89207-9

ORDER INFORMATION

For USA and Canada
ELSEVIER SCIENCE INC.
P.O. Box 945
Madison Square Station
New York, NY 10160-0757
Fax: (212) 633 3880

In all other countries
ELSEVIER SCIENCE B.V.
P.O. Box 330
1000 AH Amsterdam
The Netherlands
Fax: (+31-20) 5862 845

US$ prices are valid only for the USA & Canada and are subject to exchange rate fluctuations; in all other countries the Dutch guilder price (Dfl.) is definitive. Customers in the European Community should add the appropriate VAT rate applicable in their country to the price(s). Books are sent postfree if prepaid.

0003-2670(19940819)294:2;1-Z